Fall 2007

Magnetohydrodynamic power generation in a scramjet using a post combustor generator

Nathan Lee Mundis

Department:

MAGNETOHYDRODYNAMIC POWER GENERATION IN A SCRAMJET USING A POST COMBUSTOR GENERATOR

by

NATHAN L. MUNDIS

A THESIS

Presented to the Faculty of the Graduate School of the

UNIVERSITY OF MISSOURI – ROLLA

In Partial Fulfillment of the Requirements for the Degree

MASTER OF SCIENCE IN AEROSPACE ENGINEERING

2007

Approved by

Dr. David W. Riggins, Advisor	**Dr. Walter Eversman**

Dr. Jerry Peacher

ABSTRACT

A scramjet with a post combustor MHD generator is examined. A quasi-one-dimensional model is developed to calculate the flow path from tip to tail. The model includes losses due to combustion irreversibility, incomplete combustion, chemically reacting flow, friction, MHD losses, and nozzle plume modeling. Flight Mach number, magnetic field strength, gas conductivity, MHD load factor, and MHD generator expansion angle are all varied in order to assess their effects on MHD power generated and thrust lost in the engine. The trends produced through the above variations are summarized in a set of model-fit equations. It is concluded that a post combustor MHD generator is a viable means of power generation in a scramjet and its power output can be regulated by controlling the input variables cited above.

ACKNOWLEDGEMENTS

First and foremost, I would like to acknowledge Dr. H. F. Nelson, my first thesis advisor, who pointed me toward this field of study and kept me on track. Dr. Nelson passed away about halfway through the preparation of this thesis and is deeply missed. I'd like to thank Dr. Riggins for assuming the role of my advisor after Dr. Nelson's death and driving me to complete this thesis. I'd like to acknowledge Drs. Peacher and Eversman, the other members of my committee. Finally, I'd like to thank my family, friends, and loved ones for their continued support through this arduous work. It is only because of all these people that this document was completed.

TABLE OF CONTENTS

Page

LIST OF FIGURES

LIST OF TABLES

NOMENCLATURE

SYMBOL	DESCRIPTION
A	area at the given point
B	magnetic field strength in the MHD generator
C_f	skin friction coefficient for the given component
C_p	constant pressure specific heat at the given point
$\overline{C}_p$	constant pressure molar specific heat for the species at the given point
E	electric field strength at the given point in the MHD generator
F	force generated in the given component
H	height at the given point
I_{sp}	pecific impulse for the given configuration
L	ength of the given component
M	Mach number at the given point
MHD_{sp}	specific MHD impulse for the given configuration
M_w	molecular weight of the given species or mixture
N_{st}	Stanton number
P	static pressure at the given point
P_t	total pressure at the given point
$\dot{Q}$	power, i.e. rate of energy flow for the component or configuration
R	specific gas constant at the given point
$\overline{R}$	universal gas constant, 8.3145 J/(K*mol)
T	static temperature at the given point

T_t	total temperature at the given point
W	width of the vehicle
Y	mole fraction of the given species at the given point
c	circumference or perimeter at the given point
f_{ST}	stoichiometric fuel to air ratio
f_c	friction loss at the given point
g_0	acceleration from gravity at sea level on Earth
h	altitude or specific enthalpy, at the given point
h_c	heat-transfer coefficient at the given point
h_f^o	specific enthalpy of formation for the given species
h_t	specific total enthalpy at the given point
h_v	fuel heating value
$\dot{m}$	mass flow rate at the given point
q	specific heat addition at the given point
s	specific entropy at the given point
s_t	specific total entropy at the given point
u	velocity at the given point
w	specific work extraction at the given point
x	coordinate of the flow direction at the given point
β	shock angle of the given shockwave
γ	ratio of specific heats at the given point
η_{MHD}	MHD load factor in the MHD generator
η_{burn}	combustion efficiency at the given point in the combustor

θ	geometry angle of the component, either compression or expansion
$\nu(M)$	Prandtl-Meyer function at the given point in the open nozzle
ρ	density at the given point
σ	conductivity of the flow in the MHD generator
τ_R	wall temperature relaxation coefficient in the given component
%MHD	percent of total power generated as electricity for the configuration

1. INTRODUCTION

Since the 1950s, engineers have been researching the use of magnetohydrodynamics (MHD), the manipulation of electric and magnetic fields in conjunction with fluid flow, in relation to hypersonic aircraft propulsion. Past research has focused primarily on the concept of an inverse cycle engine where energy is extracted by a MHD generator upstream of the combustor and is subsequently returned to the flow via a MHD accelerator downstream of the combustor but before the nozzle. This engine design seeks to improve engine efficiency at very high speeds (>Mach 10) by circumventing the high temperatures and velocities that would normally complicate efficient combustor operation. Though an interesting concept that on the surface appears promising, more recent investigations have indicated the inverse cycle approach is likely not feasible.

The present study, however, does not research the inverse cycle concept; rather, this study places a MHD generator between the exit of the combustor and the entrance to the nozzle. This generator extracts work from the flow in the form of electrical energy which can then in turn be utilized in myriad ways. Most simply, the electricity generated could be used to power the onboard systems of the craft on-demand, thereby providing a weight savings from reduction in necessary power storage and transmission systems. Other suggested uses for the electricity generated are far more conceptual but include powering lasers, microwave generators, or other means that could be used to modify the flow field upstream of the vehicle in such a way as to reduce external drag on the vehicle, thereby providing an overall energy savings. In such a case, if the drag reduction exceeded the thrust loss caused by the MHD energy extraction within the propulsion flow path, there would be a net gain in

terms of overall vehicle performance. Exploring this use of the energy extracted by the MHD generator, however, is not a topic covered in this study, which focuses on performance impacts in terms of lost thrust and derivative quantities, as well as the magnitude of power able to be generated though MHD.

The present study, while relatively straight forward in terms of modeling, provides a wealth of information that the researcher has been unable to find in any study already conducted and reported in the literature. This study specifically examines how the thrust, engine power, and electrical power extracted change as a function of a variety of parameters including Mach number, magnetic field strength, fluid conductivity, electromagnetic load factor, and MHD generator expansion angle. It examines the trends inherent in these changes and draws conclusions about the behavior of those trends and the impact on the design of an engine configuration containing a MHD generator.

To achieve the stated purpose, this thesis first reviews the research published in the literature related to its subject. Next, the engine geometry is specified. Then, the construction of the numerical model is described and its validation given. Subsequently, results are presented and discussed. The results are then used to derive equations that describe the trends in those model results. Finally, conclusions are drawn about this entire work.

2. LITERATURE REVIEW

When the literature on aerospace magnetohydrodynamics and associated applications was reviewed, no study or text was found that considered the model (quasi-one-dimensional) and configuration (a post combustor MHD generator) presented in this thesis; however, what has been discussed in related areas proved instrumental in facilitating the work completed and presented here. In this section, the literature relevant to this study is reviewed.

2.1. GENERAL MHD THEORY

General magnetohydrodynamic theory can be found in a variety of texts ranging from electrodynamics, to plasma physics, to (some) fluid mechanics texts. In general, the type of MHD model used in this investigation is covered most explicitly in fluid dynamics texts which are focused on fluids applications. Electrodynamics texts [1,2] usually have a chapter on electric and magnetic fields in detail while also covering Maxwell's equations in general. These two sections of such a book can be used to derive the MHD relations as used in the present model. However, doing this requires much derivation and a rather great knowledge of electrodynamics. Most books which are centered on plasmadynamics (rather than fluid dynamic applications of MHD, such as *Magnetohydrodynamics* and other similar titles [3,4]) are in general more geared toward the exploration and study of aspects of MHD that do not particularly relate to its use in aerospace applications, e.g. concentrating on the relation of MHD to solar physics. Collections of papers on MHD, like *Engineering Aspects of Magnetohydrodynamics* [5] give an interesting and broad overview of much of the research that has been done in the field. This particular volume contains a section on "Flight Applications" that covers many of the possible uses of MHD with regards to aerospace, and a section on

"Power Conversion" that focused on the use of MHD for generating power (as is done in this particular study); however, the power generation covered in this text is generally terrestrial in nature. Angrist's *Direct Energy Conversion* [6] is the first text mentioned that explicitly derives a set of MHD equations similar to the ones used in the present model. In addition, this reference covers a great variety of aspects of MHD power generation including possible limitations that might arise. Refs. 7, 8, 9, and 10 were very instrumental in understanding the nature of MHD phenomena, its applications both in aerospace and elsewhere, and the derivation of related and useful equations. Finally, Hill and Peterson's *Mechanics and Thermodynamics of Propulsion* [11] provided the best reference for the present study. In this volume, the quasi-one-dimensional MHD equations are derived more explicitly than in any other text examined. Additionally, different cases of the application of these equations are investigated and discussed. While no single reference found covers the precise form of the equations used in the model developed in this thesis, this last reference provides a closely related treatment of the MHD configuration and was used extensively (see the derivation of the MHD equations presented in Appendix B).

2.2. EARLY MHD INVESTIGATIONS

Early work in aerospace applications utilizing MHD focus on showing that MHD is a valuable area of research for aerospace engineers and gas dynamicists, establishing methods for analysis, and showing the basic trends expected in flows with MHD. In their 1958 paper, "The Prospects for Magneto-Aerodynamics" [12], Resler and Sears examine the equations describing MHD flow, attempt to estimate the probable significance of magneto-aerodynamic effects, and characterize several different flows. They present examples of MHD induced drag and one and two dimensional channel flows. In their follow-up paper,

"Magneto-Gasdynamic Channel Flow" [13], they use a simplified quasi-one-dimensional approach to analyze constant-density and constant-area channel flow in the presence of MHD. In their analysis of constant-area flow, they show that eight distinct flow regions exist, four subsonic and four supersonic, depending on the magnetic and electric field strengths and the velocity of the flow. Though this work was simplistic compared to modern equivalents and no precise calculations were made, it established that MHD could have noticeable and positive effects in terms of aerospace engineering applications and spurred further research. In the same period, Jack Kerrebrock was investigating methods by which higher conductivity of flow gases could be maintained by the use of non-equilibrium ionization [14]. Kerrebrock concluded that non-equilibrium ionization is only feasible in a generator that produces a large Hall Effect, which (because of large electrical losses) is something to be avoided, especially in the type of generator investigated in this work. The research outlined above was performed in the late fifties and early sixties of the twentieth century but laid the ground work for much of the subsequent research into MHD, including this thesis.

2.3. MODERN MHD STUDIES

Modern aerospace MHD studies focus mainly on the specific applications of MHD to aerospace propulsion systems and particularly to the concept of the so-called "MHD Bypass Engine" in which an MHD generator and accelerator are linked such that energy is diverted around the engine's combustor. This concept is based on the somewhat obscure Soviet design known within the hypersonic community by the acronym "AJAX." AJAX is reviewed at a basic level in the paper, "An Electro-magnetic-chemical Hypersonic Propulsion System" [15], which explores the feasibility of the various components that are supposedly

integral to the Soviet AJAX, including an inverse cycle (MHD-based) engine whose stated purpose is to remove enough energy before the flow enters the combustor so that the flow would not transition to supersonic-though-flow in the combustor. The removed energy would then be delivered back into the flow via a MHD accelerator, located downstream of the combustor. The paper concludes that such a complicated system reduces entropy generation within the combustor and could provide tangible benefits in comparison to a traditional (hydrogen fueled) scramjet.

Park, Bogdanoff, and Mehta further examine the MHD bypass engine in a series of three papers published in 2001 and 2003 [16, 17, 18]. Their papers are based on the assumption that a critical velocity limit is imposed on the flow through a scramjet combustor because of limitations on the ability of the fuel and air to mix effectively within the combustor. Based on this assumption, they examine the difference between systems that achieve this velocity through inlet compression alone and inlet compression combined with MHD bypass. The first of these three papers examines a frictionless system and concludes that (if their assumed combustor entrance velocity restriction is valid) the MHD bypass engine outperforms the standard scramjet engine, especially at higher flight velocities. In the second of this series of papers, the authors examine the same MHD bypass concept with the addition of viscous effects, a three-dimensional inlet compression system, and equilibrium chemistry kinetics modeled throughout the length of the nozzle. Though acknowledging that the MHD bypass discussed in the paper is technologically infeasible due to the high magnetic fields needed (higher magnetic fields correspond to heavier magnets) and neglected electrical line losses between the generator and accelerator, the authors conclude that, with the assumption of a combustor entrance velocity limit, the MHD bypass engine outperforms the traditional

scramjet engine at flight speeds above 3000 meters per second (about Mach 10) The third paper referenced in this series introduces the concepts of nonequilibrium ionization by electrical discharge and/or ultraviolet irradiation. The authors hypothesize that this ionization will allow lower compression ratios, and therefore lower entropy increase, in the engine inlet. This concept is based on the fact that nonequilibrium ionization uses external power to ionize a flow whose temperature is not high enough to cause sufficient equilibrium ionization. The authors conclude in this third paper that the power cost of nonequilibrium ionization causes an engine employing this method to underperform non-MHD scramjets consistently, and always to underperform equilibrium ionized bypass engines as explored in the first and second of their three papers. Overall, from this series of works, it appears that the concept of the MHD bypass engine might offer some tangible benefits.

Reference 19 continues the investigation on the MHD bypass concept by limiting the maximum temperature allowed in the combustor and then comparing a traditional scramjet, a traditional MHD bypass concept as proposed in the AJAX model, and a third concept that incorporates the MHD generator into the combustor and the MHD accelerator into the nozzle. The authors of this work conclude that the traditional scramjet exceeds the maximum allowed combustion temperature and is therefore infeasible, while the traditional MHD bypass engine keeps the combustion temperature below the limiting value but impacts thrust too negatively to be feasible. However, they determine that the third (combusting MHD bypass) concept both satisfies the temperature limit and provides adequate thrust. However, they admit that the physics of combustion under such intense magnetic and electric fields has yet to be studied.

Riggins undertakes a detailed analysis of the MHD bypass engine and compares it to the traditional scramjet engine [20]. He states that even if only the losses resulting from the inverse cyclic nature of the engine are considered, the total pressure loss is significant enough to cast serious doubt on the viability of the concept. Further, he concludes that when all aspect of a MHD bypass engine are considered, such an engine produces lower specific impulse and specific thrust at a higher heat load (i.e. heat absorbed by cryogenic fuel or other coolant) than the traditional scramjet engine. However, he notes that there may still be promise in the use of an MHD generator alone to extract power from the flow to be used elsewhere in the overall vehicle system. This work raises serious concerns about the practicality of the MHD bypass engine.

The authors of "MHD Control in Hypersonic Aircraft" summarize three MHD topics they have studied perviously: the MHD bypass engine, a MHD controlled inlet, and MHD power generation [21]. For the MHD bypass engine they conclude that benefits can be relized using a nonequilibrium electron-beam ionization MHD generator at Mach numbers less than the design Mach number of the engine. The further the engine is operated off-design, the more benefit is produced by the MHD bypass system; at the design point the MHD bypass and the traditional scramjet converge in terms of performance. In relation to a MHD controlled inlet they conclude that using MHD to increase inlet mass capture or otherwise manipulate the flow at the inlet can increase the thrust produced by up to sixteen percent for some off-design cases. Finally, the authors briefly examine the use and positioning of an MHD generator for the purpose of power extraction. They conclude that for flight Mach numbers less than Mach 9, a generator placed upstream of the combustor has less negative or even a positive impact in terms of specific impulse as compared to a generator

placed downstream of the combustor. They also conclude that for Mach numbers greater than Mach 10, the post combustor MHD generator is superior. This paper provides the earliest reference found that mentions using a MHD generator to produce power that is not subsequently returned to the propulsive flow path.

Shneider and Macheret explore the uses of MHD and plasma physics for manipulating the flow around and in the inlet and isolator areas of a scramjet engine in order to maximize off design performance [22]. First, they examine the effects of using a nonequilibrium electron beam ionization MHD generator placed near the nose of the vehicle for restoring shock-on-lip conditions at Mach numbers in excess of flight design Mach number. This system is entirely self-contained, requiring no outside energy and can restore shock on lip with only a five-percent thrust loss. The authors postulate that this thrust penalty might be acceptable if it precludes the possibility of shocks reflecting into the combustor and "unstarting" the engine. Next, the paper investigates the use of energy "beamed" by electron beam or laser deposition to an area ahead of the vehicle's lower cowl's forward edge in order to eliminate "spillage" (i.e. lost mass flow caused by the vehicle bow shockwave missing the cowl) and restore full mass capture at Mach numbers below design. Without consideration of where the energy to create the "virtual cowl" will be obtained, they conclude that a ten-percent thrust gain can be achieved by use of such a "virtual cowl." Finally, the authors investigate the use of heat addition upstream of the combustor to eliminate the isolator component that is usually needed to buffer the combustor from the inlet at low flight Mach number in a scramjet engine. They report that a sixteen-percent thrust loss will accompany the elimination of the isolator by this method for Mach numbers significantly below design. They conclude that this thrust loss will likely be more than compensated by the weight

savings of not needing an isolator, especially at the design Mach number where the isolator serves no function. Finally, the authors postulate that an excellent source of power to create a virtual cowl or eliminate the isolator would be a post-combustor MHD generator, though they do not spend much time developing or examining the concept. The purpose of this thesis is to explore just the sort of generator they have proposed.

2.4 THE LATEST MHD WORK

All of the works covered in the previous subsections of this section were published before the present model was developed; however, the works discussed in this section were published after the work on the present model had commenced. In other words, these works were published while the data presented in this thesis was being compiled and organized, thus they reflect the very latest MHD work.

The work of Lee and Lu [23] returns to the MHD bypass engine, but in it, they consider the effects of MHD parameters such as load factor, magnetic field strength, and conductivity on the allowable MHD generator inlet Mach number. They constrain their analysis by placing an upward limit on combustor inlet static and total temperatures, limits on the amount of MHD interaction allowed in the generator, and self sustainability, i.e. the generator must produce enough electricity to maintain the non-equilibrium ionization used. These authors conclude that moving the load factor farther from unity, increasing the magnetic field strength, and/or increasing the conductivity all narrow the operating range of a given generator inlet Mach number; however, that same generator will have increased performance over the narrowed range. The paper titled, “Simulation of Supersonic MHD Channel Flow” [24] examines the modeling of MHD flow through a constant area duct using the Navier-Stokes equations. The authors examine four cases: 1) no MHD interaction, 2)

constant magnetic field interaction, 3) case 2 plus the effects of the induced magnetic field, and 4) case 3 plus the Baldwin-Lomax turbulence model. This work concludes that the analysis method used is feasible but that more work needs to be done to determine its validity.

Finally, Ref. 25 is unique in that it, like this thesis, analyzes a post-combustor MHD generator; however, the similarity ends with the generator positioning, as a three-dimensional analysis is performed and a diagonally conducting sidewall generator is used. The authors of this paper attempt to replicate numerically the experimental results of the Hypersonic Vehicle Electric Power System (HVEPS) program, which is descried in Refs. 26, 27, and 28, but not explicitly discussed in this thesis. Their analysis focuses on the production of a numerical model that will describe these results, and they do not assess the impact the generator has on the scramjet's ability to produce thrust. They conclude that the results of their analysis match the experimental results if the conductivity in the MHD generator is taken to be 81.3% of the value predicted by the HVEPS research team. They further conclude that the model does not describe the relatively large voltage loss near the anode and cathode nor the large electrical losses in the MHD entrance and exit regions. This last work is the most recent publication related to the subject of this thesis that was found. With its discussion complete, the literature review is concluded.

3. DESCRIPTION OF ENGINE GEOMETRY

The engine design used for this study is based on the waverider design and geometry used in NASA's X-43 project in which a scramjet-integrated air-breathing vehicle was flown at flight Mach numbers of 7 and 10 in 2004, breaking the previous air-breathing record of Mach 3.3 held by the SR-71. Figure 3.1 below is a schematic of the engine configuration used in the present study. The heavy black lines are the engine surfaces, the blue lines are the dimensioning lines, the red dashed lines are shockwaves, and the green dot-dashed line at the rear is the nozzle expansion plume.

H_I is the inlet height, which for this study is always one (1.0) meter. θ_T is the angle of the top of the waverider – the angle between the top of the engine and the horizontal – which is always one (1.0) degree; θ_T only affects the characteristics of the vehicle by its contribution in determining the expansion angle of the nozzle which will be described below.

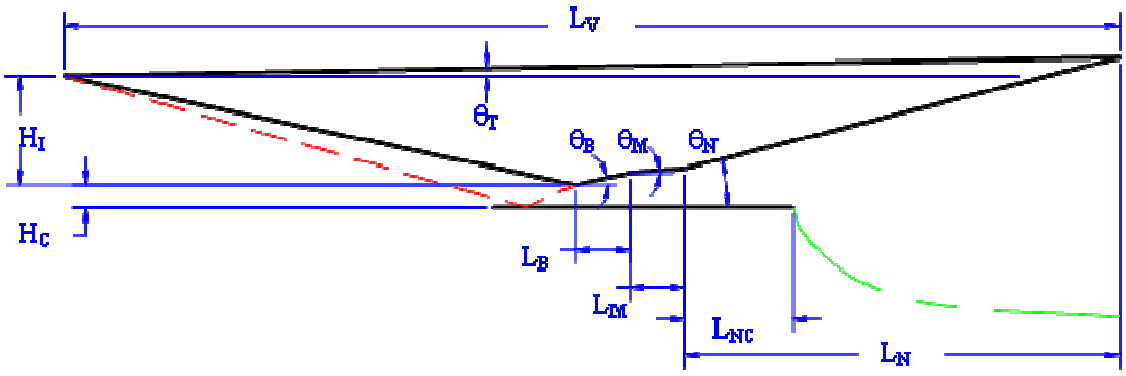

Figure 3.1: A schematic of the engine used in the study with symbolic dimensions shown.

θ_I, which is not dimensioned in Fig. 3.1, is the inlet compression angle – the angle between the lower surface of the inlet and the horizontal – which has the value of twelve (12.0) degrees throughout this study. The length of the inlet L_I, which is also not dimensioned above, can then be determined from two previous quantities as follows:

$$L_I = H_I \cdot \cot(\theta_I) \tag{3.1}$$

H_C is the cowl height, i.e. the distance between the lower surface of the engine (cowl) and the lowest point of the upper surface of the engine; this quantity is determined by the shock angles as given below in the description of the numerical model used in the inlet. L_B is the length of the combustor which is taken to be one-half (0.5) meter throughout this investigation, while θ_B is the combustor expansion angle, which is taken to be the smallest angle possible (rounded up to the nearest two-tenths of a degree) to prevent the engine from choking as described in the combustor description below. L_M is the length of the MHD generator which is constantly one-half (0.5) meter throughout this study. θ_M is the expansion angle of the MHD generator, which is one of the variables in the study. L_N is the length of the nozzle, which is held at four (4.0) meters, while L_{NC} is the length of the closed portion of the nozzle, i.e. the portion for whose length the cowl extends, which is taken to be twenty-five percent (25.0%) of L_N, i.e. one (1.0) meter. L_V is the overall engine length (also the vehicle length) which is the sum of all the component lengths:

$$L_V = L_I + L_B + L_M + L_N \tag{3.2}$$

θ_N is the expansion angle of the nozzle which is ultimately determined by the rest of the geometry of the vehicle described above according to the following equation:

$$\theta_N = \arctan\left[\frac{\left(H_I + L_V \cdot \tan\theta_T\right) - \left(L_B \cdot \tan\theta_B + L_M \cdot \tan\theta_M\right)}{L_N}\right] \tag{3.3}$$

4. DESCRIPTION OF NUMERICAL MODEL

Throughout the model, mass, momentum, energy, entropy and state equations must constantly be satisfied. These equations are derived as needed in different forms for each section of the engine from the basic equations given below:

MASS $$\dot{m} = \rho_1 u_1 A_1 = \rho_2 u_2 A_2 = constant \tag{4.1}$$

MOMENTUM $$P_1 A_1 + \rho_1 U_1^{\,2} A_1 + \int_{A_1}^{A_2} P dA + F_v = P_2 A_2 + \rho_2 U_2^{\,2} A_2 \tag{4.2}$$

ENERGY $$h_{t1} + {}_1q_2 - {}_1w_2 = h_{t2} \tag{4.3}$$

where $$h_t = h + \frac{u^2}{2} = C_p T + \frac{u^2}{2} = C_p T_t \tag{4.3b}$$

ENTROPY $${}_1s_{t2} = {}_1s_2 = \int_{h_1}^{h_2} \frac{dh}{T} - R \cdot \ln\left(\frac{P_2}{P_1}\right) \tag{4.4}$$

STATE $$P = \rho RT \tag{4.5}$$

In Eq. 4.2, F_v is the force exerted by friction on the walls. In all sections of the engine except the combustor, it is assumed that chemistry is frozen, i.e. no chemical reaction occurs; therefore, the specific heats in these sections are functions of temperature only. Also following from the above assumption, in the combustor, the specific heats are functions of both the chemical composition of the flow and its temperature. The equations for the temperature variation of the specific heats have the following form:

$$\overline{C}_p = \left(a_1 + a_2 T + a_3 T^2 + a_4 T^3 + a_5 T^4\right)\overline{R} \tag{4.6}$$

The coefficients $a_1 - a_5$ have the values given in Tables 4.1 and 4.2 depending on the temperature of the fluid [29]. For low temperatures from 200K – 1000K, the coefficients from Table 4.1 are used; for higher temperatures from 1000K – 6000K, the coefficients from Table

4.2 are used. The overall specific heat of the mixture $\overline{C}_{p,mix}$ can then be found by using the specific heats of each species $\overline{C}_{p,i}$ and that specie's mole fraction in the mixture Y_i:

$$\overline{C}_{p,mix} = Y_{N_2}\overline{C}_{p,N_2} + Y_{O_2}\overline{C}_{p,O_2} + Y_{H_2}\overline{C}_{p,H_2} + Y_{H_2O}\overline{C}_{p,H_2O} \tag{4.7}$$

Thus, the value for the ratio of specific heats γ can be found, by definition:

$$\gamma = \frac{\overline{C}_{p,mix}}{\overline{C}_{p,mix} - \overline{R}} \tag{4.8}$$

With the fluid and thermo-chemical assumptions that are used throughout the model given, the focus in the following sections will be on detailed descriptions of modeling in the individual components of the engine.

Table 4.1: Coefficients for Eq. 4.6 for 200K $\leq T \leq$ 1000K.

	a_1	a_2	a_3	a_4	a_5
N_2	3.53100528E+00	-1.23660987E-04	-5.02999437E-07	2.43530612E-09	-1.40881235E-12
O_2	3.78245636E+00	-2.99673415E-03	9.84730200E-06	-9.68129508E-09	3.24372836E-12
H_2	2.34433112E+00	7.98052075E-03	-1.94781510E-05	2.01572094E-08	-7.37611761E-12
H_2O	4.19864056E+00	-2.03643410E-03	6.52040211E-06	-5.48797062E-09	1.77197817E-12

Table 4.2: Coefficients for Eq. 4.6 for 1000K $\leq$ T $\leq$ 6000K.

	a_1	a_2	a_3	a_4	a_5
N_2	2.95257626E+00	1.39690057E-03	-4.92631691E-07	7.86010367E-11	-4.60755321E-15
O_2	3.66096083E+00	6.56365523E-04	-1.41149485E-07	2.05797658E-11	-1.29913225E-15
H_2	2.93286579E+00	8.26607967E-04	-1.46402335E-07	1.54100359E-11	-6.88804432E-16
H_2O	2.67703787E+00	2.97318329E-03	-7.73769690E-07	9.44336689E-11	-4.26900959E-15

4.1. AMBIENT CONDITIONS

The first part of the model that must be established is the method by which the ambient conditions at which the engine operates are described. Although the model can accommodate any combination of initial conditions, a guideline for maintaining the dynamic pressure of the air entering the engine was chosen. This criterion helps limit variance in engine mass flow rates, in lift produced on any vehicle housing the engine, and in heat transfer both within the engine and outside it. The present work is based on a constant dynamic pressure, q_0, of one atmosphere (101,325 Pa) for defining the ambient conditions at which the vehicle operates. Dynamic pressure is defined as follows:

$$q_0 = \tfrac{1}{2}\rho_0 u_0^{\,2} = \tfrac{1}{2}\gamma_0 P_0 M_0^{\,2} \tag{4.1.1}$$

With the dynamic pressure and Mach number known (and assuming a value of 1.4 for gamma) the pressure can be backed out of the second of the relations in Eq. 4.2. The pressure then can be used with a table of the Standard Atmosphere to find a corresponding altitude which can in turn be used to find the atmospheric temperature at that altitude. The Standard Atmosphere is first defined by a temperature profile as shown in Figure 4.2. This profile is composed of three isothermal layers (the vertical lines) and four gradient layers (the diagonal lines). This temperature profile is then used to calculate the pressure profile by using the hydrostatic equation:

$$dP = -\rho g_0 dh \tag{4.1.2}$$

For the isothermal regions, this becomes:

$$P = P_1 \cdot e^{-\left[g_0 / (RT)\right](h-h_1)} \tag{4.1.3}$$

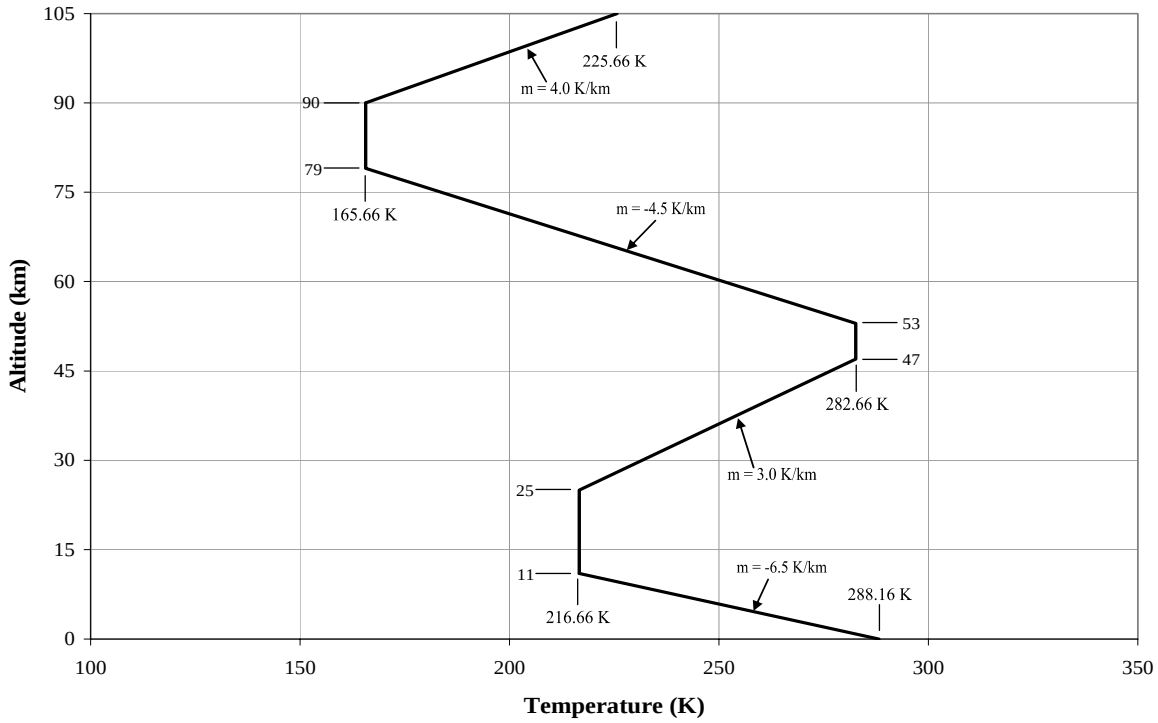

Figure 4.1: The Standard Atmosphere temperature profile.

In the above equation, P_1 and h_1 are the pressure and geopotential altitude, respectively, at the start of the isothermal region. Similarly, for the gradient regions the hydrostatic equation becomes:

$$P = P_1 \cdot \left(T / T_1 \right)^{-\left\{ \left[g_0 / (mR) \right] + 1 \right\}} \tag{4.1.4}$$

Here, P_1 and T_1 are the pressure and temperature, respectively, at the start of the gradient region. After the pressure variation is found, the density is easily calculated from the state equation (4.1). It should be noted that the values of the Standard Atmosphere calculated differ slightly from that of the *1976 Standard Atmosphere* [30] most commonly referenced because the present model assumes air to be 79% N_2 and 21% O_2, which leads to a slightly

different value for the molecular weight of air and thereby a slightly different value for the gas constant, *R*.

4.2. INLET DESCRIPTION

The inlet component in a scramjet is used to slow and compress the freestream flow to allow for more efficient combustor operation. When the supersonic flow encounters the inlet an oblique shock is formed. Since, in the model used, specific heats are a function of temperature, both the shock angle and the resulting properties behind the shock must be found iteratively. First, the mass equation (4.1) is used, assuming a constant area, to define a value on which to iterate. For a normal shockwave, this mass relation is:

$$\rho_1 u_1 = \rho_2 u_2 \tag{4.2.1}$$

However, when dealing with oblique shocks, the component of velocity normal to the shock must be used in place of the flow velocity in all normal shock equations, so Eq. 4.2.1 becomes:

$$\rho_1 u_{1N} = \rho_2 u_{2N} \tag{4.2.2}$$

With rearrangement of Eq. 4.2.2, the iteration parameter, δ, can be defined:

$$\delta = \frac{\rho_1}{\rho_2} = \frac{u_{2N}}{u_{1N}} = \frac{\tan(\beta - \theta)}{\tan(\beta)} \tag{4.2.3}$$

The last of the relations in Eq. 4.2.3 follows from the geometry of the velocities before and after the shock with angle β and the fact that when dealing with oblique shocks:

$$u_{1T} = u_{2T} \tag{4.2.4}$$

To begin the process of finding a solution, a value is "guessed" for δ; in this case an initial guess of 0.1 is used. Then, a reasonable range of possible shock angles β is chosen.

The minimum angle is selected to be equal to the inlet compression angle θ since as Mach number approaches infinity, shock angle approaches the compression angle. The maximum angle is determined by considering the range of Mach numbers and compression angles for which the model will be used. For example, if the minimum Mach number is eight (8.0) and the maximum compression angle is twenty (20.0) degrees, a maximum shock angle of at least thirty (30.0) degrees must be used. With δ and θ known, the last relation from Eq. 4.2.3 can be iterated to find the shock angle, β. Next, u_{1N} can be found from the following geometrical relation:

$$u_{1N} = u_1 \cdot \sin(\beta) \tag{4.2.5}$$

Then, the pressure aft the shock can be found via the momentum equation (4.2), with the integral term being zero:

$$P_2 = P_1 + \rho_1 {u_{1N}}^2 - \rho_2 {u_{2N}}^2 = P_1 + \rho_1 u_{1N}\left(1 - \frac{\rho_1}{\rho_2}\right) = P_1 + \rho_1 u_{1N}(1-\delta) \tag{4.2.6}$$

At the same time, the energy equation (4.3), with no heat or work addition, is used to find the enthalpy behind the shock:

$$h_2 = C_{p2}T_2 = C_{p1}T_1 + \frac{1}{2}\left({u_{1N}}^2 - {u_{2N}}^2\right) = C_{p1}T_1 + \frac{1}{2}{u_{1N}}^2\left(1-\delta^2\right) \tag{4.2.7}$$

At this point, a temperature, T_2, and the specific heat, C_{p2}, aft the shock must be found iteratively, so a value for T_2 is assumed. In this case, the smallest value T_2 could be, T_1, is chosen. This guessed temperature value is then used to calculate C_{p2} from the specific heat functions. Then, the calculated C_{p2} and h_2 from Eq. 4.2.7 are used to arrive at a new value for T_2. This new value of T_2 is then used to repeat the process until the values of T_2 at the beginning and end of the iteration match within a very small margin of error. Next, the equation of state (4.5) is used to calculate the density behind the shock:

$$\rho_2 = \frac{P_2}{RT_2} \tag{4.2.8}$$

The density calculated in Eq. 4.2.8 is then used in the first relation in Eq. 4.2.3 to arrive at a new value for δ. The new value of δ is then used to repeat the entire process until the starting and ending δ's match to within a very small margin of error. After the iterative process is completed, all of the properties behind the first shock can be easily calculated, including the velocity behind the shock which is:

$$u_2 = \frac{u_{2N}}{\sin(\beta - \theta)} \tag{4.2.9}$$

At this point, the properties behind the second, reflected, shock can be found using the exact same method as outlined above. Please note that the entropy equation (4.4) is not used because the system is frictionless, thus it has a constant value for entropy before the shock and a different (larger) constant value for entropy after the shock. As noted in the previous section, with the two shock wave angles found, the height of the cowl H_C can be found by the following equation:

$$H_C = \frac{L_I - H_I \cot(\beta_1)}{\cot(\beta_1) + \cot(\beta_2 - \theta_I)} \tag{4.2.10}$$

With the cowl height known, the total area of the inlet can be calculated:

$$A_{in} = (H_I + H_C)W \tag{4.2.11}$$

Thus, the mass flow rate of air through the engine can also be calculated:

$$\dot{m}_{air} = \rho_0 U_0 A_{in} \tag{4.2.12}$$

The force generated is calculated for each engine component and then summed when the entire engine analysis is complete to find the total thrust generated by the engine. The force generated in the inlet is found by the following equation:

$$F_I = \dot{m}_{air}\left(U_{out} - U_0\right) + P_{out}A_{out} - P_0 A_{in} \tag{4.2.13}$$

The quantities with the subscript "out" refer to the values at the end of the inlet. Once these calculations are complete, the flow moves into the combustor.

4.3. COMBUSTOR DESCRIPTION

As soon as the flow enters the combustor, it is assumed that the fuel is instantly and completely mixed with the compressed air stream. It is also assumed this process occurs adiabatically, with the new properties of the mixed stream calculated from Eqs. 4.1, 4.2, 4.3, and 4.5 in their original form. It is further assumed that the fuel enters parallel to the airflow with a given Mach number and pressure, $M_f = 2.0$ and $P_f = 2\ ATM$. The fuel also has a temperature T_f determined by thermal balancing requirements as described in Section 4.5, below. The amount of fuel added to the flow depends on the amount of air entering the engine:

$$\dot{m}_f = f_{ST} \cdot \dot{m}_{air} \tag{4.3.1}$$

The stoichiometric fuel to air ratio f_{ST} for hydrogen fuel is 0.02913 kilograms of fuel per kilogram of air. The total mass flow through the combustor and the subsequent components is simply the sum of the air and fuel mass flow rates:

$$\dot{m}_T = \dot{m}_{air} + \dot{m}_f \tag{4.3.2}$$

Following from mass conservation, the area of the duct must increase when the fuel is added as follows:

$$A_f = \frac{\dot{m}_f}{\rho_f U_f} \tag{4.3.3}$$

This area is added to the area of the duct before fuel addition to get the area after fuel addition:

$$A_2 = A_1 + A_f \tag{4.3.4}$$

Though the fuel addition and mixing process is adiabatic, force is still generated in the flow which is given by the following equation:

$$F_{mix} = \dot{m}_T U_2 - \dot{m}_{air} U_1 + P_2 A_2 - P_1 A_1 \tag{4.3.5}$$

The properties subscripted with 2 are those after the fuel and air is mixed while those subscripted 1 are those of the air before it has mixed.

After this mixing occurs, the flow is allowed to combust and evolve though the combustor. This evolution is governed by the quasi-one-dimensional flow equations which are derived from Eqs. 4.1 – 4.5. In differential form these equations become:

MASS $$0 = \frac{d\rho}{\rho} + \frac{du}{u} + \frac{dA}{A} \tag{4.3.6}$$

MOMENTUM $$\frac{dP}{\rho} + udu = dq - Tds \tag{4.3.7}$$

ENERGY $$dh_t = dh + udu = C_p dT + TdC_p + udu = C_p dT_t + T_t dC_p = dq \tag{4.3.8}$$

ENTROPY $$ds_t = ds = \frac{dh}{T} - R\frac{dP}{P} = \frac{dq + df_c}{T} \tag{4.3.9}$$

STATE $$\frac{dP}{P} = \frac{d\rho}{\rho} + \frac{dR}{R} + \frac{dT}{T} \tag{4.3.10}$$

The heat exchange, *dq*, is actually the sum of two sources of heat addition and loss. First, the heat addition from the combustion of the fuel is calculated:

$$dq_{combustion} = q_{combustion} \cdot d\eta_{burn} \tag{4.3.11}$$

In Eq. 4.3.11, $q_{combustion}$, is the total possible heat generated by the stoichiometric combustion of hydrogen with air, which is found as follows:

$$q_{combustion} = h_v \cdot \frac{f_{ST}}{1 + f_{ST}} \tag{4.3.12}$$

where h_v is the heating value of the fuel; for hydrogen, $h_v = 1.3 \times 10^8$ J/kg. and f_{ST} is the stoichiometric fuel to air ratio; $f_{ST} = 0.02913$ kg_f/kg_a for the combustion of hydrogen and air. The $q_{combustion}$ calculated above is an external heat addition when, in actuality, the energy addition from combustion is a combination of the change in static enthalpy Δh resulting from a difference in temperature and molecular weight of the fluid and a change in heat of formation Δh_f^o from the difference in composition. The *dCp* term described below accounts for Δh but does not account for Δh_f^o, which is what $q_{combustion}$ truly represents, for simplicity:

$$q_{combustion} \cong \Delta h_f^o \tag{4.3.13}$$

The burning efficiency, η_{burn}, is a model used to determine the rate at which combustion occurs throughout the combustor:

$$\eta_{burn}(x) = 1 - e^{-\alpha \frac{x}{u_B \cdot \tau}} \tag{4.3.14}$$

α is a fit coefficient whose value is calculated according to a condition provided by the researcher. τ is the chemical time for the reaction, in this case $\tau = 1 \times 10^{-3}$ seconds. And u_B is the velocity of the flow as it enters the combustor, which varies with the free stream conditions and configuration of the engine. Because the combustor results proved to be extremely sensitive to the amount of heat added by combustion at each step, it was decided to have two conditions to determine the step size. At the beginning of the combustor, a constant

$d\eta_{burn} = 1\times10^{-4}$ step size is used. The η_{burn} at each step is then found by adding the $d\eta_{burn}$ to the value from the previous step:

$$\eta_{burn,step} = \eta_{burn,previous} + d\eta_{burn} \tag{4.3.15}$$

This value is then used in Eq. 4.3.14 to back-out the value for the spatial location in the combustor, x_{step}:

$$x_{step} = -\frac{u_B \cdot \tau}{\alpha}\ln\left(1-\eta_{burn,step}\right) \tag{4.3.16}$$

Finally, the spatial length of the step is found by subtracting the *x*-value at the previous step from the current *x*-value:

$$dx = x_{step} - x_{previous} \tag{4.3.17}$$

When $dx > 1\times10^{-4}$, the step size is switched to the second condition $dx = 1\times10^{-4}$, $d\eta_{burn}$ is then found as follows:

$$x_{step} = x_{previous} + dx \tag{4.3.18}$$

$$\eta_{burn,step} = 1 - e^{-\alpha\frac{x_{step}}{u_B\cdot\tau}} \tag{4.3.19}$$

$$d\eta_{burn} = \eta_{burn,step} - \eta_{burn,previous} \tag{4.3.20}$$

With a systematic approach to determining the step sizes found, the description of the remaining combustor model can be given.

The next component of the heat exchange *dq* is the heat loss to the walls of the combustor. Using the heat-transfer coefficient h_c and its definition results in:

$$\dot{m}\cdot dq_{wall} = h_c\left(T_w - T_t\right)c\cdot dx \tag{4.3.21}$$

T_w in the above equation is the wall temperature. In the combustor model, T_w is given a value of 1000 K. Next the Stanton number N_{St} is introduced as defined by:

$$N_{St} = \frac{h_c A}{\dot{m} C_p} \approx \frac{C_f}{2} \tag{4.3.22}$$

The second part of Eq. 4.3.19 is called the "Reynolds analogy," which relates N_{St} and the skin friction coefficient C_f and holds over a wide range of flow conditions. With these introductions, Eq. 4.3.18 becomes:

$$dq_{wall} = \frac{C_f}{2} C_p \left(T_w - T_t\right) \frac{c}{A} dx \tag{4.3.23}$$

Finally, a "relaxation coefficient" τ_R is introduced to account for velocity slip at the walls, a condition which exists in very high velocity combustors, in which the velocity at the walls of the combustor does not actually reach zero. For the present study, a value of 0.9 is used for τ_R. With the relaxation coefficient added Eq. 4.3.23 finally reaches the form used in the present model:

$$dq_{wall} = \frac{C_f}{2} C_p \left(T_w - \tau_R T_t\right) \frac{c}{A} dx \tag{4.3.24}$$

It should be noted that, Eq. 4.3.24 is intended to calculate heat loss to the combustor walls so the value should always be negative; however, if $T_w > \tau_R T_t$, the value would be positive, representing a heat addition to the flow from the walls. Since this condition would not physically occur in a real aircraft combustor, when $T_w > \tau_R T_t$, dq_{wall} is assumed to be zero. Thus the original dq found in Eqs. 4.3.7 – 4.3.9 can be written as the sum of these two components:

$$dq = dq_{combustion} + dq_{wall} \tag{4.3.25}$$

The effect of friction within the combustor is accounted for through the df_c term in Eq. 4.3.9:

$$df_c = \frac{u^2}{2} C_f \frac{c}{A} dx \tag{4.3.26}$$

As noted earlier, C_f is the skin friction coefficient, which is assumed to have a value of $C_f = 0.007$ in the combustor. The value is so high to account for the intrusive nature of the injection and mixing systems.

As explained previously, chemistry is not frozen in the combustor because, of course, combustion is occurring. It was also noted that it is assumed that at each step combustion of a fraction of the fuel-air mixture occurs as determined by the value of $d\eta_{burn}$ at that step. The balanced equation for the complete combustion of the fraction of hydrogen that combusts with air at each step is given as follows:

$$d\eta_{burn}\left[H_2 + \tfrac{1}{2}\left(O_2 + 3.762N_2\right)\right] \Rightarrow d\eta_{burn}\left(H_2O + 1.881N_2\right) \tag{4.3.27}$$

Thus at the end of each step, the gas mixture has a composition given by:

$$\left[1-\eta_{burn}\left(x_{step}\right)\right]H_2 + \tfrac{1}{2}\left[1-\eta_{burn}\left(x_{step}\right)\right]O_2 + \eta_{burn}\left(x_{step}\right)H_2O + 1.881N_2 \tag{4.3.28}$$

This composition can then be used to calculate the molecular weight of the gas mixture at the end of the step:

$$Mw_{mix,step} = Y_{N_2} Mw_{N_2} + Y_{O_2} Mw_{O_2} + Y_{H_2} Mw_{H_2} + Y_{H_2O} Mw_{H_2O} \tag{4.3.29}$$

In turn the molecular weight can be used to calculate the value of the mass-based gas constant at the end of the step:

$$R_{step} = \frac{\overline{R}}{Mw_{mix,step}} \tag{4.3.30}$$

The change in the gas constant term which appears in the state equation can then be calculated by simply finding the difference between the gas constants at the beginning and end of the step:

$$dR = R_{step} - R_{previous} \tag{4.3.31}$$

Finding the change in the specific heat term that appears in the energy equation 4.3.8 proves to be more complicated as it is a result of both change in the chemistry of the flow and its temperature. Because the specific heat at the end of the step $C_{p,step}$ is a function of the temperature at the end of the step, which is in turn a result of the evaluation of the quasi-one-dimensional equations, this quantity must be found iteratively.

To start the iterative process, it is assumed that the specific heat does not change across the step, i.e. dC_p equals zero. With this assumption, the quasi-one-dimensional flow equations 4.3.6– 4.3.10 can be utilized. First, the energy equation 4.3.8 can be solved to find the total temperature change dT_t. Next, the entropy change ds can be calculated from Eq.4.3.9. Then, the mass, momentum, energy, and state equations can all be combined to form the following equation to calculate the change in velocity du:

$$\frac{du}{u} = \frac{\frac{dq-\gamma Tds+\gamma TdC_p-TdC_p}{\gamma RT} + \frac{dA}{A} - \frac{dR}{R}}{M^2 - 1} \tag{4.3.32}$$

With the velocity change found, the pressure dP change can be found simply from the momentum equation 4.3.7. These few property changes provide everything needed to calculate all the properties at the end of the step, including the temperature T_{step}. This temperature can then be used in Eq.4.6 with coefficients from either Table 4.1 or 4.2, depending on the value of T_{step}, to find the specific heat of each individual species. Next, a new value of the specific heat $C_{p,step}$ and the ratio of specific heats γ_{step} of the overall mixture at the end of the step can be found via Eq. 4.7 and 4.8. The change in specific heat across the step dC_p found in Eq. 4.3.8 can then be calculated:

$$dC_p = C_{p,step} - C_{p,previous} \tag{4.3.33}$$

This new value for dC_p can then be used to start a new iteration of the quasi-one-dimensional equations. Iterations continue in this fashion until the percentage difference between the $C_{p,step}$ calculated at the end of the iteration and that used at the start is within a small margin of error and the process is considered complete. In fact by completing this process, the quasi-one-dimensional equations have also been solved and the entire process may begin again with the next step. It should be noted that most models the researcher has seen omit the dC_p term from the energy equation; however, the inclusion of the term is mathematically correct and was seen by the researcher to have a noticeable impact on the results. It should also be noted that if at any point in the combustor the flow Mach number drops below 1.1, the flow is considered choked, and the combustor expansion angle is increased by 0.2 degrees.

Finally, the force generated in the combustor can be found as follows:

$$F_B = \dot{m}_T \left(U_{out} - U_{in}\right) + P_{out} A_{out} - P_{in} A_{in} \tag{4.3.34}$$

It should be noted that the "in" conditions are those of flow after the fuel-air mixing has occurred while the "out" conditions are those at the end of the combustor. With these calculations complete, the flow continues to the MHD generator.

4.4. MHD GENERATOR DESCRIPTION

After the combustor analysis is complete, signaling that the flow has exited the combustor, the flow immediately enters the magnetohydrodynamic generator. While the quasi-one-dimensional equations in the MHD generator are similar to those in the combustor, there are minor differences that necessitate the display of the equations again:

MASS
$$0 = \frac{d\rho}{\rho} + \frac{du}{u} + \frac{dA}{A} \tag{4.4.1}$$

MOMENTUM $$\frac{dP}{\rho} + udu = dq - Tds \tag{4.4.2}$$

ENERGY $$dh_t = dh + udu = C_p dT + TdC_p + udu = C_p dT_t + T_t dC_p = dq \tag{4.4.3}$$

ENTROPY $$ds_t = ds = \frac{dh}{T} - R\frac{dP}{P} = \frac{dq - dw_{EM} + df_c}{T} \tag{4.4.4}$$

STATE $$\frac{dP}{P} = \frac{d\rho}{\rho} + \frac{dT}{T} \tag{4.4.5}$$

One difference occurs in the entropy equation 4.3.9 with the inclusion of the dw_{EM} term which will be discussed further in this section, while the other difference is in the state equation 4.3.10 where the dR term has been dropped. First, the dq term is again the sum of two terms. There is the heat loss dq_{wall} to the wall as was discussed in the combustor:

$$dq_{wall} = \frac{C_f}{2} C_p \left(T_w - \tau_R T_t\right) \frac{c}{A} dx \tag{4.4.6}$$

In the MHD generator, T_w is 800 K, C_f is 0.001, and τ_R is 0.9, as in the combustor. The wall temperature T_w is lower in the MHD generator because the electrodes must be kept at a lower temperature than the combustor walls in order to function effectively, while C_f is less because there are no major obtrusions for which to account in the MHD generator. The other component of the heat addition dq is the heat generated through the electromagnetic interactions of the MHD generator itself (as derived in Appendix B):

$$dq_{EM} = \frac{\sigma u B^2 \left(\frac{1}{\eta_{MHD}^2} - \frac{1}{\eta_{MHD}}\right)}{\rho} dx \tag{4.4.7}$$

It should be noted that the above dq_{EM} is in fact the total energy generation from the electromagnetic forces, i.e. heat and work, which accounts for why the work term dw_{EM} appears in the entropy equation 4.4.4 above. Thus, in the MHD generator:

$$dq = dq_{EM} + dq_{wall} \tag{4.4.8}$$

There is an additional term in the MHD generator that represents the portion of dq_{EM} that can effectively be used for electrical power (as derived in Appendix B):

$$dw_{EM} = \frac{\sigma u B^2 \left(\frac{1}{\eta_{MHD}} - 1\right)}{\rho} dx \tag{4.4.9}$$

It should be noted that both electromagnetic terms assume the degradation due to the Hall Effect to be negligible, a reasonable assumption for such a high velocity flow since the high velocity shortens the time between collisions. The friction on the walls is calculated exactly as it was in the combustor:

$$df_c = \frac{u^2}{2} C_f \frac{c}{A} dx \tag{4.4.10}$$

The only change is the value of the skin friction coefficient C_f, which is equal to 0.001 for the reason stated previously. In the MHD generator, the change in the specific heat C_p is function of only the temperature of the flow as discussed in introduction to the model section, and the dC_p term is calculated as it was in the combustor, though an iterative process that also solves the quasi-one-dimensional equations.

At this point the quasi-one-dimensional equations have been solved, the property changes calculated at each step, and the MHD generator can be fully evaluated. After this evaluation has been completed, the force generated in the MHD generator can be calculated as follows:

$$F_M = \dot{m}_T \left(U_{out} - U_{in}\right) + P_{out} A_{out} - P_{in} A_{in} \tag{4.4.11}$$

Here the “in” and “out” quantities refer to the flow entering and exiting the MHD generator, respectively. After the flow is modeled through the MHD generator, the thermal balance of the engine must be considered.

4.5. THERMAL BALANCING

The heat lost to the walls in the combustor and MHD generator does not simply disappear. To address this issue, it is assumed that the hydrogen fuel is used not only as a source of chemical power to the engine, but also as a coolant for the walls of the combustor and MHD generator. Since the MHD generator's walls are maintained at a lower temperature, the hydrogen is first routed to those walls. The heat lost to the MHD generator's walls can be found as a sum of the differential heat lost at each step:

$$q_{wall.M} = \sum_{MHD}^{steps} dq_{wall} \tag{4.5.1}$$

This heat loss, though, is specific (per unit mass); thus in order to convert it into a usable quantity, it is multiplied by the mass flow rate through the MHD generator to find the energy per unit time lost to the walls:

$$\dot{Q}_{wall,M} = \dot{m}_T q_{wall,M} \tag{4.5.2}$$

A sufficient quantity of hydrogen must be circulated to absorb energy at this rate:

$$\dot{Q}_{abs,M} = \dot{Q}_{wall,M} \tag{4.5.3}$$

To match these two rates, one of two quantities can be varied, either the temperature of the hydrogen when it completes its cooling of the MHD generator or the flow rate of the hydrogen if the hydrogen reaches the wall temperature of the MHD generator. To figure which of these two quantities is varied, first the maximum rate of heat absorption by the hydrogen needed for combustion is calculated:

$$\dot{Q}_{abs,M.\max} = \dot{m}_f C_{p_f} \left(T_{w,M} - T_{f,i} \right) \tag{4.5.4}$$

The fuel mass flow rate referenced above is that calculated for the stoichiometric combustion of hydrogen with air referenced in the combustor section. If $\dot{Q}_{wall,M} > \dot{Q}_{abs,M,\max}$ then the fluid

will reach its maximum temperature of $T_{w,M}$ and the mass flow rate of fuel must be higher than that required for combustion:

$$T_{f,M} = T_{w,M} \tag{4.5.5}$$

$$\dot{m}_{f,M} = \frac{\dot{Q}_{wall,M}}{C_{p_f}\left(T_{f,M} - T_{f,i}\right)} \tag{4.5.6}$$

On the other hand, if $\dot{Q}_{wall,M} < \dot{Q}_{abs,M,\max}$ then the mass flow rate of fuel to the combustor $\dot{m}_f$ is used and the temperature which the hydrogen reaches must be calculated:

$$\dot{m}_{f,M} = \dot{m}_f \tag{4.5.7}$$

$$T_{f,M} = \frac{\dot{Q}_{wall,M}}{\dot{m}_{f,M} C_{p_f}} + T_{f,i} \tag{4.5.8}$$

After the MHD generator has been thermally balanced by the above method, the combustor is balanced similarly. The heat lost to the walls of the combustor is as follows:

$$\dot{Q}_{abs,\mathbf{B}} = \dot{Q}_{wall,B} = \dot{m}_T \sum_{Comb}^{steps} dq_{wall} \tag{4.5.9}$$

The maximum heat that can be absorbed by the hydrogen passing these walls is then calculated:

$$\dot{Q}_{abs,B.\max} = \dot{m}_{f,M} C_{p_f}\left(T_{w,B} - T_{f,M}\right) \tag{4.5.10}$$

If $\dot{Q}_{wall,B} > \dot{Q}_{abs,B,\max}$ then:

$$T_{f,B} = T_{w,B} \tag{4.5.11}$$

$$\dot{m}_{f,B} = \frac{\dot{Q}_{wall,B}}{C_{p_f}\left(T_{f,B} - T_{f,M}\right)} \tag{4.5.12}$$

Whereas, if $\dot{Q}_{wall,B} < \dot{Q}_{abs,B,\max}$ then:

$$\dot{m}_{f,B} = \dot{m}_{f,M} \tag{4.5.13}$$

$$T_{f,B} = \frac{\dot{Q}_{wall,B}}{\dot{m}_{f,M} C_{p_f}} + T_{f,i} \tag{4.5.14}$$

The temperature of the fuel as it finishes its cooling of the combustor $T_{f,B}$ is the temperature at which it enters the engine when the fuel and air are mixed as was described at the beginning of the combustor model. Since the temperature of the fuel effects the temperature of the flow through the combustor which in turn effects how much heat is lost to the walls, it is necessary that the entire combustor and MHD generator sections are within a loop that iterates until a true thermal balance is found. Though this task might sound daunting, a solution is quickly reached with this process taking no more than five iterations for any of the cases run. If it is found that additional fuel was needed to cool the vehicle, $\dot{m}_{f,B} > \dot{m}_f$, it is assumed that either this additional fuel is somehow itself cooled and the excess fuel remains on board the vehicle to be used, or it is released to the atmosphere in such a way that it does not impact the thrust generated by the engine. In the results section, specific impulse is given for both of these assumptions. Now that the engine has been thermally balanced, all that remains is the discussion of the modeling required in the nozzle.

4.6. NOZZLE DESCRIPTION

In the nozzle, the quasi-one-dimensional equations become more simplified than they are in the other components of the engine. It is assumed that there is no heat interaction in the nozzle, i.e. no heat loss to the walls. This assumption is valid if it is assumed that the nozzle is constructed of a material that can withstand the highest temperatures encountered, at the nozzle entrance. With this assumption, the quasi-one-dimensional flow equations have the following form:

MASS $$0 = \frac{d\rho}{\rho} + \frac{du}{u} + \frac{dA}{A} \tag{4.6.1}$$

MOMENTUM $$\frac{dP}{\rho} + udu = -Tds \tag{4.6.2}$$

ENERGY $$dh_t = dh + udu = C_p dT + TdC_p + udu = C_p dT_t + T_t dC_p = 0 \tag{4.6.3}$$

ENTROPY $$ds_t = ds = \frac{dh}{T} - R\frac{dP}{P} = \frac{df_c}{T} \tag{4.6.4}$$

STATE $$\frac{dP}{P} = \frac{d\rho}{\rho} + \frac{dT}{T} \tag{4.6.5}$$

The nozzle is divided into two separate sections: a closed section, which is merely an expanding area duct, and an open section, in which the flow is able to expand both against the engine's top surface and downward into the atmosphere. The model allows the possibility that as little as twenty-five percent (25%) and as much as one-hundred percent (100%) of the nozzle is closed. For the purposes of this study, the minimum of one-fourth (25%) of the nozzle being closed was used. It is necessary to have this minimum amount closed because, if the flow were allowed to expand into the atmosphere immediately after exiting the MHD generator, the expansion would be so abrupt that first, it would be very difficult to calculate and second, much of the thrust would be lost because of unrestrained plume expansion into the atmosphere. However, it is desirable to have as little of the nozzle closed as possible since this both reduces the friction the nozzle creates on the flow and the weight of the engine itself as less material is required to contain the flow. In the following sections, the model for each section of the nozzle is discussed.

4.6.1. Closed Section. As noted previously, the closed section of the nozzle is just an expanding area duct, and, as such, the calculation of the flow properties within it is rather straightforward. Were it not for the change of the specific heat as a function of temperature

and the friction on the nozzle walls, this section of the engine could be modeled by the isentropic flow expansion equations. As in the combustor and MHD generator, the friction is calculated as follows:

$$df_c = \frac{u^2}{2} C_f \frac{c}{A} dx \tag{4.6.1.1}$$

Likewise, the change in specific heat is calculated by iteratively solving the quasi-one-dimensional equations as done in the previous sections of the engine. As earlier, this iterative solution provides all the properties at the end of the step and the next step can begin until the closed section of the nozzle is fully evaluated. Once the end of the closed section of the nozzle has been reached, the force generated therein can be found as follows:

$$F_{NC} = \dot{m}_T \left(U_{out} - U_{in}\right) + P_{out} A_{out} - P_{in} A_{in} \tag{4.6.1.2}$$

The "in" and "out" quantities are the entrance and exit conditions, respectively, of the closed section of the nozzle. After the closed section, the flow moves into the open section of the nozzle.

4.6.2. Open Section (Plume Modeling). The evaluation of the open section of the nozzle is decidedly more complicated as it requires the development of a plume model. To develop this model, it is assumed that at each step the engine flow experiences a Prandtl-Meyer expansion while the atmospheric flow experiences an oblique shockwave. The angle of the pseudo-surface assumed to be causing these effects is unknown and must be found iteratively until some other condition is met. Since the higher pressure of the engine flow drives the expansion, the boundary condition imposed is that the pressure of the engine flow after expansion equals the pressure of the atmospheric flow behind the shock within a small margin. To begin this process, a value for the deflection angle θ of the pseudo-surface is assumed and the resulting expansion angle and shockwave angle found. The shock angle β

and post shock pressure P_{shock} is found using the oblique shockwave relation for a calorically perfect gas:

$$\tan\theta = 2\cot\beta \frac{M_0^2 \sin^2\beta - 1}{M_0^2(\gamma + \cos 2\beta) + 2} \tag{4.6.2.1}$$

$$M_{n,0} = M_0 \sin\beta \tag{4.6.2.2}$$

$$P_{shock} = P_0\left[1 + \frac{2\gamma}{\gamma+1}\left(M_{n,0}^2 - 1\right)\right] \tag{4.6.2.3}$$

While the expansion wave angles $\nu(M)$ and post expansion pressure P_{exp} can be found via the Prandtl-Meyer relations:

$$\nu(M) = \sqrt{\frac{\gamma+1}{\gamma-1}}\tan^{-1}\sqrt{\frac{\gamma-1}{\gamma+1}\left(M^2-1\right)} - \tan^{-1}\sqrt{M^2-1} \tag{4.6.2.4}$$

$$\nu\left(M_{\exp}\right) = \theta + \nu\left(M_{nozzle}\right) \tag{4.6.2.5}$$

$$P_{\exp} = P_{nozzle}\left(\frac{1 + \frac{\gamma-1}{2}M_{nozzle}^2}{1 + \frac{\gamma-1}{2}M_{\exp}^2}\right)^{\frac{\gamma}{\gamma-1}} \tag{4.6.2.6}$$

These equations are iterated while the deflection angle θ is adjusted until:

$$P_{\exp} \cong P_{shock} \tag{4.6.2.7}$$

Once this condition is met, the angle of the pseudo-surface for the particular step is found. An example plume profile is shown below in Figure 4.2 with the first meter of the engine being the closed section and the remaining three meters the open section.

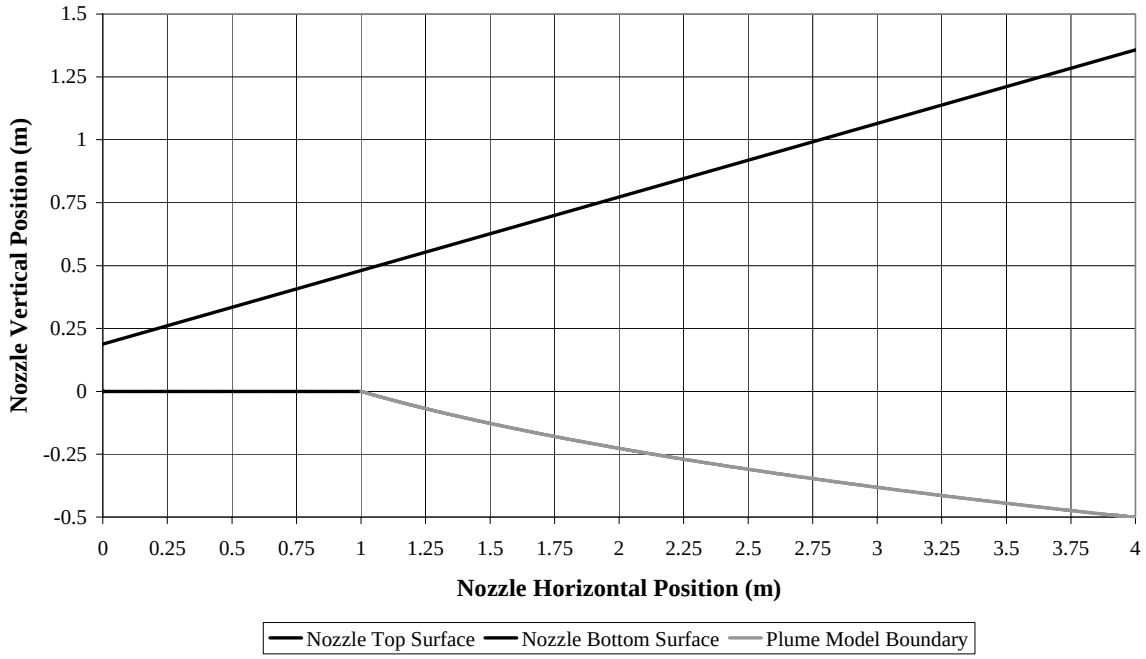

Figure 4.2: Example plume profile at a Mach number of 8.0.

When calculating the property changes of the flow within the nozzle, this pseudo-surface is treated as the lower boundary of the nozzle which is directly used in the calculation of the area change dA for each step in the nozzle. An additional advantage of having a portion of the nozzle open is a reduction in the friction generated by the walls of the nozzle since friction is only generated on the solid surfaces of the nozzle. In the equation for the differential friction df_c, the perimeter of the nozzle c usually has the following value:

$$c = 2H + 2W \tag{4.6.2.8}$$

Where H is the height of the duct at the particular position and W is its width. For the open section of the nozzle, however, because there are no side walls or bottom surface, c simply becomes:

$$c = W \tag{4.6.2.9}$$

Thus, the equation for the differential friction in the open part of the nozzle is as follows:

$$df_c = \frac{u^2}{2} C_f \frac{W}{A} dx \tag{4.6.2.10}$$

It should also be noted that the area *A* in the above equation uses the full height of the flow, including the portion contributed by the height of the plume which serves to increase the area and thereby further reduce friction in the nozzle. After the friction is found for the step, the quasi-one-dimensional equations are solved along with the changes in the specific heat as was done in the closed section of the nozzle. The force generated by the open section of the nozzle has a significantly different form as that found in the previous sections of the engine. Because the flow is open to the atmosphere, only the force on the top surface in the axial direction contributes to the thrust generated by the engine. This force is found as the sum of the differential force generated on that surface at each step:

$$F_{NO} = \sum_{nozzle,open}^{steps} dF_{top} \tag{4.6.2.11}$$

The differential force on the top is found by multiplying the average pressure across the step by the change in area of that step:

$$dF_{top} = \frac{\left(P_{begin} + P_{end}\right)}{2} dA_{top} \tag{4.6.2.12}$$

With this final force found, the analysis of the engine is complete and the quantities for comparison are found and compared in the results section. Before that is done, however, the model needs to be validated as will be done in the next section of this thesis.

4.7. VALIDATION OF THE MODEL

In order to ensure that the model was programmed and is working correctly, it must be validated against known data and methods. To do this, each section of the engine is

analyzed as if it were a stand alone component. The various effects in each section are analyzed individually and compared to the results generated by more simplified methods.

4.7.1 Validation of the Inlet. To validate the inlet, the properties and shock angles generated by the model are compared to those generated by the standard calorically perfect oblique shock relations:

$$\tan\theta = 2\cot\beta \frac{M_1^2 \sin^2\beta - 1}{M_1^2(\gamma + \cos 2\beta) + 2} \tag{4.1.2.1}$$

$$M_{n,1} = M_1 \sin\beta \tag{4.7.1.2}$$

$$M_{n,2} = \sqrt{\frac{1 + \frac{\gamma-1}{2} M_{n,1}^2}{\gamma M_{n,1}^2 - \frac{\gamma-1}{2}}} \tag{4.7.1.3}$$

$$M_2 = \frac{M_{n,2}}{\sin(\beta - \theta)} \tag{4.7.1.4}$$

$$\frac{P_2}{P_1} = 1 + \frac{2\gamma}{\gamma+1}\left(M_{n,1}^2 - 1\right) \tag{4.7.1.5}$$

$$\frac{\rho_2}{\rho_1} = \frac{(\gamma+1)M_{n,1}^2}{2 + (\gamma-1)M_{n,1}^2} \tag{4.7.1.6}$$

$$\frac{T_2}{T_1} = \frac{P_2}{P_1}\frac{\rho_1}{\rho_2} \tag{4.7.1.7}$$

The results of this comparison are summarized in Table 4.3. As can be seen from the results in Table 4.3, the complete model calculations are relatively close to those of the standard baseline. When the change in C_p that exists in the model was disabled and the model was allowed to proceed as if the flow was calorically perfect, the results are virtually identical to the baseline standard case. Because of these comparable data, it can be concluded that the inlet model is correct and validated.

Table 4.3: Calculations to validate the inlet model.

M_0	P_0	T_0	ρ_0	β_1	M_1	P_1	T_1	ρ_1	β_2	M_2	P_2	T_2	ρ_2
	(Pa)	(K)	(kg/m^3)	(deg.)		(Pa)	(K)	(kg/m^3)	(deg.)		(Pa)	(K)	(kg/m^3)
Complete Modelled Calculations													
8.0	2261.7	218.76	0.0359	17.464	5.424	14957	440.00	0.1180	19.885	4.237	58625	660.26	0.3081
12.0	1005.2	234.96	0.0148	15.658	6.983	12398	660.90	0.0651	17.594	5.344	64613	1063.80	0.2108
15.0	643.3	244.38	0.0091	14.996	7.896	11560	857.76	0.0468	16.826	5.903	70171	1453.50	0.1675
Calorically Perfect Modelled Calculations													
8.0	2261.7	218.76	0.0359	17.599	5.341	15058	450.29	0.1160	20.607	4.007	59561	716.93	0.2883
12.0	1005.2	234.96	0.0148	15.981	6.617	12634	717.60	0.0611	18.793	4.705	64876	1289.90	0.1745
15.0	643.3	244.38	0.0091	15.463	7.201	11901	988.71	0.0418	18.219	4.988	68392	1881.10	0.1262
Calorically Perfect Standard Calculations													
8.0	2261.7	218.76	0.0359	17.600	5.340	15062	450.31	0.1161	20.607	4.007	59573	716.93	0.2885
12.0	1005.2	234.96	0.0148	15.981	6.617	12633	717.61	0.0609	18.793	4.705	64870	1289.87	0.1740
15.0	643.3	244.38	0.0091	15.463	7.201	11897	988.71	0.0416	18.219	4.988	68370	1881.10	0.1256

4.7.2 Validation of the Combustor. The validation of the combustor is more complicated than the validation of the inlet since there are many more parameters affecting the flow than there were in the inlet. To validate the combustor, each of the affecting parameters was analyzed as if it were the only effect the combustor experienced. First, however, a null case where all of the effects were disabled was considered to ensure that, with nothing affecting the flow, it experienced no change. When this was done, all of the flow properties entering the combustor were exactly equal to those exiting it, validating the null case. Next the case of calorically perfect heat addition with frictionless walls was considered to validate that heat was being properly added to the flow. This was done by comparing the properties of the flow exiting the combustor, with all effects except combustion disabled, to calculations made with the Rayleigh Flow equations:

$$\frac{T_{t2}}{T_{t1}} = 1 + \frac{\Delta q_{1-2}}{C_p T_{t1}} = \frac{f\left(M_2^2\right)}{f\left(M_1^2\right)} \tag{4.7.2.1}$$

$$f\left(M^2\right) = \frac{1 + \frac{\gamma-1}{2} M^2}{\left(1+\gamma M^2\right)^2} M^2 \tag{4.7.2.2}$$

$$M^2 = \frac{2f\left(M^2\right)}{1-2\gamma f\left(M^2\right)-\left[1-2(\gamma+1)f\left(M^2\right)\right]^{1/2}} \tag{4.7.2.3}$$

$$\frac{P_2}{P_1} = \frac{1+\gamma M_1^2}{1+\gamma M_2^2} \tag{4.7.2.4}$$

The results of these calculations as well as the output of the model are given below in Table 4.4. The close agreement of the two sets of data presented in the Table validates the heat addition model used in the combustor.

Table 4.4: Calculations to validate the combustor heat addition model.

M_i	P_i	T_i	ρ_i	$\Delta q_{1\text{-}2}$	M_e	P_e	T_e	ρ_e
	(Pa)	(K)	(kg/m^3)	(J/kg)		(Pa)	(K)	(kg/m^3)
Modeled Constant Area Heat Addition Calculations								
4.0	60000	700	0.29742	2038300	1.1006	520730	3993.0	0.45251
5.0	65000	1000	0.22554	3225900	1.7338	449250	5744.4	0.27137
6.0	70000	1500	0.16193	2794100	2.9663	270150	5460.5	0.17167
Theoretical Rayleigh Calculations								
4.0	60000	700	0.29742	2038300	1.0995	521438	3994.8	0.45292
5.0	65000	1000	0.22554	3225900	1.7337	449296	5744.6	0.27139
6.0	70000	1500	0.16193	2794100	2.9662	270160	5460.7	0.17167

Next, the combustor friction model is validated by comparing the results from the combustor with all effects except friction disabled to the theoretical Fanno Flow equations:

$$\gamma C_f \frac{c}{A} dx = \frac{1-M^2}{M^4\left(1+\frac{\gamma-1}{2}M^2\right)} dM^2 \tag{4.7.2.5}$$

$$F\left(M^2\right) = \frac{\gamma+1}{2}\ln\left(\frac{1+\frac{\gamma-1}{2}M^2}{M^2}\right) - \frac{1}{M^2} \tag{4.7.2.6}$$

$$\chi_2 - \chi_1 = F\left(M_2^2\right) - F\left(M_1^2\right) = \gamma C_f \frac{c}{A} L_B \tag{4.7.2.7}$$

$$\frac{T_2}{T_1} = \frac{1+\frac{\gamma-1}{2}M_1^2}{1+\frac{\gamma-1}{2}M_2^2} \tag{4.7.2.8}$$

$$\frac{P_2}{P_1} = \frac{M_1}{M_2}\left(\frac{1+\frac{\gamma-1}{2}M_1^2}{1+\frac{\gamma-1}{2}M_2^2}\right)^{1/2} \tag{4.7.2.9}$$

The results of this comparison are given below in Table 4.5. Once again, the results from the model closely mirror those produced by the more simplified theoretical equations thereby validating the friction model used in the combustor.

Table 4.5: Calculations to validate the combustor friction model.

M_i	P_i	T_i	ρ_i	$\chi_2-\chi_1$	M_e	P_e	T_e	ρ_e
	(Pa)	(K)	(kg/m^3)			(Pa)	(K)	(kg/m^3)
Modeled Friction Calculations								
4.0	60000	700	0.29742	0.07660	3.4274	78411	877.8	0.30997
5.0	65000	1000	0.22554	0.12859	3.6500	113930	1637.3	0.24145
6.0	70000	1500	0.16193	0.16685	3.7410	164940	3237.7	0.17677
Theoretical Fanno Flow Calculations								
4.0	60000	700	0.29742	0.07660	3.4274	78415	877.8	0.30997
5.0	65000	1000	0.22554	0.12859	3.6498	113945	1637.4	0.24146
6.0	70000	1500	0.16193	0.16685	3.7408	164956	3237.9	0.17677

Although the combustor does not need to expand to prevent the flow from choking for any of the cases run, the ability of it to do so is part of the model. Therefore, the expansion capabilities, with all other effects disabled, of the combustor are validated against the theoretical expanding flow equations (also known as the nozzle flow equations):

$$T_{t1} = T_t^* = T_{t2} \tag{4.7.2.10}$$

$$P_{t1} = P_t^* = P_{t2} \tag{4.7.2.11}$$

$$C^* = \left(\frac{\gamma+1}{2}\right)^{\frac{\gamma+1}{2(\gamma-1)}} \sqrt{\frac{RT_t^*}{\gamma}} \tag{4.7.2.12}$$

$$A^* = \frac{\dot{m}C^*}{P_t^*} \tag{4.7.2.13}$$

$$\frac{A}{A^*} = \left[\frac{2}{\gamma+1}\left(1+\frac{\gamma-1}{2}M^2\right)\right]^{\frac{\gamma+1}{2(\gamma-1)}} \frac{1}{M} \tag{4.7.2.14}$$

The results of this comparison are given in Table 4.6. Because the two sets of data match so closely, the expansion capabilities of the combustor have been validated. With these three combustor effects validated individually, the overall model used in the combustor has been validated.

Table 4.6: Calculations to validate the combustor expansion model.

M_i	P_i	T_i	ρ_i	θ_B	M_e	P_e	T_e	ρ_e
	(Pa)	(K)	(kg/m^3)	(deg.)		(Pa)	(K)	(kg/m^3)
Modeled Expansion Calculations								
4.0	60000	700	0.29742	4.00	4.2423	43658	639.2	0.23699
5.0	65000	1000	0.22554	2.00	5.2433	49157	923.3	0.18474
6.0	70000	1500	0.16193	1.00	6.1860	57984	1421.4	0.14155
Theoretical Expanding Flow Calculations								
4.0	60000	700	0.29742	4.00	4.2423	43655	639.2	0.23698
5.0	65000	1000	0.22554	2.00	5.2434	49154	923.3	0.18473
6.0	70000	1500	0.16193	1.00	6.1860	57983	1421.4	0.14155

4.7.3 Validation of the MHD Generator. The MHD generator, which proves to be the most complex component to be validated, is evaluated next. First, the friction model of the MHD unit is validated by comparing it to the same Fanno Flow equations used in the combustor (4.7.2.5-4.7.2.9). The results of this comparison are given in Table 4.7. Because

of the close agreement of the modeled and theoretical data, the friction model in the MHD generator is considered to be validated.

Next, the expansion model of the MHD unit is validated by juxtaposing the modeled expansion data with data generated by the theoretical expanding flow equations (4.7.2.10-4.7.2.14). The results of this comparison are summarized in Table 4.8, below. The agreement of the data presented above serves to validate the MHD generator expansion model.

Table 4.7: Calculations to validate the MHD generator friction model.

M_i	$P_{t,i}$	$T_{t,i}$	R	$\chi_2 - \chi_1$	M_e	$P_{t,e}$	$T_{t,e}$
	(Pa)	(K)	(J/(kg*K))			(Pa)	(K)
Modeled Friction Calculations							
1.4	1000000	3660	340	0.00777	1.3862	992490	3660.0
2.7	4400000	5640	345	0.01078	2.6687	4232400	5640.0
3.4	12000000	7710	350	0.01364	3.3404	11106000	7710.0
Theoretical Fanno Flow Calculations							
1.4	1000000	3660	340	0.00777	1.3862	992492	3660.0
2.7	4400000	5640	345	0.01078	2.6687	4232424	5640.0
3.4	12000000	7710	350	0.01364	3.3405	11105638	7710.0

Table 4.8: Calculations to validate the MHD generator expansion model.

M_i	$P_{t,i}$	$T_{t,i}$	R	θ	M_e	$P_{t,e}$	$T_{t,e}$
	(Pa)	(K)	(J/(kg*K))	(deg.)		(Pa)	(K)
Modeled Expansion Calculations							
1.4	1000000	3660	340	4.00	1.6497	1000000	3660.0
2.7	4400000	5640	345	2.00	2.8007	4400000	5640.0
3.4	12000000	7710	350	1.00	3.4643	12000000	7710.0
Theoretical Expanding Flow Calculations							
1.4	1000000	3660	340	4.00	1.6497	1000000	3660.0
2.7	4400000	5640	345	2.00	2.8007	4400000	5640.0
3.4	12000000	7710	350	1.00	3.4643	12000000	7710.0

Finally, the actual magnetohydrodynamic interactions of the MHD unit must be validated. Finding a theoretical means for comparison, however, proves difficult as the full MHD interaction affects both the energy and the momentum of the flow which leads to differential equations that cannot be explicitly solved. To addresses this problem, the two MHD interactions were analyzed as if they could occur separately. Although this is not physically possible, nothing prevents it from being done in a theoretical and modeled fashion. First, the MHD energy interaction will be analyzed with the momentum interaction disabled. This interaction can then be compared to results from the Rayleigh flow equations (4.7.2.1-4.7.2.4), where $\Delta q_{1\text{-}2}$ is defined as follows:

$$\Delta q_{1-2} = \sum_{MHD}^{steps} dq_{EM} = \int_0^{L_M} \frac{\sigma E(x)\left[E(x) - B \cdot u(x)\right]}{\rho(x) u(x)} dx \qquad (4.7.3.1)$$

The results of this comparison are summarized in Table 4.9, which is presented below. As can be seen, the modeled results agree closely with the theoretical results validating the MHD energy interaction model.

Table 4.9: Calculations to validate the MHD generator energy interaction model.

M_i	$P_{t,i}$	$T_{t,i}$	R	$\Delta q_{1\text{-}2}$	M_e	$P_{t,e}$	$T_{t,e}$
	(Pa)	(K)	(J/(kg*K))			(Pa)	(K)
Modeled MHD Energy Interaction Calculations							
1.4	1000000	3660	340	-13796	1.4066	1002600	3652.1
2.7	4400000	5640	345	-54540	2.7221	4510400	5609.4
3.4	12000000	7710	350	-99746	3.4428	12642000	7654.9
Theoretical Rayleigh Calculations							
1.4	1000000	3660	340	-13796	1.4066	1002626	3652.1
2.7	4400000	5640	345	-54540	2.7221	4510432	5609.4
3.4	12000000	7710	350	-99746	3.4428	12641876	7654.8

Next, the momentum interaction of the MHD generator is analyzed with the energy interaction disabled. To perform this analysis, a theoretical basis for comparison must be found. By comparing the MHD momentum interaction to that offered by the friction model of Fanno flow, this theoretical basis was found. With a little manipulation, an equation comparable to Eq. 4.7.2.5 for Fanno flow was found:

$$-2\gamma\sigma B^2 \frac{A}{\dot{m}}\left(\frac{1}{\eta_{MHD}}-1\right)dx = \frac{1-M^2}{M^4\left(1+\frac{\gamma-1}{2}M^2\right)}dM^2 \qquad (4.7.3.2)$$

$$\chi_2 - \chi_1 = F\left(M_2^2\right) - F\left(M_1^2\right) = -2\gamma\sigma B^2 \frac{A}{\dot{m}}\left(\frac{1}{\eta_{MHD}}-1\right)L_B \qquad (4.7.3.3)$$

The other equations for Fanno flow (4.7.2.6, 4.7.2.8, and 4.7.2.9) hold. The results of this comparison are summarized in Table 4.10, below. The close agreement of the two sets of data presented above validates the MHD unit's MHD momentum interaction model. With these four effect in the MHD generator validated, the overall MHD generator model is considered to be completely validated.

Table 4.10: Calculations to validate the MHD generator momentum interaction model.

M_i	$P_{t,i}$	$T_{t,i}$	R	$\chi_2-\chi_1$	M_e	$P_{t,e}$	$T_{t,e}$
	(Pa)	(K)	(J/(kg*K))			(Pa)	(K)
Modeled MHD Momentum Interaction Calculations							
1.4	1000000	3660	340	0.02229	1.3602	978990	3660.0
2.7	4400000	5640	345	0.02303	2.6338	4054100	5640.0
3.4	12000000	7710	350	0.02438	3.2950	10468000	7710.0
Theoretical MHD Fanno Flow Calculations							
1.4	1000000	3660	340	0.02229	1.3602	978990	3660.0
2.7	4400000	5640	345	0.02303	2.6338	4054122	5640.0
3.4	12000000	7710	350	0.02438	3.2950	10468102	7710.0

4.7.4 Validation of the Nozzle. The nozzle, which proves to be easiest to validate, is validated in this section. The main effect in the nozzle is the expansion of the flow, so this effect is validated first by comparing the results of the nozzle expansion model to those of the nozzle flow equations (4.7.2.10-4.7.2.14). This comparison was made for both a completely closed nozzle and one with twenty-five percent closed and seventy-five percent open, with a plume model. The results of these comparisons are show in Tables 4.11 and 4.12.

Table 4.11: Calculations to validate the nozzle expansion model with a closed nozzle.

M_i	$P_{t,i}$	$T_{t,i}$	R	θ	M_e	$P_{t,e}$	$T_{t,e}$
	(Pa)	(K)	(J/(kg*K))	(deg.)		(Pa)	(K)
Modeled Expansion Calculations							
1.4	1000000	3650	340	16.2962	3.2311	999890	3650.0
2.7	4300000	5620	345	16.2962	4.4954	4299400	5620.0
3.3	11000000	7670	350	16.2962	5.3281	10998000	7670.0
Theoretical Nozzle Flow Calculations							
1.4	1000000	3650	340	16.2962	3.2309	1000000	3650.0
2.7	4300000	5620	345	16.2962	4.4952	4300000	5620.0
3.3	11000000	7670	350	16.2962	5.3278	11000000	7670.0

Table 4.12: Calculations to validate the nozzle expansion model with plume modeling.

M_i	$P_{t,i}$	$T_{t,i}$	R	A_2/A_1	M_e	$P_{t,e}$	$T_{t,e}$
	(Pa)	(K)	(J/(kg*K))			(Pa)	(K)
Modeled Expansion Calculations							
1.4	1000000	3650	340	9.6632	3.4624	999860	3650.0
2.7	4300000	5620	345	12.2916	4.6622	4299300	5620.0
3.3	11000000	7670	350	14.9199	5.4675	10998000	7670.0
Theoretical Nozzle Flow Calculations							
1.4	1000000	3650	340	9.6632	3.4621	1000000	3650.0
2.7	4300000	5620	345	12.2916	4.6619	4300000	5620.0
3.3	11000000	7670	350	14.9199	5.4672	11000000	7670.0

These data agree closely; however, it was expected that the total pressures would agree precisely since no total pressure change should be taking place. The inaccuracy of the modeled total pressure is a result of a compounding of numerical computational error. Total pressure change is not calculated explicitly in the model; rather, total temperature change, static pressure change, and velocity change are calculated and then used to find the values of those quantities at the end of the step. The remaining quantities, including the total pressure, are then calculated from the three explicitly calculated above. The error causing the disagreement in the total pressure is noticeably present in the nozzle, whereas it was not in either the combustor or MHD generator, because the nozzle is eight times as long and undergoes an expansion at least four times greater than either of the two previously validated components. With all this taken into account, the lack of precise agreement in the total pressure is understandable and it can be concluded that the nozzle expansion model is validated.

The only other effect present in the calorically perfect version of the nozzle being analyzed here is friction. As before, the results of calculations for the friction model in the nozzle (with nozzle expansion set to zero) are compared to those from the theoretical Fanno flow equations (4.7.2.5-4.7.2.9). The results of this comparison are given in Table 4.13.

The very close agreement of these data validates the nozzle friction model. With this last validation, all effects except the changes in specific heat C_p, gas constant R, and ratio of specific heats γ, which cannot be validated by any theoretical comparison, have been validated in all components. It is considered, therefore, that the entire model has been validated.

Table 4.13: Calculations to validate the nozzle friction model.

M_i	$P_{t,i}$	$T_{t,i}$	R	$\chi_2 - \chi_1$	M_e	$P_{t,e}$	$T_{t,e}$
	(Pa)	(K)	(J/(kg*K))			(Pa)	(K)
Modeled Friction Calculations							
1.4	1000000	3650	340	0.0621	1.2857	945420	3650.0
2.7	4300000	5620	345	0.0862	2.6440	3227000	5620.0
3.3	11000000	7670	350	0.1091	2.8952	6529800	7670.0
Theoretical Fanno Flow Calculations							
1.4	1000000	3650	340	0.0621	1.2857	945417	3650.0
2.7	4300000	5620	345	0.0862	2.4644	3227008	5620.0
3.3	11000000	7670	350	0.1091	2.8952	6529810	7670.0

5. RESULTS

This section summarizes the mains results obtained in this study, in which a number of parameters in the MHD system and relating to the propulsion system in general were varied. The vehicle performance for each of these parameter combinations was then calculated using the model described in earlier sections. Results of the current study are mainly shown in terms of the common figure of merit specific impulse, as defined below. This quantity allows the comparison of different vehicle/engine configurations in terms of thrust-based efficiency of fuel utilization. Also of importance is the MHD-based power effectiveness which will be defined in terms of a MHD-based "specific impulse."

For each configuration modeled, the total propulsive thrust is calculated as a sum of the axial forces generated in each component as described in Section 4:

$$Thrust = F_I + F_{mix} + F_B + F_M + F_{NC} + F_{NO} \tag{5.1}$$

Thrust is a vehicle-specific quantity and thus is not directly comparable for different engine geometries especially due to cooling issues (i.e. the cooling fuel requirements as discussed earlier). The standard parameter of merit (effectiveness) is the specific impulse (thrust per unit weight flow rate of on-board propellant) which is useful for assessing the performance effectiveness of different geometries:

$$I_{sp} = \frac{Thrust}{\dot{m}_f \cdot g_0} \tag{5.2}$$

The calculation of the specific impulse in Eq. 5.2 uses the stoichiometric fuel mass flow from Eq. 4.3.1, which assumes that the fuel needed for thermal balancing is somehow retained onboard and cooled. If this excess fuel flow required for thermal balancing must be dumped (without affecting thrust), the thermally balanced specific impulse becomes:

$$I_{sp,bal} = \frac{Thrust}{\dot{m}_{f,B} \cdot g_0} \tag{5.3}$$

Here $\dot{m}_{f,B}$ is the mass flow of fuel after thermally balancing the combustor as derived and discussed in Section 4.5. The total power extracted by the MHD generator as electricity is as follows:

$$\dot{Q}_{MHD,out} = -\dot{m}_T \sum_{MHD}^{steps} dw_{EM} \tag{5.4}$$

As with thrust, this is a vehicle/configuration specific quantity. It is manipulated in order to obtain a parameter comparable to specific impulse; this parameter will be called the specific MHD impulse:

$$MHD_{sp} = \frac{\dot{Q}_{MHD,out}}{U_0 \cdot \dot{m}_f \cdot g_0} \tag{5.5}$$

As with standard specific impulse, this can also be written for a thermally balanced engine (i.e. one requiring cooling fuel):

$$MHD_{sp,bal} = \frac{\dot{Q}_{MHD,out}}{U_0 \cdot \dot{m}_{f,B} \cdot g_0} \tag{5.6}$$

By taking the sum the specific impulse and specific MHD impulse, a total specific impulse metric can be found for both the stoichiometric and thermally balanced cases:

$$I_{sp,T} = I_{sp} + MHD_{sp} \tag{5.7}$$

$$I_{sp,T,bal} = I_{sp,bal} + MHD_{sp,bal} \tag{5.8}$$

Finally, the fraction of the MHD contribution to the total specific impulse can be found:

$$\%MHD = 100\frac{MHD_{sp}}{I_{sp,T}} = 100\frac{MHD_{sp,bal}}{I_{sp,T,bal}} \tag{5.9}$$

The fractional MHD contibution is equal for both the stoichiometric and thermally balanced cases because the fuel mass flows "cancel out" in this calculation. It should also be noted that the ratio of any of the above specific impulses is as follows:

$$\frac{balanced}{stoichiometric} = \frac{\dot{m}_f}{\dot{m}_{f,B}} \tag{5.10}$$

For the purposes of easy comparison a "MHD base case" will be defined as follows:

$$B = 0.5\ Tesla; \quad \eta_{MHD} = 1.6; \quad \sigma = 100\ mho/m; \quad \theta_M = 0.0\ deg.$$

The parameters given represent the parameters that are varied in this study in order to generate performance comparisons. The magnetic field strength *B* base case value was chosen as a representative value for a light-weight electromagnet. Modern electromagnets with iron cores can achieve field strengths as high as 2 Teslas while modern superconducting electromagnets extend this range to (or in excess of) 10 Teslas. The load factor η_{MHD} used in the base case is typical for MHD generators, though this parameter can theoretically range anywhere between one and infinity. The definition of the load factor is given and discussed in Appendix B. The base conductivity σ was chosen as the maximum theoretically possible for a potassium *K* seed under equilibrium ionization for an expected combustor exit temperature of 3500 K. Finally, in the base case the MHD generator was assumed to have a constant cross-sectional area, i.e. $\theta_M = 0.0\ deg.$

5.1. COMPARISON TO AN IDEAL SCRAMJET

The base case without any MHD is first compared to an ideal scramjet (no losses, fully expanded); results in terms of specific impulse are in Figure 5.1. As can be seen, the specific impulse of the modeled engine with no MHD interaction is less than that of the ideal by between 2615 and 2746 seconds. In addition, thermal balancing has no discernable effect

for flight Mach numbers below 13. Even above Mach 13, thermal balancing has a maximum impact of just 4.3% of ideal in contrast to the other non-ideal effects which have a maximum impact of 88% of ideal specific impulse. Therefore, for the remainder of the results discussion, the effect of thermal balancing on specific impulse will be ignored.

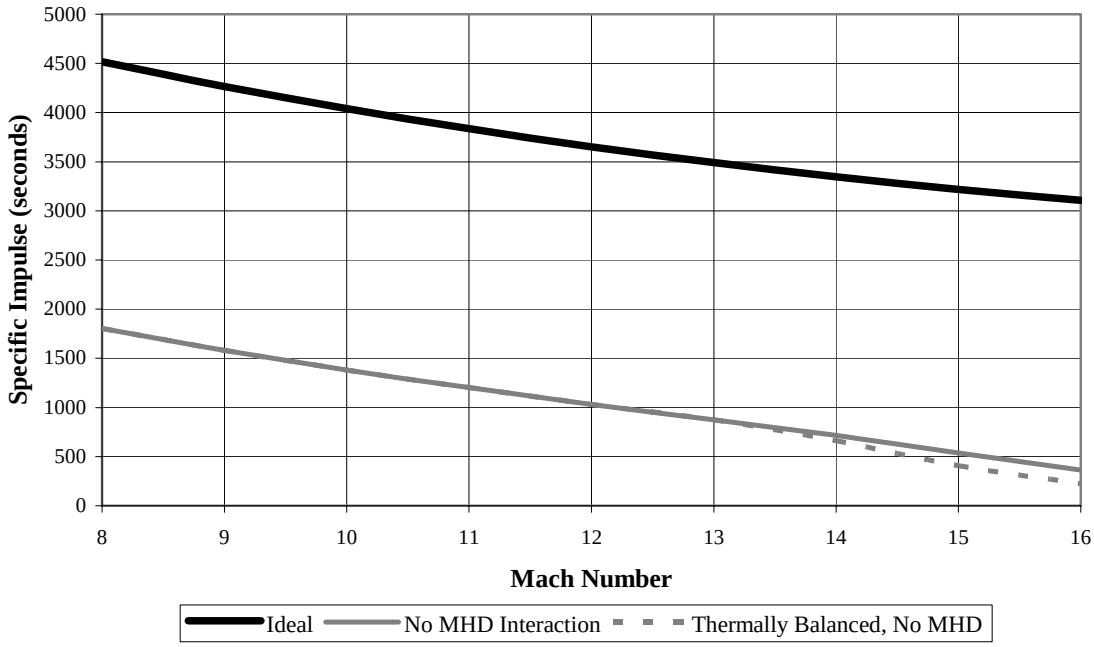

Figure 5.1: Comparison of the specific impulse of the ideal scramjet to the modeled engine, both stoichiometric and thermally balanced.

Figure 5.2 compares the modeled engine both with no MHD and the MHD base case to the ideal scramjet. As can be seen, the MHD base case further reduces the specific impulse between 26.4 seconds at Mach 8 and 108 seconds at Mach 16. This is consistent with the fact that the MHD generator is removing energy from the flow to be used as electricity.

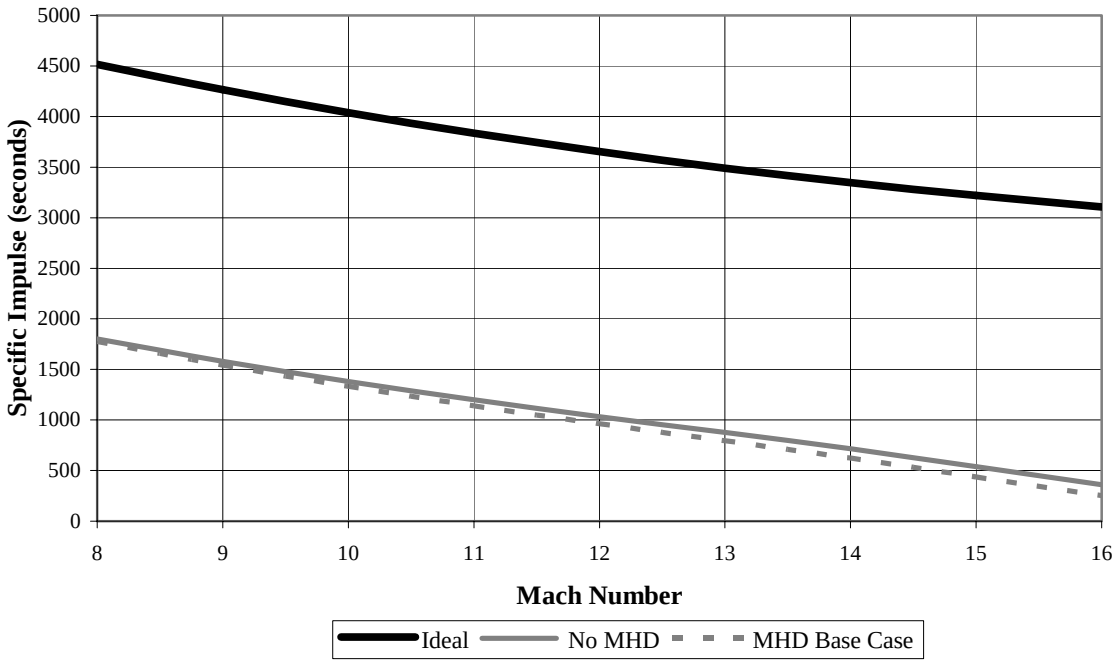

Figure 5.2: Comparison of the specific impulse of the ideal scramjet to the modeled engine with no MHD and the MHD base case.

5.2. RESULTS AS MACH NUMBER VARIES

One of the variables of interest for the performance output of the engine and the MHD generator is the flight Mach number. In general, as was seen in the previous section, specific impulse decreases as Mach number increases. Figures 5.3 – 5.5 are plots of specific impulse, specific MHD impulse, and total specific impulse versus Mach number for a number of MHD generator configurations. It should be noted that each of the conditions is simply varied in terms of the single parameter (as shown in the legend) around the MHD base case. Figure 5.3 shows that at a variety of magnetic field strengths, the same trends are observed: specific impulse decreases as Mach increases, specific MHD impulse increases as Mach increases, and total specific impulse decreases as Mach increases, but not as rapidly as specific impulse decreased. It can also be observed from Figure 5.3 that at higher magnetic

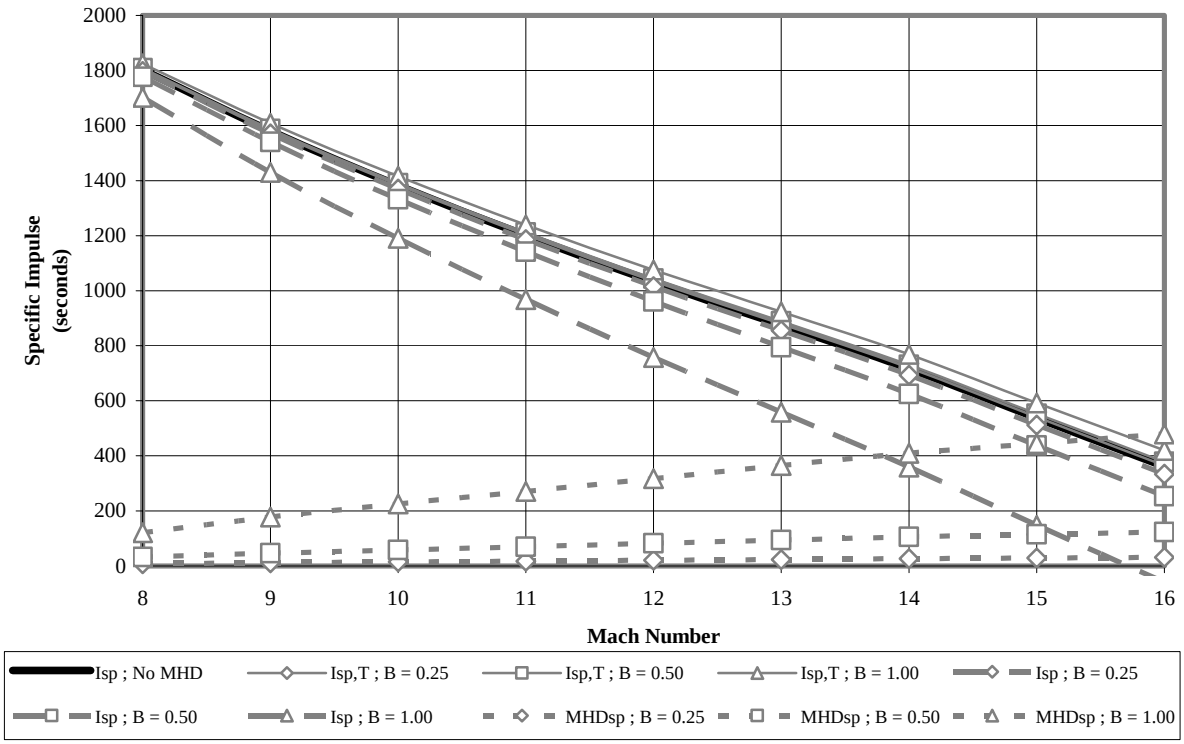

Figure 5.3: Specific impulses versus Mach number for varying magnetic field strength.

field strengths, all of the above trends occur more rapidly than at lower field strengths. Figure 5.4 shows the same general characteristics for the three specific impulse quantities with varying Mach number and at various gas conductivities. This figure, however, also demonstrates that at higher gas conductivities the trends are more drastic than at lower gas conductivities (but not as drastic as the trends are at higher magnetic field strength).

Figure 5.5 once again demonstrates the same general characteristics for the specific impulse with Mach and also shows that at higher load factor the same trends occur, albeit more rapidly. Both the specific impulse trends (with varying Mach) and the observed differences among them (for different magnetic field strengths, gas conductivities, and load factors) follow logically from the MHD equations Eqs. 4.4.7 and 4.4.9.

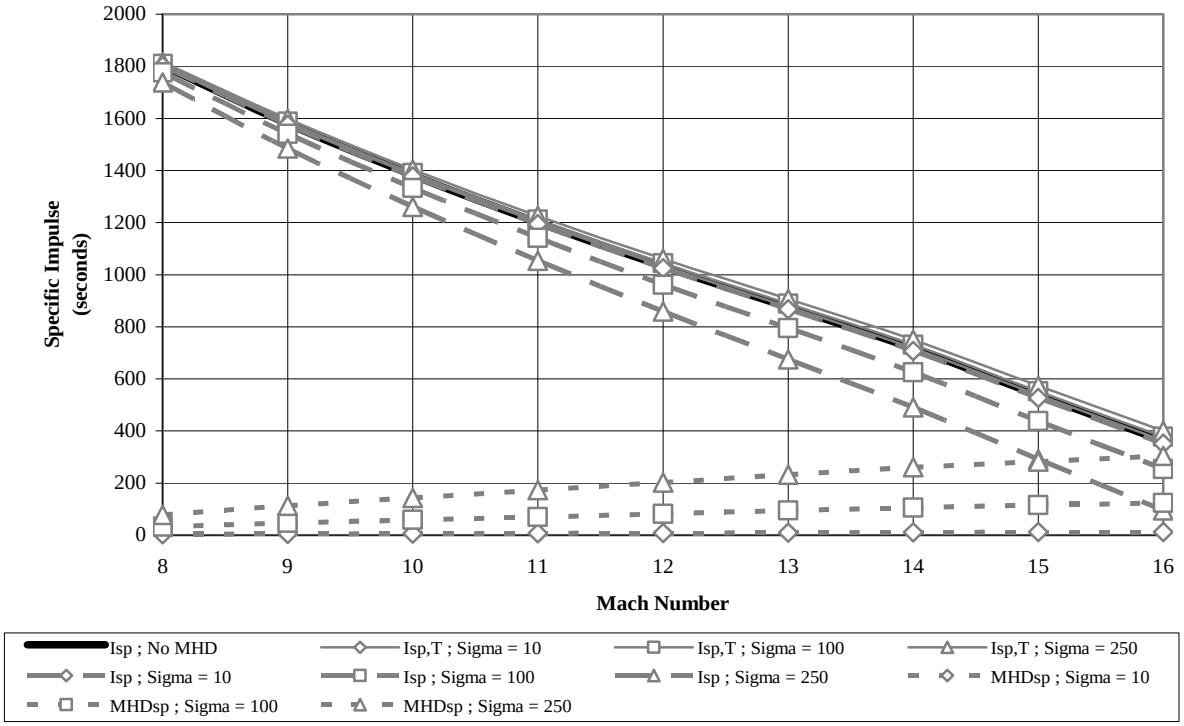

Figure 5.4: Specific impulses versus Mach number for varying gas conductivity.

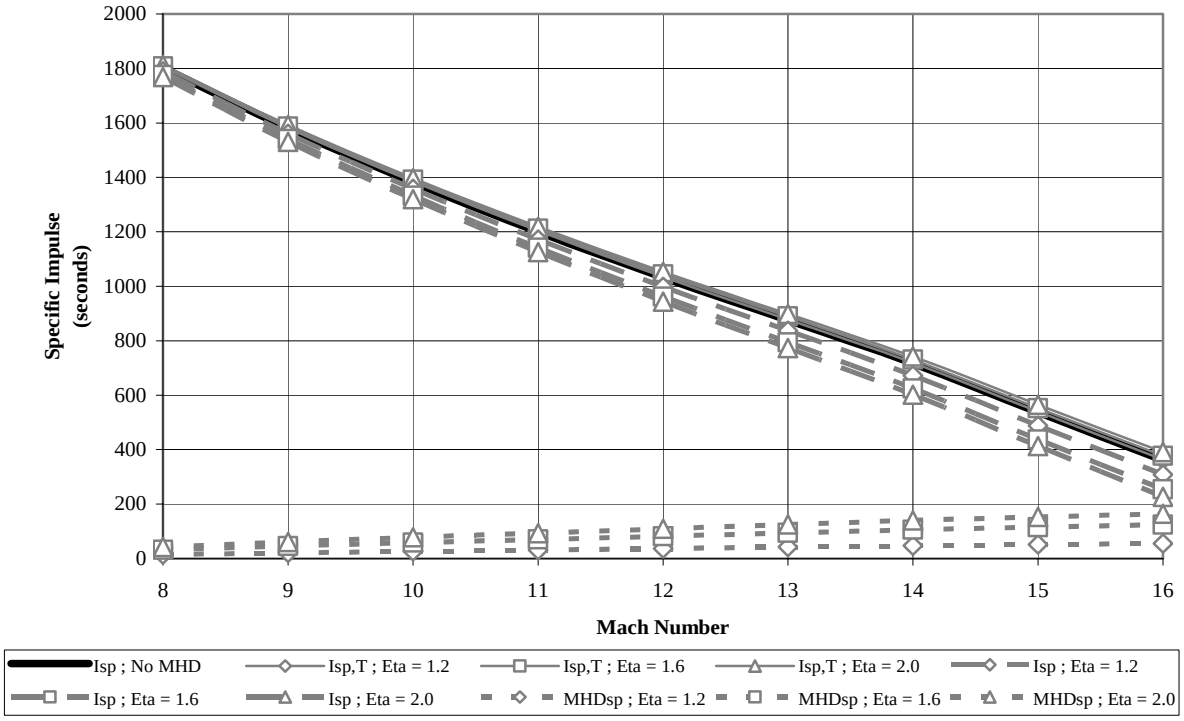

Figure 5.5: Specific impulses versus Mach number for varying load factor.

Finally, Figure 5.6 shows how the percentage of the total power produced by the MHD generator varies with Mach number for a variety of different electromagnetic configurations. All of the characteristics shown in this figure follow logically from those discussed previously in this section.

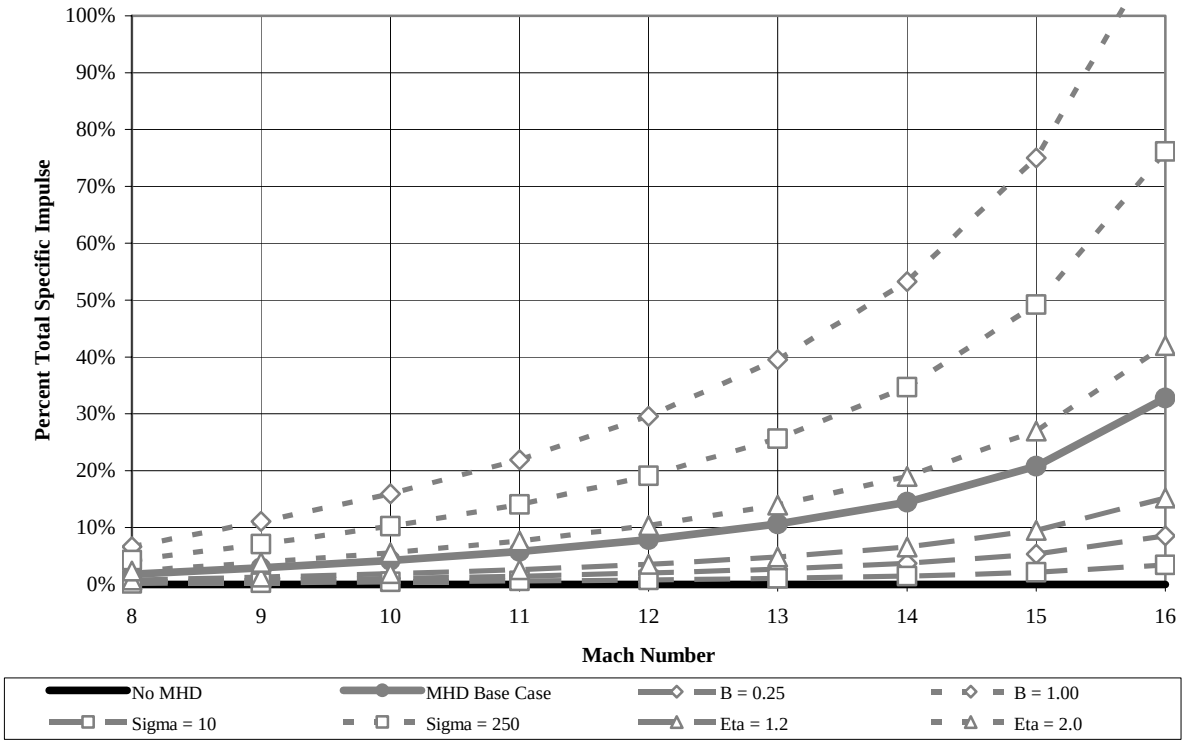

Figure 5.6: Percent power generated by MHD versus Mach number for different MHD generator configurations.

5.3. RESULTS AS MAGNETIC FIELD STRENGTH VARIES

This section briefly discusses the results obtained when the electrodynamic characteristics of the MHD generator are changed. First, the magnetic field strength is varied to

assess its impact of the specific impulses as shown in Figure 5.7. This figure demonstrates that at three flight Mach numbers, as magnetic field strength increases, specific impulse decreases and specific MHD impulse increases at exponentially increasing rates. This observation indicates that these quantities vary quadratically, cubically, or perhaps at a higher order with magnetic field strength. The figure also shows that total specific impulse increases at an exponential rate, though not increasing exponentially as fast as the other two parameters. This trend is likely a result of the fact that specific MHD impulse exceeds specific impulse lost from the MHD generators interaction at all Mach numbers and magnetic field strengths, and this difference grows with increasing magnetic field strength.

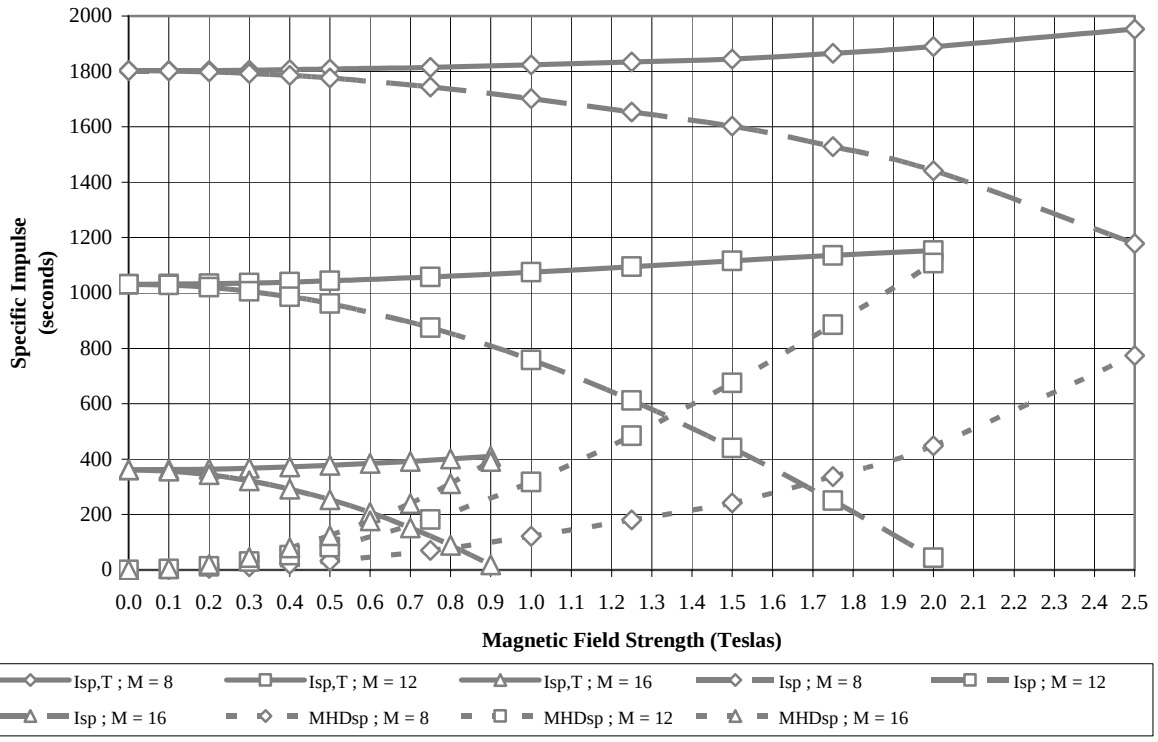

Figure 5.7: Specific impulses versus magnetic field strength at three Mach numbers.

Figure 5.8 illustrates that the growth of the specific MHD impulse with magnetic field strength dominates the slower growth observed in total specific impulse. This figure also indicates that the percent of power produced by the MHD generator grows more rapidly with magnetic field strength at higher Mach number. These trends illustrate that, for a given Mach number, gas conductivity, load factor, and MHD expansion angle, increasing the magnetic field strength is an effective approach to augmenting generator output. It should be noted, however, that losses from the Hall effect, which are neglected in the current study, become more severe at higher magnetic field strengths, thus caution must be shown when varying this particular parameter in the model.

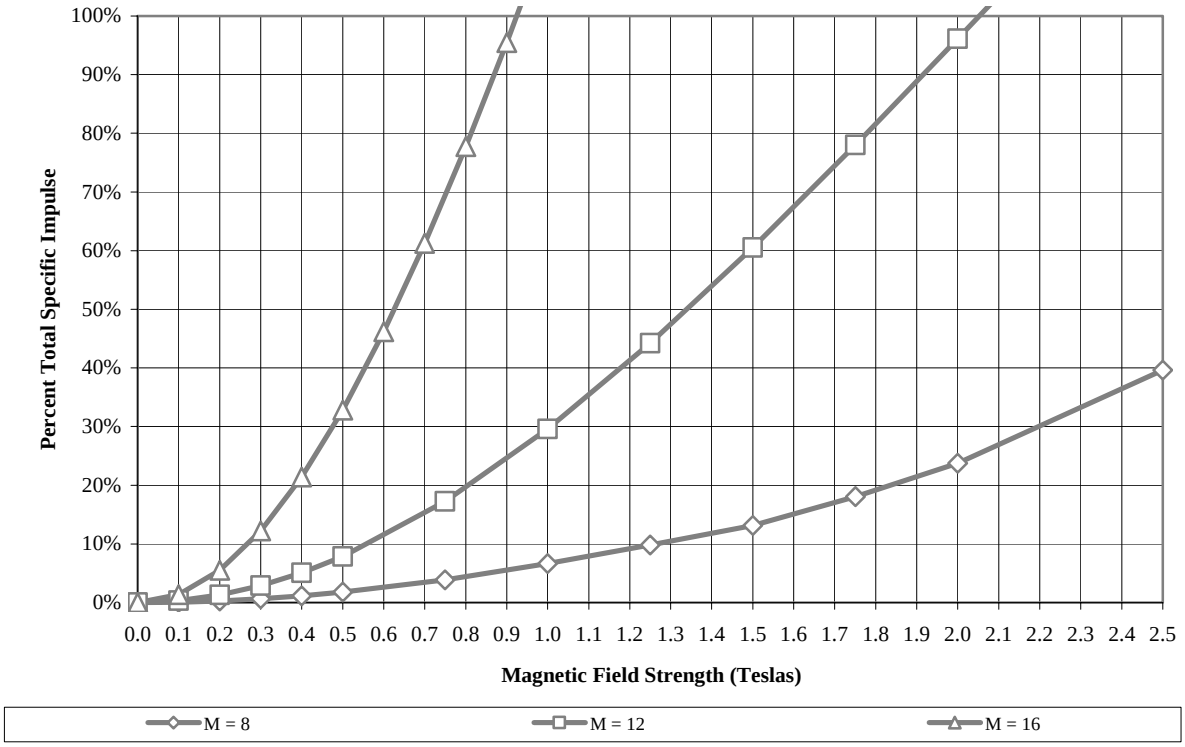

Figure 5.8: Percent power generated by MHD versus magnetic field strength for three different Mach numbers.

5.4. RESULTS AS GAS CONDUSTIVITY VARIES

Results are discussed in this section for variable gas conductivities. In this work (to define completely the potential), the upper extent of conductivity was extended to 1000 mhos per meter, about ten times the equilibrium ionization possible with a potassium seed at the temperatures generated. As shown in Figure 5.9, all three specific impulses vary linearly with gas conductivity throughout the extended range. The positive slope of total specific impulse curves demonstrate that specific MHD impulse grows faster with gas conductivity than the specific impulse declines.

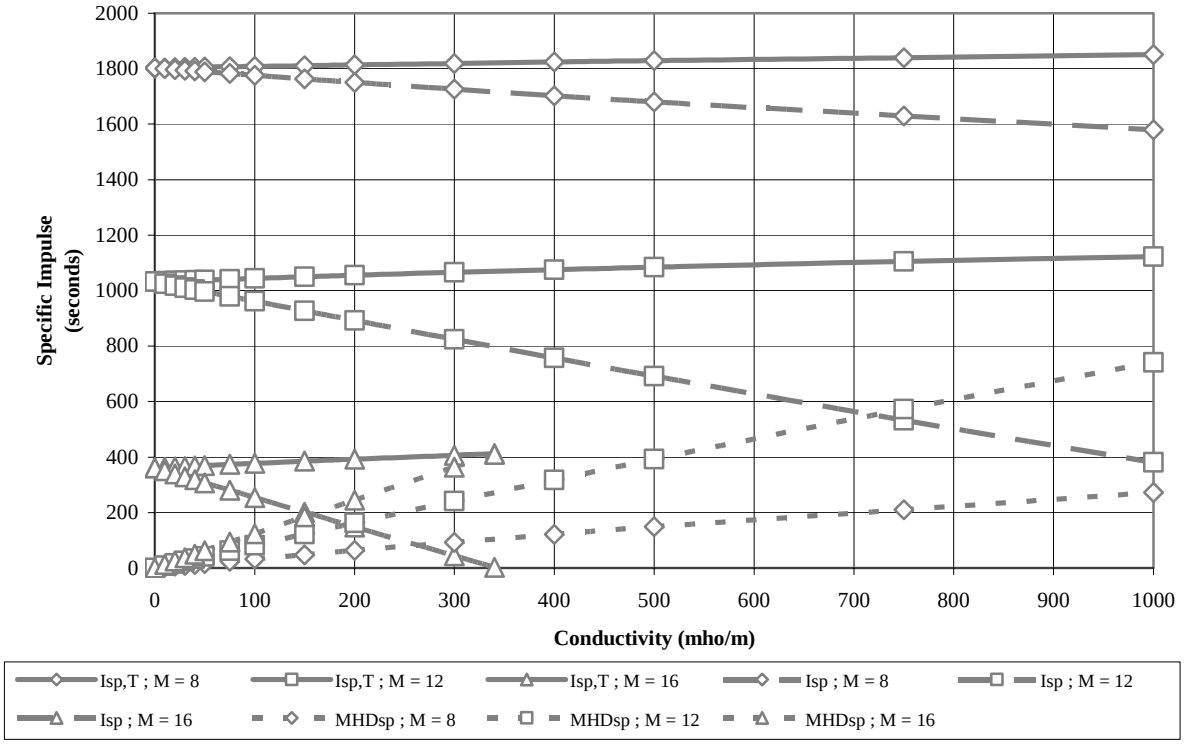

Figure 5.9: Specific impulses versus gas conductivity at three Mach numbers.

Figure 5.10 plots the percent of power generated by the MHD unit against varying gas conductivity. As expected, this quantity increases approximately linearly with conductivity. Additionally, as expected, the percent MHD increases more rapidly at higher Mach numbers. These results demonstrate that when compared to increasing magnetic field strength, increasing gas conductivity is a somewhat less effective approach, although still useful.

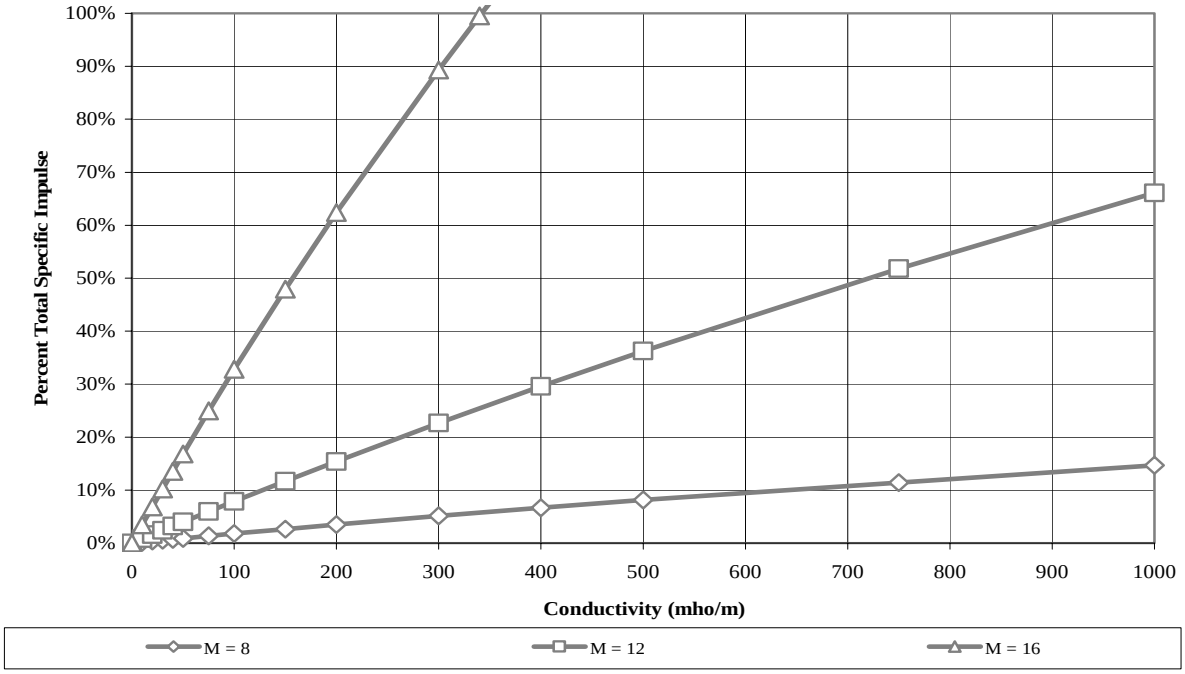

Figure 5.10: Percent power generated by MHD versus gas conductivity for three different Mach numbers.

5.5. RESULTS AS MHD LOAD FACTOR VARIES

In this section, the variation of the MHD generator load factor is examined against performance obtained. Figure 5.11 shows that with increasing load factor, specific impulse

decreases, specific MHD impulse increases, and total specific impulse increases. These performance changes as functions of MHD load factor are asymptotic. This observation follows from a close examination of the MHD equations since MHD power extracted varies with $1 - 1/\eta_{MHD}$. In addition, this observation leads to the conclusion that a load factor much above 3.0 would have such diminishing returns as to be unnecessary.

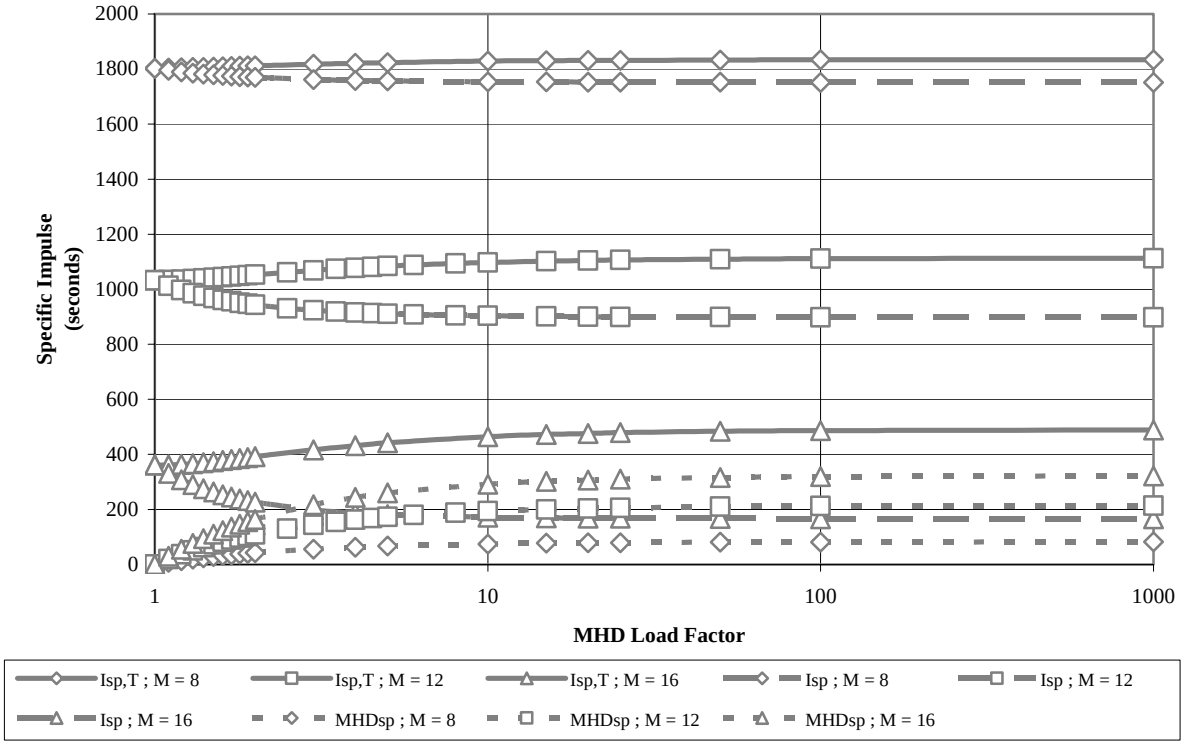

Figure 5.11: Specific impulses versus MHD load factor at three Mach numbers.

Figure 5.12 shows the percent power generated by MHD versus MHD load factor. Once again an asymptotic trend is shown with percent MHD increasing more rapidly at

higher Mach numbers, as expected. The trends related to load factor demonstrate that it is a less effective parameter when used to manipulate the generator output than either conductivity or magnetic field strength.

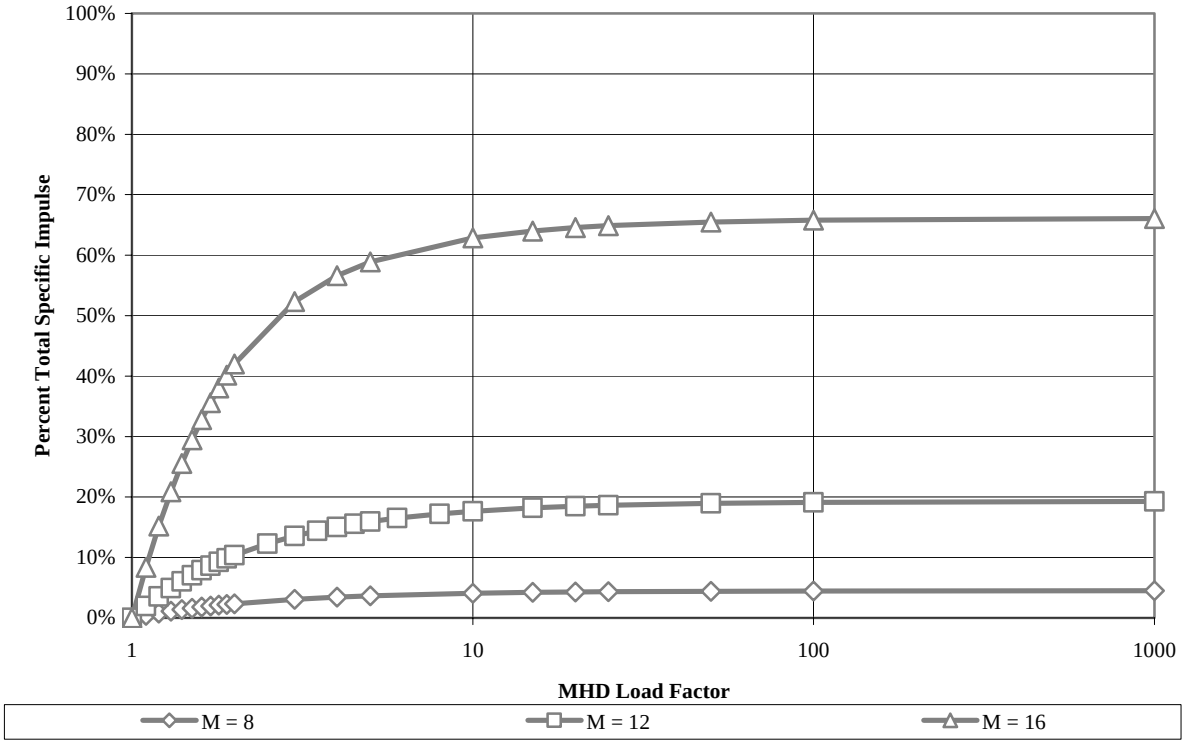

Figure 5.12: Percent power generated by MHD versus MHD load factor for three different Mach numbers.

5.6. RESULTS AS MHD GENERATOR EXPANSION VARIES

Though not an electromagnetic property, another parameter that can be varied within the engine system is the MHD generator expansion angle θ_M (see Figure 3.1). In Figure 5.13, an interesting result of varying this parameter can be seen; specifically, specific impulse with

no MHD interaction increases as expansion angle increases. This increase results because, at all conditions, the flow exiting the nozzle is under-expanded, so more expansion means more thrust. Additionally, since the downstream 75% of the nozzle length is open (aft of the lower cowl trailing edge), more expansion in a closed portion of the engine inevitably produces more thrust. Basically, it is seen that with the MHD turned off, an expanding MHD generator acts like additional closed nozzle length. When the MHD is turned on however, results differ substantially. First, for all three Mach numbers, specific MHD impulse and total specific impulse increase throughout the expansion angle range. Specific impulse increases throughout the expansion angle range for Mach 8. For Mach 12, specific impulse increases

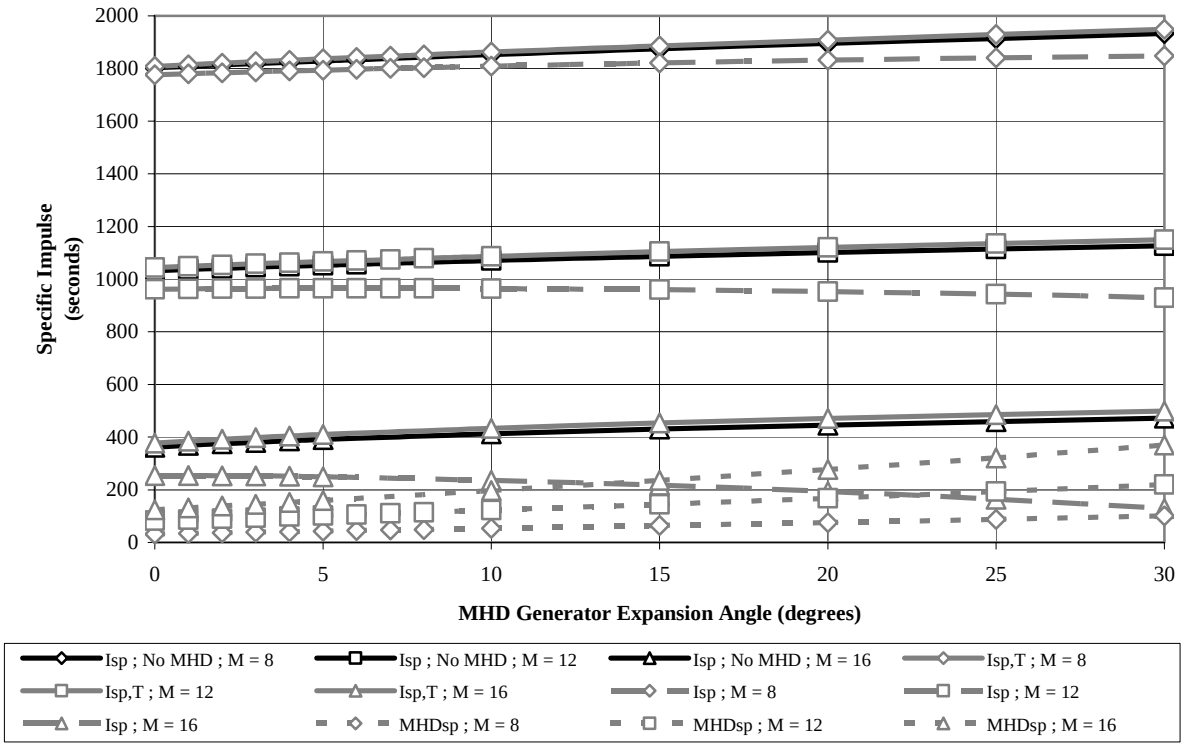

Figure 5.13: Specific impulses versus MHD generator expansion angle at three Mach numbers.

up to an expansion angle of six degrees and then begins decreasing. For Mach 16, specific impulse increases only gradually up to an angle of three degrees and then begins decreasing. The trend for the specific impulse results from two contrary interactions, the production of more thrust resulting from more closed expansion as noted above, and the fact that the MHD generator is extracting more energy. This increased energy extraction is explained as follows: in an expanding duct the velocity increases (for supersonic flow); the greater the rate at which the duct is expanding, the greater the rate at which the velocity is increasing; since the MHD equations contain the velocity as a variable, MHD power generation increases with increasing velocity. Thus at some peak angle, the velocity will be increasing rapidly enough such that any thrust increase that would have been realized (without MHD) is simply absorbed into MHD power generation. Additionally, it would be expected that stronger MHD interactions in the generator, i.e. higher magnetic field strength or gas conductivity, would tend to shift this peak angle lower, as does higher Mach numbers.

Figure 5.14 relates the percentage of power generated in the MHD unit to the expansion angle. This figure shows that at all three Mach numbers, the percent power generated in the MHD unit varies linearly with expansion angle with the observed increase more rapid at higher Mach numbers (than seen with all previous parameter variations). The results with varying expansion angle show that an expanding MHD generator benefits the engine at all conditions. Not only is more thrust generated with no MHD interaction, lower magnetic field and gas conductivities could be used to generate the same amount of electric power.

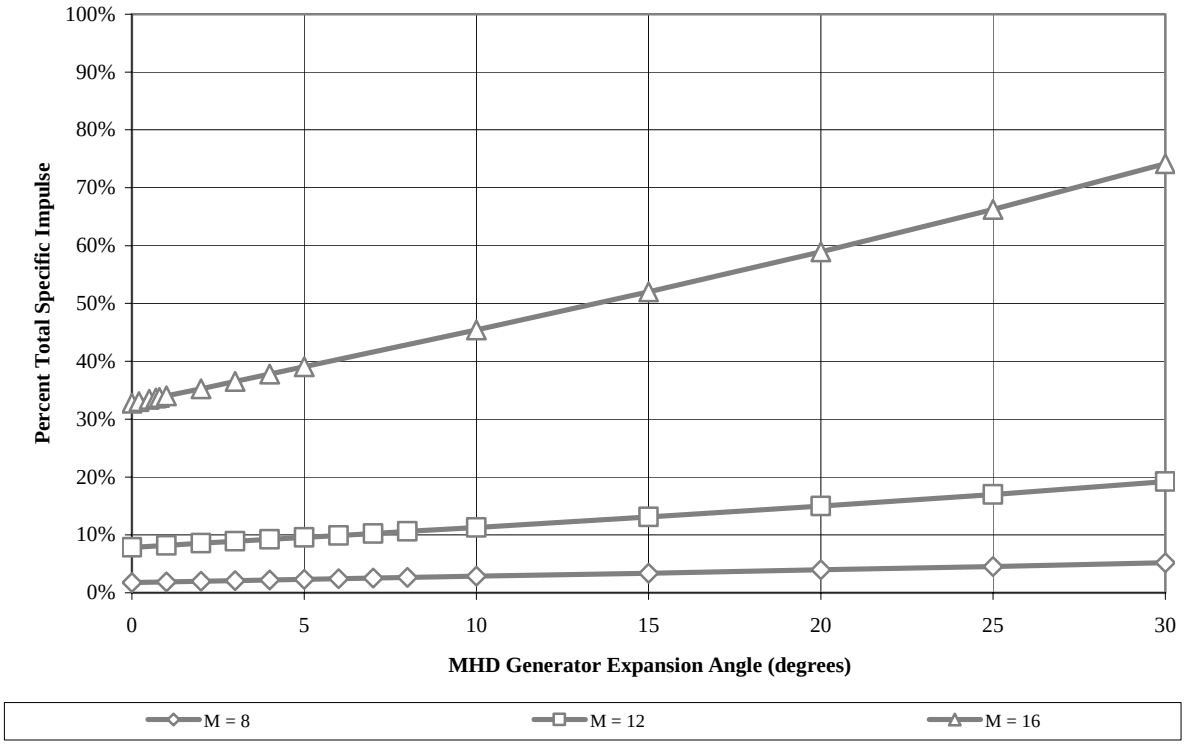

Figure 5.14: Percent power generated by MHD versus MHD generator expansion angle for three different Mach numbers.

6. SUMMARY OF IMPORTANT DATA TRENDS

For convience in summarizing important data trends developed in this work, a series of model equations (curve-fits) were developed directly from the results obtained to usefully describe vehicle performance with the MHD generator. Essentially, these model equations are simplified curve-fit equations to allow rapid assessment of performance for ranges of the parameters tested in this work. To begin this process, a curve-fit equation for the ideal specific impulse versus flight Mach number is found. Symbolically, the ideal specific impulse is:

$$I_{sp,ideal} = \frac{(1+f_{ST})U_9 - U_0}{f_{ST} g_0}$$

This is converted to be in terms of Mach number, using the result of the ideal process that $M_9 = M_0$ (as shown in Appendix C). Further, it can be found that the exit temperature T_9 is equal to the quotient of two functions of Mach squared:

$$T_9 = \frac{g(M^2)}{h(M^2)}$$

With all of the above taken into account, the model form of the ideal specific impulse equation becomes:

$$I_{sp,ideal} \cong \left[72.35 \left(\frac{43.33 M_0{}^2 + 3970}{.2 M_0{}^2 + 1} \right)^{1/2} - 1034.8 \right] M_0 \qquad (6.1)$$

The non-ideal specific impulse as produced by the model with no MHD is taken to be a fraction of the ideal specific impulse. This fraction is itself a function of Mach number and MHD generator expansion angle:

$$\frac{I_{sp,noMHD}}{I_{sp,ideal}} \cong 0.46 + 0.0045M_0 - 0.0016{M_0}^2 + 0.0011\theta_M \tag{6.2}$$

The equations describing the effects of the MHD generator are found to be independent of engine's specific impulse with no MHD interaction. First, to find the specific MHD impulse, its definition from Eqs. 5.4 and 5.5 should be examined. This definition coupled with the observations made in Section 5 leads to the following for the specific MHD impulse curve-fit equation:

$$MHD_{sp} \cong \zeta\left[\sigma M_0^2 B^2\left(1-\frac{1}{\eta_{MHD}}\right)\right]$$

Here ζ is a proportionality constant that is itself a function of MHD generator expansion angle. Through analysis, it was found that $\zeta = 0.0582 + 0.0032\theta_M$. Thus the complete equation for specific MHD impulse can be written as follows:

$$MHD_{sp} \cong \sigma M_0^2 B^2\left(1-\frac{1}{\eta_{MHD}}\right)\left(0.0582 + 0.0032\theta_M\right) \tag{6.3}$$

Next, the impact of the MHD interactions on the thrust is found, i.e. the thrust loss because of MHD interactions as compared to the thrust with no MHD. It can be determined that the thrust loss will be proportional to the irreversibility introduced by the MHD generator, thus:

$$I_{sp,noMHD} - I_{sp} \approx q_{EM} - w_{EM}$$

Substituting in the previously defined expressions for q_{EM} and w_{EM}, the following equation is constructed:

$$I_{sp,noMHD} - I_{sp} \cong \xi\left[\sigma M_0^2 B^2\left(1-\frac{1}{\eta_{MHD}^2}\right)\right]$$

The only differences between this equation and that for specific MHD impulse is the exponent on the load factor and the value of the proportionality constant which is once again a linear function of MHD generator expansion angle. The proportionality constant is found to be $\xi = 0.0304 + 0.0018\theta_M$, which makes the complete expression for the specific impulse loss due to the MHD generator the following:

$$I_{sp,noMHD} - I_{sp} \cong \sigma M_0^2 B^2 \left(1 - \frac{1}{\eta_{MHD}^2}\right)(0.0304 + .0018\theta_M) \tag{6.4}$$

Total specific impulse and percent power of the MHD generator can be found by substituting the performance quantities calculated from Eqs. 6.2 – 6.4 into the relevant place within Eqs. 5.7 and 5.9, respectively.

Equations 6.1 through 6.4 (with 5.7 and 5.9) summarize all of the trends found in this study, though as modeled curve-fit relationships they are approximate. It should be noted that these equations have not been tested rigorously within the solution domain, so it may be possible to find cases that they do not describe. This is especially true for the MHD generator expansion angle terms as the effect of this angle was only examined with no MHD and for the MHD base case. However, the solution domain over which these equations should be essentially useful is:

$$8 \le M_0 \le 16 \quad 0 \le B \le 2.5 Teslas \quad 0 \le \sigma \le 500 mho/m \quad 1 \le \eta_{MHD} \le 3 \quad 0 \le \theta_M \le 15 \deg.$$

To venture outside this range would introduce great uncertainty.

7. CONCLUSIONS

A magnetohydrodynamic generator placed between the combustor and the nozzle of a scramjet engine can be used to remove energy from the flow and convert it into electrical energy. Using this approach, the amount of power that can be extracted and converted into electricity ranges from no power on the low end to an amount in excess of the complete thrust power of the engine on the high end (making the engine produce a force opposite the direction the vehicle is moving). Of course, since the purpose of the engine is the generation of thrust, it is not desirable to remove all of the thrust power. It was also found that in general, the amount of power produced by the MHD generator and the resulting loss of thrust both vary quadratically with Mach number and magnetic field strength, linearly with conductivity and MHD generator expansion angle, and asymptotically with MHD load factor, though to different degrees. Relationships are developed by curve-fitting the results obtained in this investigation in order to allow rapid approximate assessment of vehicle performance for the ranges of parameters tested. It is concluded that a post combustor MHD generator can be used to remove energy from a scramjet flow field to power onboard systems or other devices. Further, at a given Mach number, the amount of power generated can be controlled by varying the magnetic field strength, gas conductivity (through the amount of seed material), and the MHD load factor (via the electrical field strength). Finally, the configuration should include an expanding area MHD generator since this can both improve overall engine specific impulse and the amount of power produced by the MHD generator.

APPENDIX A: COMPLETE COMPUTER CODE OF THE MODEL

```
clear all

PSL=101325; %Pascals

TSL=288.16; %Kelvin
Runiv=8314.4;
gSL=9.81; %m/s^2 Sea Level Gravity
RadiusEarth=6.356766E6; %meters


epsilon=.00001; %Error in numerically solved calculations

%Air Thermodynamic Properties
PercO2Air=.21;
PercN2Air=.79;
MwO2=31.999;
MwN2=28.013;
MwAir=PercO2Air*MwO2+PercN2Air*MwN2;
Rair=Runiv/MwAir;
yIdeal=1.4;

%Inlet Compressor Parameters – 2-shock
thetaC=12*pi/180; %Inlet Compression Angle, must not exceed 20 deg.
Inlet=1; %Vertical distance from Nose to Top of Combustor
CompLength=Inlet*cot(thetaC);
Width=1;

%Combustor Parameters
CombLength=.5;
CfComb=0.007; %Combustor Friction Coefficient
thetaCombI=0*pi/180.;
TwComb=1000; %Combustor Wall Temperature, K
CombRelax=.9;

%Fuel Properties – H2
numC=0; %number of Carbon atoms in fuel
numH=2; %number of Hydrogen atome in fuel
h=130000000; %Fuel Heating Value
FuelToAirRatio=(36*numC+3*numH)/(103*(4*numC+numH)); %Stoichiometic Fuel to Air Ratio
qmax=h*FuelToAirRatio/(1+FuelToAirRatio);
Mwf=2.016;
Rf=Runiv/Mwf;
yf=1.4;
Cpf=yf/(yf-1)*Rf;
Tfl=100; %Cryogenic Hydrogen initial temperature
Mfinj=2.0; %Injection mach number of the fuel
Ptfinj=2*PSL;
Pfinj=Ptfinj/(1+(yf-1)/2*Mfinj^2)^(yf/(yf-1));

%Combustion Product Thermodynamic Properties
Mwp=18.015;
Rp=Runiv/Mwp;
yp=1.327;
Cpp=yp/(yp-1)*Rp;

%Fuel Mixing Parameters: EtaMix=1-exp(-MixPow*(CombLength/(U2*MixTime)))
MixPow=13.3;
MixTime=1e-3;

%MHD Generator Properties
MHDLength=.5;
CfMHD=.001; %MHD Generator Friction Coefficient
thetaMHDI=0.0*pi/180;
TwMHD=800; %MHD Gen. Wall Temp., K
MHDRelax=.9;
Bfield=0.5; %Magnetic Field Strength in Teslas
EtaMHD=1.6; %EtaMHD=uB/Ey Second Law effectiveness of the generator, aka load factor
Cond=100;
```

```
dxMHD=.0001;

%Nozzle Properties
CfNoz=0.001;%Nozzle Friction Coefficient
NozzleLength=4.0;
dxNoz=.0001;
PercNozCl=25;%Percent of Nozzle Enclosed

%Vehicle Properties
VehicleLength=CompLength+CombLength+MHDLength+NozzleLength;
thetaT=1*pi/180;
Exit=Inlet+VehicleLength*tan(thetaT);


%Specified Vehicle Freestream Parameters
M0=[8]; %Mach is limited from 8 to 25
q0=101325; %Flight Dynamic pressure, 1ATM
P0=q0*2*(yIdeal*M0.^2).^-1;

%Standard Atmosphere Calculation
AltGp=0:10:105000; %meters
for cnt=1:1:max(size(AltGp));
    if AltGp(cnt)<=11000;
        Tatm(cnt)=TSL-6.5e-3*AltGp(cnt);
        Patm(cnt)=PSL*(Tatm(cnt)/TSL)^(-gSL/(-6.5e-3*Rair));
        if AltGp(cnt)==11000;
            cnt1=cnt;
        end
    elseif AltGp(cnt)<=25000;
        Tatm(cnt)=216.66;
        Patm(cnt)=Patm(cnt1)*exp(-gSL/(Rair*Tatm(cnt))*(AltGp(cnt)-11000));
        if AltGp(cnt)==25000;
            cnt1=cnt;
        end
    elseif AltGp(cnt)<=47000;
        Tatm(cnt)=216.66+3e-3*(AltGp(cnt)-25000);
        Patm(cnt)=Patm(cnt1)*(Tatm(cnt)/Tatm(cnt1))^(-gSL/(3e-3*Rair));
        if AltGp(cnt)==47000;
            cnt1=cnt;
        end
    elseif AltGp(cnt)<=53000;
        Tatm(cnt)=282.66;
        Patm(cnt)=Patm(cnt1)*exp(-gSL/(Rair*Tatm(cnt))*(AltGp(cnt)-47000));
        if AltGp(cnt)==53000;
            cnt1=cnt;
        end
    elseif AltGp(cnt)<=79000;
        Tatm(cnt)=282.66-4.5e-3*(AltGp(cnt)-53000);
        Patm(cnt)=Patm(cnt1)*(Tatm(cnt)/Tatm(cnt1))^(-gSL/(-4.5e-3*Rair));
        if AltGp(cnt)==79000;
            cnt1=cnt;
        end
    elseif AltGp(cnt)<=90000;
        Tatm(cnt)=165.66;
        Patm(cnt)=Patm(cnt1)*exp(-gSL/(Rair*Tatm(cnt))*(AltGp(cnt)-79000));
        if AltGp(cnt)==90000;
            cnt1=cnt;
        end
    else
        Tatm(cnt)=165.66+4e-3*(AltGp(cnt)-90000);
        Patm(cnt)=Patm(cnt1)*(Tatm(cnt)/Tatm(cnt1))^(-gSL/(4e-3*Rair));
    end
    muatm(cnt)=1.46e-6*((Tatm(cnt)^(2/3))/(Tatm(cnt)+111));%Absolute Viscosity, Sutherland's Law
    katm(cnt)=1.99e-3*((Tatm(cnt)^(2/3))/(Tatm(cnt)+112));%Air Thermal Conductivity, Sutherland's Law
    rhoatm(cnt)=Patm(cnt)/(Rair*Tatm(cnt));%Density
end

AltGm=RadiusEarth*AltGp.*(RadiusEarth-AltGp).^-1;
```

```
%End Standard Atmosphere Calculation

%Beginning of Engine Evaluation
for here=1:1:max(size(M0));
%Calculation of Freestream Properites based on Constant Dynamic Pressure
   match=1e100;
   for place=1:1:max(size(AltGp))
     if abs(P0(here)-Patm(place))<match;
         AltGp0(here)=AltGp(place);
         AltGm0(here)=AltGm(place);
         T0(here)=Tatm(place);
         rho0(here)=rhoatm(place);
         match=abs(P0(here)-Patm(place));
     else
         break
     end
   end
   TI=T0(here);
   if TI>1000;
      CpN2barI=Runiv*(2.95257626+1.39690057e-3*TI-4.92631691e-7*TI^2+7.86010367e-11*TI^3-4.60755321e-15*TI^4);
      CpO2barI=Runiv*(3.66096083+6.56365523e-4*TI-1.41149485e-7*TI^2+2.05797658e-11*TI^3-1.29913248e-15*TI^4);
   else
      CpN2barI=Runiv*(3.53100528-1.23660987e-4*TI-5.02999437e-7*TI^2+2.43530612e-9*TI^3-1.40881235e-12*TI^4);
      CpO2barI=Runiv*(3.78245636-2.99673415e-3*TI+9.84730200e-6*TI^2-9.68129508e-9*TI^3+3.24372836e-12*TI^4);
   end
   CpIbar=PercN2Air*CpN2barI+PercO2Air*CpO2barI;
   Cp0(here)=CpIbar/MwAir;
   y0(here)=Cp0(here)/(Cp0(here)-Rair);
   Tt0(here)=T0(here)*(1+(y0(here)-1)/2*M0(here)^2);
   a0(here)=(y0(here)*Rair*T0(here))^.5;
   U0(here)=M0(here)*a0(here);
%End Freestream Property Evalutaion


%Compressor Evaluation
   %Calculation for the first oblique shock
   delta1=.1;

   beta1AGUp=33*pi/180;
   beta1AGDn=thetaC;
   beta1A(here)=(beta1AGDn+beta1AGUp)/2;
   while abs(tan(beta1A(here)-thetaC)/tan(beta1A(here))-delta1)>epsilon;
      if tan(beta1A(here)-thetaC)/tan(beta1A(here))-delta1<0;
         beta1AGDn=beta1A(here);
      else
         beta1AGUp=beta1A(here);
      end
      beta1A(here)=(beta1AGDn+beta1AGUp)/2;
   end
   M0N=M0(here)*sin(beta1A(here));
   U0N=M0N*a0(here);

   P1A(here)=P0(here)+rho0(here)*U0N^2*(1-delta1);
   h1A=Cp0(here)*T0(here)+U0N^2/2*(1-delta1^2);

   TI=T0(here);
   if TI>1000;
      CpN2barI=Runiv*(2.95257626+1.39690057e-3*TI-4.92631691e-7*TI^2+7.86010367e-11*TI^3-4.60755321e-15*TI^4);
      CpO2barI=Runiv*(3.66096083+6.56365523e-4*TI-1.41149485e-7*TI^2+2.05797658e-11*TI^3-1.29913248e-15*TI^4);
   else
      CpN2barI=Runiv*(3.53100528-1.23660987e-4*TI-5.02999437e-7*TI^2+2.43530612e-9*TI^3-1.40881235e-12*TI^4);
      CpO2barI=Runiv*(3.78245636-2.99673415e-3*TI+9.84730200e-6*TI^2-9.68129508e-9*TI^3+3.24372836e-12*TI^4);
   end
   CpIbar=PercN2Air*CpN2barI+PercO2Air*CpO2barI;
   Cp1A=CpIbar/MwAir;
   y1A=Cp1A/(Cp1A-Rair);
   T1A(here)=h1A/Cp1A;
```

```
while abs(T1A-TI)/T1A>epsilon;
   TI=T1A;
   if TI>1000;
      CpN2barI=Runiv*(2.95257626+1.39690057e-3*TI-4.92631691e-7*TI^2+7.86010367e-11*TI^3-4.60755321e-15*TI^4);
      Cp02barI=Runiv*(3.66096083+6.56365523e-4*TI-1.41149485e-7*TI^2+2.05797658e-11*TI^3-1.29913248e-15*TI^4);
   else
      CpN2barI=Runiv*(3.53100528-1.23660987e-4*TI-5.02999437e-7*TI^2+2.43530612e-9*TI^3-1.40881235e-12*TI^4);
      Cp02barI=Runiv*(3.78245636-2.99673415e-3*TI+9.84730200e-6*TI^2-9.68129508e-9*TI^3+3.24372836e-12*TI^4);
   end
   CpIbar=PercN2Air*CpN2barI+Perc02Air*Cp02barI;
   Cp1A=CpIbar/MwAir;
   y1A=Cp1A/(Cp1A-Rair);
   T1A(here)=h1A/Cp1A;
end
rho1A=P1A(here)/(Rair*T1A(here));
delta1Chk=rho0(here)/rho1A;
i=1;
while abs((delta1-delta1Chk)/delta1)>epsilon;
   delta1=delta1Chk;
   beta1AGUp=33*pi/180;
   beta1AGDn=thetaC;
   beta1A(here)=(beta1AGDn+beta1AGUp)/2;
   while abs(tan(beta1A(here)-thetaC)/tan(beta1A(here))-delta1)>epsilon;
      if tan(beta1A(here)-thetaC)/tan(beta1A(here))-delta1<0;
         beta1AGDn=beta1A(here);
      else
         beta1AGUp=beta1A(here);
      end
      beta1A(here)=(beta1AGDn+beta1AGUp)/2;
   end
   M0N=M0(here)*sin(beta1A(here));
   U0N=M0N*a0(here);
   P1A(here)=P0(here)+rho0(here)*U0N^2*(1-delta1);
   h1A=Cp0(here)*T0(here)+U0N^2/2*(1-delta1^2);

   TI=T0(here);
   if TI>1000;
      CpN2barI=Runiv*(2.95257626+1.39690057e-3*TI-4.92631691e-7*TI^2+7.86010367e-11*TI^3-4.60755321e-15*TI^4);
      Cp02barI=Runiv*(3.66096083+6.56365523e-4*TI-1.41149485e-7*TI^2+2.05797658e-11*TI^3-1.29913248e-15*TI^4);
   else
      CpN2barI=Runiv*(3.53100528-1.23660987e-4*TI-5.02999437e-7*TI^2+2.43530612e-9*TI^3-1.40881235e-12*TI^4);
      Cp02barI=Runiv*(3.78245636-2.99673415e-3*TI+9.84730200e-6*TI^2-9.68129508e-9*TI^3+3.24372836e-12*TI^4);
   end
   CpIbar=PercN2Air*CpN2barI+Perc02Air*Cp02barI;
   Cp1A=CpIbar/MwAir;
   y1A=Cp1A/(Cp1A-Rair);
   T1A(here)=h1A/Cp1A;

   while abs(T1A(here)-TI)/T1A(here)>epsilon;
      TI=T1A;
      if TI>1000;
         CpN2barI=Runiv*(2.95257626+1.39690057e-3*TI-4.92631691e-7*TI^2+7.86010367e-11*TI^3-4.60755321e-15*TI^4);
         Cp02barI=Runiv*(3.66096083+6.56365523e-4*TI-1.41149485e-7*TI^2+2.05797658e-11*TI^3-1.29913248e-15*TI^4);
      else
         CpN2barI=Runiv*(3.53100528-1.23660987e-4*TI-5.02999437e-7*TI^2+2.43530612e-9*TI^3-1.40881235e-12*TI^4);
         Cp02barI=Runiv*(3.78245636-2.99673415e-3*TI+9.84730200e-6*TI^2-9.68129508e-9*TI^3+3.24372836e-12*TI^4);
      end
      CpIbar=PercN2Air*CpN2barI+Perc02Air*Cp02barI;
      Cp1A=CpIbar/MwAir;
      y1A=Cp1A/(Cp1A-Rair);
      T1A(here)=h1A/Cp1A;
   end
   rho1A=P1A(here)/(Rair*T1A(here));
   delta1Chk=rho0(here)/rho1A;
   i=i+1;
   if i>=5000;
      'First Shock Loop exited'
      Perror=abs((delta1-delta1Chk)/delta1)
```

```
        break
    end
end
U1NA=U0N*delta1;
U1A=U1NA/sin(beta1A(here)-thetaC);
a1A=(y1A*Rair*T1A(here))^.5;
M1A=U1A/a1A;

%Calculation for the second, reflected oblique shock
delta2=.1;

beta1BGUp=33*pi/180;
beta1BGDn=thetaC;
beta1B(here)=(beta1BGDn+beta1BGUp)/2;
while abs(tan(beta1B(here)-thetaC)/tan(beta1B(here))-delta2)>epsilon;
    if tan(beta1B(here)-thetaC)/tan(beta1B(here))-delta2<0;
        beta1BGDn=beta1B(here);
    else
        beta1BGUp=beta1B(here);
    end
    beta1B(here)=(beta1BGDn+beta1BGUp)/2;
end
M1NA2=M1A*sin(beta1B(here));
U1NA2=M1NA2*a1A;
P1B(here)=P1A(here)+rho1A*U1NA2^2*(1-delta2);
h1B=Cp1A*T1A(here)+U1NA2^2/2*(1-delta2^2);

TI=T1A(here);
if TI>1000;
    CpN2barI=Runiv*(2.95257626+1.39690057e-3*TI-4.92631691e-7*TI^2+7.86010367e-11*TI^3-4.60755321e-15*TI^4);
    Cp02barI=Runiv*(3.66096083+6.56365523e-4*TI-1.41149485e-7*TI^2+2.05797658e-11*TI^3-1.29913248e-15*TI^4);
else
    CpN2barI=Runiv*(3.53100528-1.23660987e-4*TI-5.02999437e-7*TI^2+2.43530612e-9*TI^3-1.40881235e-12*TI^4);
    Cp02barI=Runiv*(3.78245636-2.99673415e-3*TI+9.84730200e-6*TI^2-9.68129508e-9*TI^3+3.24372836e-12*TI^4);
end
CpIbar=PercN2Air*CpN2barI+Perc02Air*Cp02barI;
Cp1B=CpIbar/MwAir;
y1B=Cp1B/(Cp1B-Rair);
T1B(here)=h1B/Cp1B;

while abs(T1B-TI)/T1B>epsilon;
    TI=T1B;
    if TI>1000;
        CpN2barI=Runiv*(2.95257626+1.39690057e-3*TI-4.92631691e-7*TI^2+7.86010367e-11*TI^3-4.60755321e-15*TI^4);
        Cp02barI=Runiv*(3.66096083+6.56365523e-4*TI-1.41149485e-7*TI^2+2.05797658e-11*TI^3-1.29913248e-15*TI^4);
    else
        CpN2barI=Runiv*(3.53100528-1.23660987e-4*TI-5.02999437e-7*TI^2+2.43530612e-9*TI^3-1.40881235e-12*TI^4);
        Cp02barI=Runiv*(3.78245636-2.99673415e-3*TI+9.84730200e-6*TI^2-9.68129508e-9*TI^3+3.24372836e-12*TI^4);
    end
    CpIbar=PercN2Air*CpN2barI+Perc02Air*Cp02barI;
    Cp1B=CpIbar/MwAir;
    y1B=Cp1B/(Cp1B-Rair);
    T1B(here)=h1B/Cp1B;
end
rho1B=P1B(here)/(Rair*T1B(here));
delta2Chk=rho1A/rho1B;
j=1;
while abs((delta2-delta2Chk)/delta2)>epsilon;
    delta2=delta2Chk;
    beta1BGUp=33*pi/180;
    beta1BGDn=thetaC;
    beta1B(here)=(beta1BGDn+beta1BGUp)/2;
    while abs(tan(beta1B(here)-thetaC)/tan(beta1B(here))-delta2)>epsilon;
        if tan(beta1B(here)-thetaC)/tan(beta1B(here))-delta2<0;
            beta1BGDn=beta1B(here);
        else
            beta1BGUp=beta1B(here);
        end
```

```
        beta1B(here)=(beta1BGDn+beta1BGUp)/2;
    end
    M1NA2=M1A*sin(beta1B(here));
    U1NA2=M1NA2*a1A;
    P1B(here)=P1A(here)+rho1A*U1NA2^2*(1-delta2);
    h1B=Cp1A*T1A(here)+U1NA2^2/2*(1-delta2^2);

    TI=T1A(here);
    if TI>1000;
        CpN2barI=Runiv*(2.95257626+1.39690057e-3*TI-4.92631691e-7*TI^2+7.86010367e-11*TI^3-4.60755321e-15*TI^4);
        Cp02barI=Runiv*(3.66096083+6.56365523e-4*TI-1.41149485e-7*TI^2+2.05797658e-11*TI^3-1.29913248e-15*TI^4);
    else
        CpN2barI=Runiv*(3.53100528-1.23660987e-4*TI-5.02999437e-7*TI^2+2.43530612e-9*TI^3-1.40881235e-12*TI^4);
        Cp02barI=Runiv*(3.78245636-2.99673415e-3*TI+9.84730200e-6*TI^2-9.68129508e-9*TI^3+3.24372836e-12*TI^4);
    end
    CpIbar=PercN2Air*CpN2barI+Perc02Air*Cp02barI;
    Cp1B=CpIbar/MwAir;
    y1B=Cp1B/(Cp1B-Rair);
    T1B(here)=h1B/Cp1B;

    while abs(T1B-TI)/T1B>epsilon;
        TI=T1B;
        if TI>1000;
            CpN2barI=Runiv*(2.95257626+1.39690057e-3*TI-4.92631691e-7*TI^2+7.86010367e-11*TI^3-4.60755321e-15*TI^4);
            Cp02barI=Runiv*(3.66096083+6.56365523e-4*TI-1.41149485e-7*TI^2+2.05797658e-11*TI^3-1.29913248e-15*TI^4);
        else
            CpN2barI=Runiv*(3.53100528-1.23660987e-4*TI-5.02999437e-7*TI^2+2.43530612e-9*TI^3-1.40881235e-12*TI^4);
            Cp02barI=Runiv*(3.78245636-2.99673415e-3*TI+9.84730200e-6*TI^2-9.68129508e-9*TI^3+3.24372836e-12*TI^4);
        end
        CpIbar=PercN2Air*CpN2barI+Perc02Air*Cp02barI;
        Cp1B=CpIbar/MwAir;
        y1B=Cp1B/(Cp1B-Rair);
        T1B(here)=h1B/Cp1B;
    end
    rho1B=P1B(here)/(Rair*T1B(here));
    delta2Chk=rho1A/rho1B;
    j=j+1;
    if j>=5000;
        'Second Shock Loop exited'
        Perror=abs((delta2-delta2Chk)/delta2)
        break
    end
end
U1NB=U1NA2*delta2;
U1B=U1NB/sin(beta1B(here)-thetaC);
a1B=(y1B*Rair*T1B(here))^.5;
M1B=U1B/a1B;

CompExit=(CompLength-Inlet*cot(beta1A(here)))/(cot(beta1A(here))+cot(beta1B(here)-thetaC));
%End Compressor Evalutaion

%Compressor Exit/Combustor Entrance Properties
M2(here)=M1B;
P2=P1B;
Pt2=P2*(1+(y1B-1)/2*M2(here)^2)^(y1B/(y1B-1));
T2=T1B;
Tt2=T2*(1+(y1B-1)/2*M2(here)^2);
U2=M2(here)*(y1B*Rair*T2)^.5;
EtaMixMax(here)=1-exp(-MixPow*(CombLength/(U2*MixTime)));

%Combustor Evaluation
A2=CompExit*Width;
mdotair(here)=P2/(Rair*T2)*U2*A2;
q(here)=qmax;
mdotfuel(here)=mdotair(here)*FuelToAirRatio;
mdottotal(here)=mdotair(here)+mdotfuel(here);
ThrustComp(here)=mdotair(here)*(U2-U0(here))+P2*A2-P0(here)*(Inlet+CompExit)*Width;
```

```
%Loop for thermal balancing and fuel-air mixture properties
balanced=0;
balcount=0;
Ttfinj=1000;
while balanced==0;
    'Thermal Balancing'

    Tt3(here)=Tt2;
    M3(here)=M2;
    T3(here)=Tt3(here)/(1+(y1B-1)/2*M3(here)^2);
    Pt3(here)=Pt2;
    P3(here)=Pt3(here)/(1+(y1B-1)/2*M3(here)^2)^(y1B/(y1B-1));
    U3(here)=M3(here)*(y1B*Rair*T3(here))^.5;
    Cp3=Cp1B;
    y3=y1B;


%Quasi-1-D Combustor Analysis
    clear xComb;
    xComb(1)=0;
    thetaComb(here)=thetaCombI;
    while max(xComb)<CombLength-5*epsilon;
        'Start of Combustor Analysis'
        dydxComb(here)=tan(thetaComb(here));

    %One Step Fuel Air mixing
        Tfinj=Ttfinj/(1+(yf-1)/2*Mfinj^2);
        Ufinj=Mfinj*(yf*Rf*Tfinj)^.5;
        rhofinj=Pfinj/(Rf*Tfinj);
        Afinj=mdotfuel(here)/(rhofinj*Ufinj);

        mdotI=mdotair(here)+mdotfuel(here);
        CombEnt(here)=CompExit+Afinj/Width;
        PercN2I=(PercN2Air*mdotair(here)/MwAir)/(mdotair(here)/MwAir+mdotfuel(here)/Mwf);
        PercO2I=(PercO2Air*mdotair(here)/MwAir)/(mdotair(here)/MwAir+mdotfuel(here)/Mwf);
        PercH2OI=0;
        PercH2I=(mdotfuel(here)/Mwf)/(mdotair(here)/MwAir+mdotfuel(here)/Mwf);
        MwI=PercN2I*MwN2+PercO2I*MwO2+PercH2OI*Mwp+PercH2I*Mwf;
        RI=Runiv/MwI;

        TIGUp=Tfinj+T3(here);
        TIGDn=0;
        TI=(TIGUp+TIGDn)/2;

        if TI>6000;
            'Combustor Temperature Too HIGH'
            pause
        elseif TI>1000;
            CpN2barI=Runiv*(2.95257626+1.39690057e-3*TI-4.92631691e-7*TI^2+7.86010367e-11*TI^3-4.60755321e-15*TI^4);
            CpO2barI=Runiv*(3.66096083+6.56365523e-4*TI-1.41149485e-7*TI^2+2.05797658e-11*TI^3-1.29913248e-15*TI^4);
            CpH2ObarI=Runiv*(2.67703787+2.97318329e-3*TI-7.73769690e-7*TI^2+9.44336689e-11*TI^3-4.26900959e-15*TI^4);
            CpH2barI=Runiv*(2.93286579+8.26607967e-4*TI-1.46402335e-7*TI^2+1.54100359e-11*TI^3-6.88804432e-16*TI^4);
        else
            CpN2barI=Runiv*(3.53100528-1.23660987e-4*TI-5.02999437e-7*TI^2+2.43530612e-9*TI^3-1.408812l35e-12*TI^4);
            CpO2barI=Runiv*(3.78245636-2.99673415e-3*TI+9.84730200e-6*TI^2-9.68129508e-9*TI^3+3.24372836e-12*TI^4);
            CpH2ObarI=Runiv*(4.19864056-2.03643410e-3*TI+6.52040211e-6*TI^2-5.48797062e-9*TI^3+1.77197817e-12*TI^4);
            CpH2barI=Runiv*(2.34433112+7.98052075e-3*TI-1.94781510e-5*TI^2+2.01572094e-8*TI^3-7.37611761e-12*TI^4);
        end
        CpIbar=PercN2I*CpN2barI+PercO2I*CpO2barI+PercH2OI*CpH2ObarI+PercH2I*CpH2barI;
        CpI=CpIbar/MwI;
        yI=CpI/(CpI-RI);

        UI=(2*((mdotfuel(here)*(CpI*Tfinj+Ufinj^2/2)+mdotair(here)*(Cp3*T3(here)+U3(here)^2/2))/mdotI-CpI*TI))^.5;
        rhoI=mdotI/(CombEnt(here)*Width*UI);
        PI=(Afinj*Pfinj+Ufinj*mdotfuel(here)+A2*P3(here)+U3(here)*mdotair(here)-UI*mdotI)/(CombEnt(here)*Width);
        TIChk=PI/(RI*rhoI);
        while abs(TI-TIChk)/TI>epsilon;
            if TI-TIChk>0;
```

```
        TIGDn=TI;
    else
        TIGUp=TI;
    end
TI=(TIGUp+TIGDn)/2;

if TI>6000;
    'Combustor Temperature Too HIGH'
    pause
elseif TI>1000;
    CpN2barI=Runiv*(2.95257626+1.39690057e-3*TI-4.92631691e-7*TI^2+7.86010367e-11*TI^3-4.60755321e-15*TI^4);
    Cp02barI=Runiv*(3.66096083+6.56365523e-4*TI-1.41149485e-7*TI^2+2.05797658e-11*TI^3-1.29913248e-15*TI^4);
    CpH20barI=Runiv*(2.67703787+2.97318329e-3*TI-7.73769690e-7*TI^2+9.44336689e-11*TI^3-4.26900959e-15*TI^4);
    CpH2barI=Runiv*(2.93286579+8.26607967e-4*TI-1.46402335e-7*TI^2+1.54100359e-11*TI^3-6.88804432e-16*TI^4);
else
    CpN2barI=Runiv*(3.53100528-1.23660987e-4*TI-5.02999437e-7*TI^2+2.43530612e-9*TI^3-1.40881235e-12*TI^4);
    Cp02barI=Runiv*(3.78245636-2.99673415e-3*TI+9.84730200e-6*TI^2-9.68129508e-9*TI^3+3.24372836e-12*TI^4);
    CpH20barI=Runiv*(4.19864056-2.03643410e-3*TI+6.52040211e-6*TI^2-5.48797062e-9*TI^3+1.77197817e-12*TI^4);
    CpH2barI=Runiv*(2.34433112+7.98052075e-3*TI-1.94781510e-5*TI^2+2.01572094e-8*TI^3-7.37611761e-12*TI^4);
end
CpIbar=PercN2I*CpN2barI+Perc02I*Cp02barI+PercH20I*CpH20barI+PercH2I*CpH2barI;
CpI=CpIbar/MwI;
yI=CpI/(CpI-RI);

UI=(2*((mdotfuel(here)*(CpI*Tfinj+Ufinj^2/2)+mdotair(here)*(Cp3*T3(here)+U3(here)^2/2))/mdotI-CpI*TI))^.5;
rhoI=mdotI/(CombEnt(here)*Width*UI);
PI=(Afinj*Pfinj+Ufinj*mdotfuel(here)+A2*P3(here)+U3(here)*mdotair(here)-UI*mdotI)/(CombEnt(here)*Width);
TIChk=PI/(RI*rhoI);
end
MI=UI/(yI*RI*TI)^.5;
TtI=TI*(1+(yI-1)/2*MI^2);
PtI=PI*(1+(yI-1)/2*MI^2)^(yI/(yI-1));
ThrustMix(here)=UI*mdotI+CombEnt*Width*PI-(U3(here)*mdotair(here)+CompExit*Width*P3(here));
'Fuel and Air are mixed'
%End One Step Fuel Air Mixing

xI=0;
EtaMixI=0;

mark=0;
clear EtaMix;
EtaMix(1)=0;
while max(EtaMix)<EtaMixMax;
    mark=mark+1;
    if mod(mark,500)==0;
        mark
    end

    dEtaMix(mark)=1E-4;
    EtaMix(mark)=EtaMixI+dEtaMix(mark);
    xI=-(U2*MixTime)/MixPow*log(1-EtaMix(mark));
    if mark>1;
        dx=xI-xComb(mark-1);
    else
        dx=xI;
    end
    if dx>1E-4;
        dx=1E-4;
        xI=xComb(mark-1)+dx;
        EtaMix(mark)=1-exp(-MixPow*xI/(U2*MixTime));
        dEtaMix(mark)=EtaMix(mark)-EtaMixI;
    end
    if xI>CombLength;
        xI=CombLength;
        EtaMix(mark)=1-exp(-MixPow*xI/(U2*MixTime));
        dEtaMix(mark)=EtaMix(mark)-EtaMixI;
    end
    EtaMixI=EtaMix(mark);
```

```
        xComb(mark)=xI;
        dxComb(mark)=dx;
        mdotComb(mark)=mdotI;
        PercO2Comb(mark)=PercO2I;
        PercN2Comb(mark)=PercN2I;
        PercH2Ocomb(mark)=PercH2OI;
        PercH2Comb(mark)=PercH2I;
        MwComb(mark)=MwI;
        gamComb(mark)=yI;
        Rcomb(mark)=RI;
        CpComb(mark)=gamComb(mark)/(gamComb(mark)-1)*Rcomb(mark);
        TtComb(mark)=TtI;
        Tcomb(mark)=TI;
        Ucomb(mark)=UI;
        PtComb(mark)=PtI;
        Mcomb(mark)=MI;
        Pcomb(mark)=PtComb(mark)/(1+(gamComb(mark)-1)/2*Mcomb(mark)^2)^(gamComb(mark)/(gamComb(mark)-1));
        TtwComb(mark)=Tcomb(mark)*(1+CombRelax*(gamComb(mark)-1)/2*Mcomb(mark)^2);
        rhoComb(mark)=Pcomb(mark)/(Rcomb(mark)*Tcomb(mark));
        mdotComb(mark)=mdotI;

        yComb(mark)=CombEnt(here)+dydxComb(here)*(xComb(mark)+dx/2);
        dyComb(mark)=dydxComb(here)*dx;
        dAComb(mark)=dyComb(mark)*Width;
        Acomb(mark)=Width*yComb(mark);
        cComb(mark)=2*(Width+yComb(mark));
        mdotCombChk(mark)=rhoComb(mark)*Acomb(mark)*Ucomb(mark);


    %Differential Analysis
        PercN2I=(PercN2Comb(mark)*mdotComb(mark)/MwComb(mark))/(PercN2Comb(mark)*mdotComb(mark)/MwComb(mark)+PercO2Comb(mark)*mdotComb(mark)/MwComb(mark)-
.5*dEtaMix(mark)*mdotfuel(here)/Mwf+PercH2Ocomb(mark)*mdotComb(mark)/MwComb(mark)+dEtaMix(mark)*mdotfuel(here)+PercH2Comb(mark)*mdotComb(mark)/MwComb(mark)-
dEtaMix(mark)*mdotfuel(here)/Mwf);
        PercO2I=(PercO2Comb(mark)*mdotComb(mark)/MwComb(mark)-
.5*dEtaMix(mark)*mdotfuel(here)/Mwf)/(PercN2Comb(mark)*mdotComb(mark)/MwComb(mark)+PercO2Comb(mark)*mdotComb(mark)/MwComb(mark)-
.5*dEtaMix(mark)*mdotfuel(here)/Mwf+PercH2Ocomb(mark)*mdotComb(mark)/MwComb(mark)+dEtaMix(mark)*mdotfuel(here)+PercH2Comb(mark)*mdotComb(mark)/MwComb(mark)-
dEtaMix(mark)*mdotfuel(here)/Mwf);

PercH2OI=(PercH2Ocomb(mark)*mdotComb(mark)/MwComb(mark)+dEtaMix(mark)*mdotfuel(here)/Mwf)/(PercN2Comb(mark)*mdotComb(mark)/MwComb(mark)+PercO2Comb(mark)*mdotComb(m
ark)/MwComb(mark)-
.5*dEtaMix(mark)*mdotfuel(here)/Mwf+PercH2Ocomb(mark)*mdotComb(mark)/MwComb(mark)+dEtaMix(mark)*mdotfuel(here)+PercH2Comb(mark)*mdotComb(mark)/MwComb(mark)-
dEtaMix(mark)*mdotfuel(here)/Mwf);
        PercH2I=(PercH2Comb(mark)*mdotComb(mark)/MwComb(mark)-
dEtaMix(mark)*mdotfuel(here)/Mwf)/(PercN2Comb(mark)*mdotComb(mark)/MwComb(mark)+PercO2Comb(mark)*mdotComb(mark)/MwComb(mark)-
.5*dEtaMix(mark)*mdotfuel(here)/Mwf+PercH2Ocomb(mark)*mdotComb(mark)/MwComb(mark)+dEtaMix(mark)*mdotfuel(here)+PercH2Comb(mark)*mdotComb(mark)/MwComb(mark)-
dEtaMix(mark)*mdotfuel(here)/Mwf);
        MwI=PercN2I*MwN2+PercO2I*MwO2+PercH2OI*Mwp+PercH2I*Mwf;
        RI=Runiv/MwI;
        dRComb(mark)=RI-Rcomb(mark);

        dCpComb(mark)=CpI-CpComb(mark);

        dqCombustion(mark)=q(here)*dEtaMix(mark);
        dqWallComb(mark)=CpComb(mark)*CfComb/2*(TwComb-TtwComb(mark))*(cComb(mark)/Acomb(mark))*dx;
        if dqWallComb(mark)>0;
            dqWallComb(mark)=0;
        end
        dqTotalComb(mark)=dqCombustion(mark)+dqWallComb(mark);
        dTtComb(mark)=(dqTotalComb(mark)-(dCpComb(mark))*TtComb(mark))/CpI;
        dFricLossComb(mark)=CfComb*Ucomb(mark)^2/2*cComb(mark)/Acomb(mark)*dx;
        TtI=TtComb(mark)+dTtComb(mark);
        dsComb(mark)=(dqTotalComb(mark)+dFricLossComb(mark))/Tcomb(mark);
        dUComb(mark)=Ucomb(mark)/(Mcomb(mark)^2-1)*(1/(gamComb(mark)*Rcomb(mark)*Tcomb(mark))*(dqTotalComb(mark)-
gamComb(mark)*Tcomb(mark)*dsComb(mark)+(gamComb(mark)-1)*dCpComb(mark)*Tcomb(mark))+dAComb(mark)/Acomb(mark)-dRComb(mark)/Rcomb(mark));
        dPComb(mark)=rhoComb(mark)*(dqTotalComb(mark)-Ucomb(mark)*dUComb(mark)-Tcomb(mark)*dsComb(mark));
        UI=Ucomb(mark)+dUComb(mark);
        PI=Pcomb(mark)+dPComb(mark);
```

```
        EtaMixI=EtaMix(mark);
        TI=(CpI*TtI-UI^2/2)/CpI;
        MI=UI/(yI*RI*TI)^.5;
        PtI=PI*(1+(yI-1)/2*MI^2)^(yI/(yI-1));

    %Adjust Cp and y for Temperature Variation
        CpII=0;
        while abs((CpI-CpII)/CpI)>epsilon;
            CpII=CpI;
            if TI>6000;
                'Combustor Temperature Too HIGH'
                pause
            elseif TI>1000;
                CpN2bar(mark)=Runiv*(2.95257626+1.39690057e-3*TI-4.92631691e-7*TI^2+7.86010367e-11*TI^3-4.60755321e-15*TI^4);
                CpO2bar(mark)=Runiv*(3.66096083+6.56365523e-4*TI-1.41149485e-7*TI^2+2.05797658e-11*TI^3-1.29913248e-15*TI^4);
                CpH2Obar(mark)=Runiv*(2.67703787+2.97318329e-3*TI-7.73769690e-7*TI^2+9.44336689e-11*TI^3-4.26900959e-15*TI^4);
                CpH2bar(mark)=Runiv*(2.93286579+8.26607967e-4*TI-1.46402335e-7*TI^2+1.54100359e-11*TI^3-6.88804432e-16*TI^4);
            else
                CpN2bar(mark)=Runiv*(3.53100528-1.23660987e-4*TI-5.02999437e-7*TI^2+2.43530612e-9*TI^3-1.40881235e-12*TI^4);
                CpO2bar(mark)=Runiv*(3.78245636-2.99673415e-3*TI+9.84730200e-6*TI^2-9.68129508e-9*TI^3+3.24372836e-12*TI^4);
                CpH2Obar(mark)=Runiv*(4.19864056-2.03643410e-3*TI+6.52040211e-6*TI^2-5.48797062e-9*TI^3+1.77197817e-12*TI^4);
                CpH2bar(mark)=Runiv*(2.34433112+7.98052075e-3*TI-1.94781510e-5*TI^2+2.01572094e-8*TI^3-7.37611761e-12*TI^4);
            end
            CpIbar=PercN2I*CpN2bar(mark)+PercO2I*CpO2bar(mark)+PercH2OI*CpH2Obar(mark)+PercH2I*CpH2bar(mark);
            CpI=CpIbar/MwI;
            dCpComb(mark)=CpI-CpComb(mark);
            yI=CpI/(CpI-RI);

            dqCombustion(mark)=q(here)*dEtaMix(mark);
            dqWallComb(mark)=CpComb(mark)*CfComb/2*(TwComb-TtwComb(mark))*(cComb(mark)/Acomb(mark))*dx;
            if dqWallComb(mark)>0;
                dqWallComb(mark)=0;
            end
            dqTotalComb(mark)=dqCombustion(mark)+dqWallComb(mark);
            dTtComb(mark)=(dqTotalComb(mark)-(dCpComb(mark))*TtComb(mark))/CpI;
            dFricLossComb(mark)=CfComb*Ucomb(mark)^2/2*cComb(mark)/Acomb(mark)*dx;
            TtI=TtComb(mark)+dTtComb(mark);

            dsComb(mark)=(dqTotalComb(mark)+dFricLossComb(mark))/Tcomb(mark);
            dUComb(mark)=Ucomb(mark)/(Mcomb(mark)^2-1)*(1/(gamComb(mark)*Rcomb(mark)*Tcomb(mark))*(dqTotalComb(mark)-
gamComb(mark)*Tcomb(mark)*dsComb(mark)+(gamComb(mark)-1)*dCpComb(mark)*Tcomb(mark))+dAComb(mark)/Acomb(mark)-dRComb(mark)/Rcomb(mark));
            dPComb(mark)=rhoComb(mark)*(dqTotalComb(mark)-Ucomb(mark)*dUComb(mark)-Tcomb(mark)*dsComb(mark));
            if dUComb(mark)>50;
                'WARNING: excessive velocity gradient'
                dUComb(mark)
                mark
            end
            UI=Ucomb(mark)+dUComb(mark);
            PI=Pcomb(mark)+dPComb(mark);
            EtaMixI=EtaMix(mark);
            TI=(CpI*TtI-UI^2/2)/CpI;
            MI=UI/(yI*RI*TI)^.5;
            PtI=PI*(1+(yI-1)/2*MI^2)^(yI/(yI-1));
        end

        drhoComb(mark)=PI/(RI*TI)-rhoComb(mark);
        dPComb(mark)=PI-Pcomb(mark);
        dTComb(mark)=TI-Tcomb(mark);
        CombStateChk(mark)=(dPComb(mark)/Pcomb(mark))/(drhoComb(mark)/rhoComb(mark)+dRComb(mark)/Rcomb(mark)+dTComb(mark)/Tcomb(mark));
        CombMassChk(mark)=(drhoComb(mark)/rhoComb(mark))/(-dUComb(mark)/Ucomb(mark)-dAComb(mark)/Acomb(mark));
        CombEnergyChk(mark)=(CpComb(mark)*dTComb(mark)+Tcomb(mark)*dCpComb(mark)+Ucomb(mark)*dUComb(mark))/(dqTotalComb(mark));
        CombMomenChk(mark)=(dPComb(mark)/rhoComb(mark)+Ucomb(mark)*dUComb(mark)+Tcomb(mark)*dsComb(mark))/(dqTotalComb(mark));
        CombEntChk(mark)=(CpComb(mark)*dTComb(mark)+Tcomb(mark)*dCpComb(mark)-dPComb(mark)/rhoComb(mark))/(Tcomb(mark)*dsComb(mark));

    %Check to Ensure that choke not before combustor exit
        if MI<1.1;
            MI
            mark
```

```
            xComb(mark)
            thetaComb(here)=thetaComb(here)+.1*pi/180
            break
        end

        if max(xComb)<CombLength;
            dFComb(mark)=(Pcomb(mark)+PI)/2*dAComb(mark);
        end
    end
end
CombExit=CombEnt(here)+CombLength*dydxComb(here);
ThrustComb=mdottotal(here)*Ucomb(max(size(Ucomb)))-mdottotal(here)*Ucomb(1)+Pcomb(max(size(Pcomb)))*CombExit*Width-Pcomb(1)*CombEnt*Width;

PercN2out=PercN2Comb(mark);
PercO2out=PercO2Comb(mark);
PercH2Oout=PercH2Ocomb(mark);
PercH2out=PercH2Comb(mark);
Mwout=PercN2out*MwN2+PercO2out*MwO2+PercH2Oout*Mwp+PercH2out*Mwf;
Rout=Runiv/Mwout;

%MHD Generator Evaluation
'Start of MHD Calculations',balcount
Pt4(here)=PtComb(mark);
Tt4(here)=TtComb(mark);
M4(here)=Mcomb(mark);

xMHD=0;
MHDEnt(here)=CombExit;
thetaMHD(here)=thetaMHDI;
chokeMHD=0;

%Quasi-1-D MHD Analysis
while max(xMHD)<MHDLength-.01*dxMHD;
    'restart'
    dydxMHD(here)=tan(thetaMHD(here));
    TtI=Tt4(here);
    PtI=Pt4(here);
    CpI=CpComb(mark);
    yI=gamComb(mark);
    MI=M4(here);
    TI=TtI/(1+(yI-1)/2*MI^2);
    UI=MI*(yI*Rout*TI)^.5;

    mdotI=mdottotal(here);
    dx=dxMHD;
    clear loc
    for loc=1:1:MHDLength/dx+1;
        if mod(loc,500)==0;
            loc
        end
        TtMHD(loc)=TtI;
        TMHD(loc)=TI;
        UMHD(loc)=UI;
        PtMHD(loc)=PtI;
        MMHD(loc)=MI;
        CpMHD(loc)=CpI;
        gamMHD(loc)=yI;
        TtwMHD(loc)=TMHD(loc)*(1+MHDRelax*(gamMHD(loc)-1)/2*MMHD(loc)^2);
        PMHD(loc)=PtMHD(loc)/(1+(gamMHD(loc)-1)/2*MMHD(loc)^2)^(gamMHD(loc)/(gamMHD(loc)-1));
        rhoMHD(loc)=PMHD(loc)/(Rout*TMHD(loc));
        mdotMHD(loc)=mdotI;
        xMHD(loc)=loc*dx-dx;
        yMHD(loc)=MHDEnt(here)+dydxMHD(here)*(xMHD(loc)+dx/2);
        dyMHD(loc)=dydxMHD(here)*dx;
        dAMHD(loc)=dyMHD(loc)*Width;
        AMHD(loc)=Width*yMHD(loc);
        cMHD(loc)=2*(Width+yMHD(loc));
        mdotMHDChk(loc)=rhoMHD(loc)*AMHD(loc)*UMHD(loc);
```

```
        EyField(loc)=UMHD(loc)*Bfield/EtaMHD;
    %MHD Differential Analysis
        dqEMt(loc)=Cond*EyField(loc)*(EyField(loc)-UMHD(loc)*Bfield)/(rhoMHD(loc)*UMHD(loc))*dx;
        dqEMeff(loc)=Cond*Bfield*(EyField(loc)-UMHD(loc)*Bfield)/(rhoMHD(loc))*dx;
        dqWallMHD(loc)=CpMHD(loc)*CfMHD/2*(TwMHD-TtwMHD(loc))*(cMHD(loc)/AMHD(loc))*dx;
        if dqWallMHD(loc)>0;
            dqWallMHD(loc)=0;
        end
        dqTotalMHD(loc)=dqWallMHD(loc)+dqEMt(loc);
        dFricLossMHD(loc)=CfMHD*UMHD(loc)^2/2*cMHD(loc)/AMHD(loc)*dx;
        dCpMHD(loc)=CpI-CpMHD(loc);
        dTtMHD(loc)=(dqTotalMHD(loc)-TtMHD(loc)*dCpMHD(loc))/CpI;
        TtI=TtMHD(loc)+dTtMHD(loc);
        dsMHD(loc)=(dqTotalMHD(loc)-dqEMeff(loc)+dFricLossMHD(loc))/TMHD(loc);
        dUMHD(loc)=UMHD(loc)/(MMHD(loc)^2-1)*(1/(gamMHD(loc)*Rout*TMHD(loc))*(dqTotalMHD(loc)-gamMHD(loc)*TMHD(loc)*dsMHD(loc)+(gamMHD(loc)-
1)*TMHD(loc)*dCpMHD(loc))+dAMHD(loc)/AMHD(loc));
        dPMHD(loc)=rhoMHD(loc)*(dqTotalMHD(loc)-UMHD(loc)*dUMHD(loc)-TMHD(loc)*dsMHD(loc));
        UI=UMHD(loc)+dUMHD(loc);
        PI=PMHD(loc)+dPMHD(loc);
        TI=(CpI*TtI-UI^2/2)/CpI;
        MI=UI/(yI*Rout*TI)^.5;
        PtI=PI*(1+(yI-1)/2*MI^2)^(yI/(yI-1));

        %Adjust Cp and y for Temperature Variation
        CpII=0;
        while abs((CpI-CpII)/CpI)>epsilon;
            CpII=CpI;
            if TI>6000;
                'MHD Temperature Too HIGH'
                pause
            elseif TI>1000;
                CpN2barM(loc)=Runiv*(2.95257626+1.39690057e-3*TI-4.92631691e-7*TI^2+7.86010367e-11*TI^3-4.60755321e-15*TI^4);
                CpO2barM(loc)=Runiv*(3.66096083+6.56365523e-4*TI-1.41149485e-7*TI^2+2.05797658e-11*TI^3-1.29913248e-15*TI^4);
                CpH2ObarM(loc)=Runiv*(2.67703787+2.97318329e-3*TI-7.73769690e-7*TI^2+9.44336689e-11*TI^3-4.26900959e-15*TI^4);
                CpH2barM(loc)=Runiv*(2.93286579+8.26607967e-4*TI-1.464023356e-7*TI^2+1.54100359e-11*TI^3-6.88804432e-16*TI^4);
            else
                CpN2barM(loc)=Runiv*(3.53100528-1.23660987e-4*TI-5.02999437e-7*TI^2+2.43530612e-9*TI^3-1.40881235e-12*TI^4);
                CpO2barM(loc)=Runiv*(3.78245636-2.99673415e-3*TI+9.84730200e-6*TI^2-9.68129508e-9*TI^3+3.24372836e-12*TI^4);
                CpH2ObarM(loc)=Runiv*(4.19864056-2.03643410e-3*TI+6.52040211e-6*TI^2-5.48797062e-9*TI^3+1.77197817e-12*TI^4);
                CpH2barM(loc)=Runiv*(2.34433112+7.98052075e-3*TI-1.94781510e-5*TI^2+2.01572094e-8*TI^3-7.37611761e-12*TI^4);
            end
            CpIbar=PercN2out*CpN2barM(loc)+PercO2out*CpO2barM(loc)+PercH2Oout*CpH2ObarM(loc)+PercH2out*CpH2barM(loc);
            CpI=CpIbar/Mwout;
            yI=CpI/(CpI-Rout);

            dqEMt(loc)=Cond*EyField(loc)*(EyField(loc)-UMHD(loc)*Bfield)/(rhoMHD(loc)*UMHD(loc))*dx;
            dqEMeff(loc)=Cond*Bfield*(EyField(loc)-UMHD(loc)*Bfield)/(rhoMHD(loc))*dx;
            dqWallMHD(loc)=CpMHD(loc)*CfMHD/2*(TwMHD-TtwMHD(loc))*(cMHD(loc)/AMHD(loc))*dx;
            if dqWallMHD(loc)>0;
                dqWallMHD(loc)=0;
            end
            dqTotalMHD(loc)=dqWallMHD(loc)+dqEMt(loc);
            dFricLossMHD(loc)=CfMHD*UMHD(loc)^2/2*cMHD(loc)/AMHD(loc)*dx;
            dCpMHD(loc)=CpI-CpMHD(loc);
            dTtMHD(loc)=(dqTotalMHD(loc)-TtMHD(loc)*dCpMHD(loc))/CpI;
            TtI=TtMHD(loc)+dTtMHD(loc);
            dsMHD(loc)=(dqTotalMHD(loc)-dqEMeff(loc)+dFricLossMHD(loc))/TMHD(loc);
            dUMHD(loc)=UMHD(loc)/(MMHD(loc)^2-1)*(1/(gamMHD(loc)*Rout*TMHD(loc))*(dqTotalMHD(loc)-gamMHD(loc)*TMHD(loc)*dsMHD(loc)+(gamMHD(loc)-
1)*TMHD(loc)*dCpMHD(loc))+dAMHD(loc)/AMHD(loc));
            dPMHD(loc)=rhoMHD(loc)*(dqTotalMHD(loc)-UMHD(loc)*dUMHD(loc)-TMHD(loc)*dsMHD(loc));
            UI=UMHD(loc)+dUMHD(loc);
            PI=PMHD(loc)+dPMHD(loc);
            TI=(CpI*TtI-UI^2/2)/CpI;
            MI=UI/(yI*Rout*TI)^.5;
            PtI=PI*(1+(yI-1)/2*MI^2)^(yI/(yI-1));
        end

        drhoMHD(loc)=PI/(Rout*TI)-rhoMHD(loc);
```

```
            dPMHD(loc)=PI-PMHD(loc);
            dTMHD(loc)=TI-TMHD(loc);
            MHDStateChk(loc)=(dPMHD(loc)/PMHD(loc))/(drhoMHD(loc)/rhoMHD(loc)+dTMHD(loc)/TMHD(loc));
            MHDMassChk(loc)=(drhoMHD(loc)/rhoMHD(loc))/(-dUMHD(loc)/UMHD(loc)-dAMHD(loc)/AMHD(loc));
            MHDEnergyChk(loc)=(CpMHD(loc)*dTMHD(loc)+TMHD(loc)*dCpMHD(loc)/(-UMHD(loc)*dUMHD(loc))+dqTotalMHD(loc));
            MHDMomenChk(loc)=(dPMHD(loc)/rhoMHD(loc))/(-UMHD(loc)*dUMHD(loc)-TMHD(loc)*dsMHD(loc)+dqTotalMHD(loc));
            MHDEntChk(loc)=(CpMHD(loc)*dTMHD(loc)+TMHD(loc)*dCpMHD(loc))/(dPMHD(loc)/rhoMHD(loc)+TMHD(loc)*dsMHD(loc));

        %Check to Ensure that choke not before MHD exit
            if MI<1.02;
                MI
                if xMHD(loc)<chokeMHD;
                    'Expansion is not helping'
                    pause
                end
                chokeMHD=xMHD(loc)
                thetaMHD(here)=thetaMHD(here)+.2*pi/180
                break
            end
            if loc<=MHDLength/dx;
                dFMHD(loc)=(PMHD(loc)+PI)/2*dAMHD(loc);
            end
        end
    end

%Thermal Balancing
    qWallMHD(here)=sum(dqWallMHD);
    PowWallMHD(here)=-qWallMHD(here)*mdottotal(here);
    qfabsMHDmax=Cpf*(TwMHD-Tfl);
    PowfabsMHDmax=mdotfuel(here)*qfabsMHDmax;
    if PowWallMHD(here)>PowfabsMHDmax;
        TfMHD(here)=TwMHD;
        mdotfMHD(here)=PowWallMHD(here)/qfabsMHDmax;
    else
        mdotfMHD(here)=mdotfuel(here);
        qfabsMHD=PowWallMHD(here)/mdotfMHD(here);
        TfMHD(here)=(qfabsMHD+Cpf*Tfl)/Cpf;
    end
    qWallComb(here)=sum(dqWallComb);
    PowWallComb(here)=-qWallComb(here)*mdottotal(here);
    qfabsCombmax=Cpf*(TwComb-TfMHD(here));
    PowfabsCombmax=mdotfMHD(here)*qfabsCombmax;
    if PowWallComb(here)>PowfabsCombmax;
        TfComb(here)=TwComb;
        PowWallCombEx=PowWallComb(here)-PowfabsCombmax;
        qfabsCombmax2=Cpf*(TwComb-Tfl);
        mdotfComb(here)=mdotfMHD(here)+PowWallCombEx/qfabsCombmax2;
    else
        mdotfComb(here)=mdotfMHD(here);
        qfabsComb=PowWallComb(here)/mdotfComb(here);
        TfComb(here)=(qfabsComb+Cpf*TfMHD(here))/Cpf;
    end
    if abs(TfComb(here)-Ttfinj)/TfComb(here)>.001;
        Ttfinj=TfComb(here)
    else
        'Engine is thermally Balanced'
        balanced=1
    end
    balcount=balcount+1
end

    MHDExit=MHDEnt(here)+MHDLength*dydxMHD(here);
    Pt5(here)=PtMHD(MHDLength/dx+1);
    Tt5(here)=TtMHD(MHDLength/dx+1);
    M5(here)=MMHD(MHDLength/dx+1);
    ThrustMHD(here)=mdottotal(here)*(UMHD(max(size(UMHD)))-UMHD(1))+PMHD(max(size(PMHD)))*MHDExit*Width-PMHD(1)*MHDEnt(here)*Width;
    Cpl=CpMHD(loc);
    yl=gamMHD(loc);
```

```
%Nozzle Analysis
    xNoz=0;
    NozEnt(here)=MHDExit;
    AI=NozEnt(here);
    MI=M5(here);
    PtI=Pt5(here);
    TtI=Tt5(here);
    TI=TtI/(1+(yI-1)/2*MI^2);
    UI=MI*(yI*Rout*TI)^.5;
    NozSlope(here)=(Exit+CombEnt(here)-NozEnt(here))/NozzleLength;
    thetaN(here)=atan(NozSlope(here));
    dx=dxNoz;

    clear spot
    'Start of Nozzle Calculations'
    for spot=1:1:NozzleLength/dx+1;
        CpNoz(spot)=CpI;
        gamNoz(spot)=yI;
        Mnoz(spot)=MI;
        PtNoz(spot)=PtI;
        Pnoz(spot)=PtNoz(spot)/(1+(gamNoz(spot)-1)/2*Mnoz(spot)^2)^(gamNoz(spot)/(gamNoz(spot)-1));
        TtNoz(spot)=TtI;
        Tnoz(spot)=TI;
        rhoNoz(spot)=Pnoz(spot)/(Rout*Tnoz(spot));
        Unoz(spot)=UI;
        xNoz(spot)=spot*dx-dx;
        dHNozTop(spot)=NozSlope(here)*dx;
        Anoz(spot)=AI;
        mdotNozChk(spot)=rhoNoz(spot)*Anoz(spot)*Unoz(spot);
        EnthFlowNoz(spot)=CpNoz(spot)*TtNoz(spot);

        if spot<(PercNozCl/100*NozzleLength)/dx+1;
            thetaExp(spot)=0;
            betaExp(spot)=0;
            vExp1(spot)=0;
            vExp2(spot)=0;
            Mexp(spot)=0;
            Pexp(spot)=0;
            Pshock(spot)=0;
        else
            if spot==(PercNozCl/100*NozzleLength)/dx+1;
                thetaExpGUp=40*pi/180;
            else
                thetaExpGUp=thetaExp(spot-1);
            end
            thetaExpGDn=0;
            thetaExp(spot)=(thetaExpGUp+thetaExpGDn)/2;
            Pdiff=1e8;
            compare=1;
            while abs(Pdiff)/Pnoz(spot)>.005;
                if spot==(PercNozCl/100*NozzleLength)/dx+1;
                    betaExpGUp=68*pi/180;
                else
                    betaExpGUp=betaExp(spot-1);
                end
                betaExpGDn=thetaExp(spot);
                betaExp(spot)=(betaExpGDn+betaExpGUp)/2;
                while abs(tan(thetaExp(spot))-2*cot(betaExp(spot))*(M0(here)^2*sin(betaExp(spot))^2-1)/(M0(here)^2*(y0(here)+cos(2*betaExp(spot)))+2))>epsilon;
                    if tan(thetaExp(spot))-2*cot(betaExp(spot))*(M0(here)^2*sin(betaExp(spot))^2-1)/(M0(here)^2*(y0(here)+cos(2*betaExp(spot)))+2)>0;
                        betaExpGDn=betaExp(spot);
                    else
                        betaExpGUp=betaExp(spot);
                    end
                    betaExp(spot)=(betaExpGDn+betaExpGUp)/2;
                    if abs(betaExpGUp-betaExpGDn)/betaExp(spot)<epsilon^2;
                        spot
                        break
```

```
        end
    end
    vExp1(spot)=((yI+1)/(yI-1))^.5*atan(((yI-1)/(yI+1)*(Mnoz(spot)^2-1))^.5)-atan((Mnoz(spot)^2-1)^.5);
    vExp2(spot)=thetaExp(spot)+vExp1(spot);

    MexpDn=1;
    MexpUp=20;
    Mexp(spot)=(MexpDn+MexpUp)/2;
    while abs(vExp2(spot)-(((yI+1)/(yI-1))^.5*atan(((yI-1)/(yI+1)*(Mexp(spot)^2-1))^.5)-atan((Mexp(spot)^2-1)^.5)))>epsilon;
        if vExp2(spot)-(((yI+1)/(yI-1))^.5*atan(((yI-1)/(yI+1)*(Mexp(spot)^2-1))^.5)-atan((Mexp(spot)^2-1)^.5))>0
            MexpDn=Mexp(spot);
        else
            MexpUp=Mexp(spot);
        end
        Mexp(spot)=(MexpDn+MexpUp)/2;
        if abs(MexpUp-MexpDn)/Mexp(spot)<epsilon^2;
            spot
            break
        end
    end
    Pexp(spot)=PtNoz(spot)/(1+(yI-1)/2*Mexp(spot)^2)^(yI/(yI-1));
    Pshock(spot)=P0(here)*(1+2*y0(here)/(y0(here)+1)*((M0(here)*sin(betaExp(spot)))^2-1));
    Pdiff=Pexp(spot)-Pshock(spot);
    if abs(Pdiff)/Pnoz(spot)>.005;
        if Pdiff<0;
            thetaExpGUp=thetaExp(spot);
        else
            thetaExpGDn=thetaExp(spot);
        end
        thetaExp(spot)=(thetaExpGUp+thetaExpGDn)/2;
        compare=compare+1;
        if compare>=1000;
            'Expansion angle could not be found within error, closest value used'
            spot
            compare
            thetaDiff=2*(thetaExpGUp-thetaExpGDn)/(thetaExpGUp+thetaExpGDn)
            Perror=Pdiff/Pnoz(spot)
            break;
        end
        if abs(thetaExpGUp-thetaExpGDn)/thetaExp(spot)<epsilon^2;
            'Expansion angle could not be found within error, closest value used'
            spot
            compare
            thetaDiff=2*(thetaExpGUp-thetaExpGDn)/(thetaExpGUp+thetaExpGDn)
            Perror=Pdiff/Pnoz(spot)
            break;
        end
    end
  end
end
dHNozBot(spot)=tan(thetaExp(spot))*dx;
dHNoz(spot)=dHNozTop(spot)+dHNozBot(spot);
if spot==1;
    Hnoz(spot)=(NozSlope(here)+tan(thetaExp(spot)))*(xNoz(spot)+dx/2)+NozEnt(here);
else
    Hnoz(spot)=Hnoz(spot-1)+(2*NozSlope(here)+tan(thetaExp(spot-1))+tan(thetaExp(spot)))*dx/2;
end
if spot<(PercNozCl/100*NozzleLength)/dx+1;
    cNoz(spot)=2*(Width+Hnoz(spot));
else
    cNoz(spot)=Width;
end
AI=Width*Hnoz(spot);
dANoz(spot)=Width*dHNoz(spot);

dFricLossNoz(spot)=CfNoz*Unoz(spot)^2/2*cNoz(spot)/Anoz(spot)*dx;
dCpNoz(spot)=CpI-CpNoz(spot);
dTtNoz(spot)=-dCpNoz(spot)*TtNoz(spot)/CpI;
```

```
        TtI=TtNoz(spot)+dTtNoz(spot);
        dsNoz(spot)=dFricLossNoz(spot)/Tnoz(spot);
        dUNoz(spot)=Unoz(spot)/(Mnoz(spot)^2-1)*(1/(gamNoz(spot)*Rout*Tnoz(spot))*(-gamNoz(spot)*Tnoz(spot)*dsNoz(spot)+(gamNoz(spot)-
1)*dCpNoz(spot)*Tnoz(spot))+dANoz(spot)/Anoz(spot));
        dPNoz(spot)=rhoNoz(spot)*(-Unoz(spot)*dUNoz(spot)-Tnoz(spot)*dsNoz(spot));
        UI=Unoz(spot)+dUNoz(spot);
        PI=Pnoz(spot)+dPNoz(spot);
        TI=(CpI*TtI-UI^2/2)/CpI;
        MI=UI/(yI*Rout*TI)^.5;
        PtI=PI*(1+(yI-1)/2*MI^2)^(yI/(yI-1));
        %Adjust Cp and y for Temperature Variation
        CpII=0;
        while abs((CpI-CpII)/CpI)>epsilon;
            CpII=CpI;
            if TI>6000;
                'Nozzle Temperature Too HIGH'
                pause
            elseif TI>1000;
                CpN2barN(spot)=Runiv*(2.95257626+1.39690057e-3*TI-4.92631691e-7*TI^2+7.86010367e-11*TI^3-4.60755321e-15*TI^4);
                CpO2barN(spot)=Runiv*(3.66096083+6.56365523e-4*TI-1.41149485e-7*TI^2+2.05797658e-11*TI^3-1.29913248e-15*TI^4);
                CpH2ObarN(spot)=Runiv*(2.67703787+2.97318329e-3*TI-7.73769690e-7*TI^2+9.44336689e-11*TI^3-4.26900959e-15*TI^4);
                CpH2barN(spot)=Runiv*(2.93286579+8.26607967e-4*TI-1.46402335e-7*TI^2+1.54100359e-11*TI^3-6.88804432e-16*TI^4);
            else
                CpN2barN(spot)=Runiv*(3.53100528-1.23660987e-4*TI-5.02999437e-7*TI^2+2.43530612e-9*TI^3-1.40881235e-12*TI^4);
                CpO2barN(spot)=Runiv*(3.78245636-2.99673415e-3*TI+9.84730200e-6*TI^2-9.68129508e-9*TI^3+3.24372836e-12*TI^4);
                CpH2ObarN(spot)=Runiv*(4.19864056-2.03643410e-3*TI+6.52040211e-6*TI^2-5.48797062e-9*TI^3+1.77197817e-12*TI^4);
                CpH2barN(spot)=Runiv*(2.34433112+7.98052075e-3*TI-1.94781510e-5*TI^2+2.01572094e-8*TI^3-7.37611761e-12*TI^4);
            end
            CpIbar=PercN2out*CpN2barN(spot)+PercO2out*CpO2barN(spot)+PercH2Oout*CpH2ObarN(spot)+PercH2out*CpH2barN(spot);
            CpI=CpIbar/Mwout;
            yI=CpI/(CpI-Rout);
            dFricLossNoz(spot)=CfNoz*Unoz(spot)^2/2*cNoz(spot)/Anoz(spot)*dx;
            dCpNoz(spot)=CpI-CpNoz(spot);
            dTtNoz(spot)=-dCpNoz(spot)*TtNoz(spot)/CpI;
            TtI=TtNoz(spot)+dTtNoz(spot);
            dsNoz(spot)=dFricLossNoz(spot)/Tnoz(spot);
            dUNoz(spot)=Unoz(spot)/(Mnoz(spot)^2-1)*(1/(gamNoz(spot)*Rout*Tnoz(spot))*(-gamNoz(spot)*Tnoz(spot)*dsNoz(spot)+(gamNoz(spot)-
1)*dCpNoz(spot)*Tnoz(spot))+dANoz(spot)/Anoz(spot));
            dPNoz(spot)=rhoNoz(spot)*(-Unoz(spot)*dUNoz(spot)-Tnoz(spot)*dsNoz(spot));
            drhoNoz2(spot)=rhoNoz(spot)*(-dUNoz(spot)/Unoz(spot)-dANoz(spot)/Anoz(spot));
            UI=Unoz(spot)+dUNoz(spot);
            PI=Pnoz(spot)+dPNoz(spot);
            TI=(CpI*TtI-UI^2/2)/CpI;
            MI=UI/(yI*Rout*TI)^.5;
            PtI=PI*(1+(yI-1)/2*MI^2)^(yI/(yI-1));
        end

        drhoNoz(spot)=PI/(Rout*TI)-rhoNoz(spot);
        dPNoz(spot)=PI-Pnoz(spot);
        dTNoz(spot)=TI-Tnoz(spot);
        NozStateChk(spot)=(dPNoz(spot)/Pnoz(spot))/(drhoNoz(spot)/rhoNoz(spot)+dTNoz(spot)/Tnoz(spot));
        NozMassChk(spot)=(drhoNoz(spot)/rhoNoz(spot))/(-dUNoz(spot)/Unoz(spot)-dANoz(spot)/Anoz(spot));
        NozEnergyChk(spot)=(CpNoz(spot)*dTNoz(spot)+Tnoz(spot)*dCpNoz(spot))/(-Unoz(spot)*dUNoz(spot));
        NozMomenChk(spot)=(dPNoz(spot)/rhoNoz(spot)+Tnoz(spot)*dsNoz(spot))/(-Unoz(spot)*dUNoz(spot));
        NozEntChk(spot)=(CpNoz(spot)*dTNoz(spot)+Tnoz(spot)*dCpNoz(spot)-Tnoz(spot)*dsNoz(spot))/(dPNoz(spot)/rhoNoz(spot));
        if spot<(PercNozCl/100*NozzleLength)/dx+1;
            dFNoz(spot)=0;
            dDNoz(spot)=Pshock(spot)*dHNozBot(spot)*Width;
        elseif spot<=NozzleLength/dx;
            dFNoz(spot)=(Pnoz(spot)+PI)/2*dHNozTop(spot)*Width;
            dDNoz(spot)=Pshock(spot)*dHNozBot(spot)*Width;
        end
    end
    ThrustNozCl(here)=mdottotal(here)*(Unoz((PercNozCl/100*NozzleLength)/dx+1)-Unoz(1))+Pnoz((PercNozCl/100*NozzleLength)/dx+1)*Anoz((PercNozCl/100*NozzleLength)/dx+1)-
Pnoz(1)*Anoz(1);
    ThrustNozOp(here)=sum(dFNoz);

    Thrust(here)=ThrustComp(here)+ThrustMix(here)+ThrustComb(here)+ThrustMHD(here)+ThrustNozCl(here)+ThrustNozOp(here)
```

```
    Cp9(here)=CpNoz(NozzleLength/dx+1);
    y9(here)=gamNoz(NozzleLength/dx+1);
    Pt9(here)=PtNoz(NozzleLength/dx+1);
    Tt9(here)=TtNoz(NozzleLength/dx+1);
    M9(here)=Mnoz(NozzleLength/dx+1);
    P9(here)=Pt9(here)/(1+(y9(here)-1)/2*M9(here)^2)^(y9/(y9-1));
    T9(here)=Tt9(here)/(1+(y9(here)-1)/2*M9(here)^2);
    rho9(here)=P9(here)/(Rout*T9(here));
    a9(here)=(y9(here)*Rout*T9(here))^.5;
    U9(here)=M9(here)*a9(here);
    Ai(here)=(Inlet+CombEnt(here))*Width;
    Ae(here)=(Exit+CombEnt(here))*Width;
    Isp(here)=Thrust(here)/(gSL*mdotfuel(here))
    FlightPower(here)=Thrust(here)*U0(here)
    qEMefi(here)=sum(dqEMefi);
    MHDPower(here)=-qEMefi*mdottotal(here)
    TotalPower(here)=FlightPower(here)+MHDPower(here)
    PercentMHD(here)=MHDPower(here)/TotalPower(here)
end

M0=M0';
AltGm0=AltGm0';
thetaComb=180/pi*thetaComb';
thetaMHD=180/pi*thetaMHD';
Tt0=Tt0';
Tt9=Tt9';
P0=P0';
P9=P9';
EtaMixMax=EtaMixMax';
TfComb=TfComb';
mdotfuel=mdotfuel';
mdotfMHD=mdotfMHD';
mdotfComb=mdotfComb';
Thrust=Thrust';
Isp=Isp';
FlightPower=FlightPower';
MHDPower=MHDPower';
TotalPower=TotalPower';
PercentMHD=PercentMHD';
Out=[M0 AltGm0 P0 Tt0 P9 Tt9 EtaMixMax TfComb thetaComb thetaMHD mdotfuel mdotfMHD mdotfComb Thrust Isp FlightPower MHDPower TotalPower PercentMHD];
save -ascii Out.dat Out;
```

APPENDIX B: DERIVATION OF THE MHD EQUATIONS

First, assume the following which is used in the MHD model:

$$\vec{u} = u\hat{x} \quad \vec{E} = E\hat{y} \quad \vec{B} = B\hat{z}$$

By using Ohm's Law for plasmas, the current density vector, $\vec{j}$ can be calculated:

$$\vec{j} = \sigma\left(\vec{E} + \vec{u} \times \vec{B}\right) + \frac{\omega_e \tau_e}{2B}\left(\vec{j} \times \vec{B}\right) \qquad \text{(Ohm's Law)}$$

In component form, this becomes:

$$j_x = \tfrac{1}{2}\omega_e \tau_e \cdot j_y$$
$$j_y = \sigma\left(E - uB\right) - \tfrac{1}{2}\omega_e \tau_e \cdot j_x$$

Solving these two components simultaneously, the current densities become:

$$j_x = \frac{\sigma \tfrac{1}{2}\omega_e \tau_e}{1 + \tfrac{1}{4}\omega_e{}^2 \tau_e{}^2}\left(E - uB\right)$$
$$j_y = \frac{\sigma}{1 + \tfrac{1}{4}\omega_e{}^2 \tau_e{}^2}\left(E - uB\right)$$

The ω_e is termed the cyclotron frequency of an electron and is given by:

$$\omega_e = \frac{eB}{m_e}$$

The τ_e is the average time between electron collisions, which, though it is difficult to calculate, has a value much less than one:

$$\tau_e << 1$$

The terms that contain $\omega_e \tau_e$ arise because of a phenomenon known as the Hall Effect, in which an electron flow is created in the plasma perpendicular to the magnetic and electric fields by the Lorentz force. If it is assumed that Hall Effect is negligible, that is:

$$\omega_e{}^2 \tau_e{}^2 << 1$$

Then the current densities reach the following forms used in the model:

$$j_x = \tfrac{1}{2}\sigma\omega_e\tau_e\left(E - uB\right) \cong 0$$
$$j_y = \sigma\left(E - uB\right)$$

The Lorentz Force Equation gives the specific force generated by the electromagnetic interaction with the plasma:

$$\vec{f} = \frac{\vec{j} \times \vec{B}}{\rho} = \frac{B\left(j_y\hat{x} - j_x\hat{y}\right)}{\rho}$$

The specific work added or removed from the flow by this specific force can be calculated by taking its dot product with the differential change in distance vector:

$$dw_{EM} = \vec{f} \bullet d\vec{x}$$

Simplified, this work interaction becomes:

$$dw_{EM} = \frac{\sigma B\left(E - uB\right)}{\rho} dx$$

By introducing the MHD load factor:

$$\eta_{MHD} = \frac{uB}{E}$$

The MHD work interaction reaches the form used in the model:

$$dw_{EM} = \frac{\sigma u B^2 \left(\frac{1}{\eta_{MHD}} - 1\right)}{\rho} dx \qquad (4.4.9)$$

It should be noted that dw_{EM} has the opposite sign convention than work in the thermodynamic sense, i.e. positive dw_{EM} is work added to the flow. The total rate per unit volume of energy, i.e. the power density, added or removed from the flow can be found by taking the dot product of the current density with the electric field:

$$\wp_{EM} = \vec{j} \bullet \vec{E} = j_y E$$

Converted to a differential specific heat interaction, this equation becomes:

$$dq_{EM} = \frac{\wp_{EM}}{\rho u} dx$$

Substituting in the power density $\wp_{EM}$ and current density $\vec{j}$, the heat interaction reaches the following form:

$$dq_{EM} = \frac{\sigma E(E - uB)}{\rho u} dx$$

Finally, by integrating the MHD load factor η_{MHD} into the above equation, the total energy interaction reaches the form used in the model:

$$dq_{EM} = \frac{\sigma u B^2 \left(\frac{1}{\eta_{MHD}^2} - \frac{1}{\eta_{MHD}}\right)}{\rho} dx \qquad (4.4.7)$$

Thus the MHD terms used in the model have been derived.

APPENDIX C: DERIVATION OF THE IDEAL SCRAMJET RELATIONS

The ideal scramjet assumes that there are no losses in the engine flow and that the flow is fully expanded. In terms of flow properties, the condition of no loss can be expressed as constant total pressure:

$$P_{t9} = P_{t0}$$

The fully expanded condition can be expressed entrance and exit static pressure equalization:

$$P_9 = P_0$$

The equation that relates total and static pressure in terms of Mach number is as follows:

$$P_t = P\left(1+\frac{\gamma-1}{2}M^2\right)^{\gamma/(\gamma-1)}$$

From these three relations and a constant gamma (which is true for an ideal scramjet), it can be seen that the exit Mach number must equal the entrance Mach number:

$$M_9 = M_0$$

Total temperature increase in the combustor is treated as a reversible heat addition:

$$\frac{T_{t9}}{T_{t0}} = 1+\frac{\Delta q}{C_p T_{t0}} = \frac{T_9}{T_0}$$

The second relation in the equation above follows from the definition of total temperature and the Mach number equivalence already noted. Thus specific impulse can be written as follows:

$$I_{sp,ideal} = \frac{(1+f_{ST})U_9 - U_0}{f_{ST} g_0} = \frac{M_0\sqrt{\gamma R}}{f_{ST} g_0}\left[(1+f_{ST})\sqrt{T_0 + \frac{\Delta q}{C_p}\frac{1}{1+\frac{\gamma-1}{2}M_0^2}} - \sqrt{T_0}\right]$$

BIBLIOGRAPHY

1. David J. Griffiths, *Introduction to Electrodynamics,* 3rd Ed., Prentice Hall: Upper Saddle River, New Jersey (1999).

2. William H. Hayt, Jr. and John A. Buck, *Engineering Electromagnetics,* 6th Ed., McGraw Hill: Boston (2001).

3. T.G. Cowling, *Magnetohydrodynamics,* Interscience Pubs.: New York (1957).

4. H.K. Moffatt, *Magnetic Field Generation in Electrically Conducting Fluids,* Cambridge Univ. Pr.: Cambridge (1978).

5. Clifford Mannal and Norman W. Mather, Eds., *Engineering Aspects of Magnetohydrodynamics,* Proceedings of the Second Symposium on the Engineering Aspects of Magnetohydrodynamics, Philadelphia, Pennsyvania, March 9 and 10, 1961, Columbia Univ. Pr.: New York (1962).

6. Stanley W. Angrist, *Direct Energy Conversion,* 2nd Ed., Chpt. 7, Allyn and Bacon: Boston (1971).

7. Ali Bulent Cambel, *Plasma Physics and Magnetofluid-mechanics*, McGraw Hill: New York (1963).

8. George W. Sutton and Arthur Sherman, *Engineering Magnetohydrodynamics*, McGraw Hill: New York (1965).

9. W.F. Hughes and F.J. Young, *The Electromagnetodynamics of Fluids,* John Wiley & Sons: New York (1966).

10. James E.A. John, *Gas Dynamics,* 2nd Ed., Chpt. 11, Allyn and Bacon: Boston (1984).

11. Philip G. Hill and Carl R. Peterson, *Mechanics and Thermodynamics of Propulsion,* Chpt. 5, Addison-Wesley: Reading, Massacheusetts (1965).

12. E.L. Resler, Jr. and W.R. Sears, "The Prospects for Magneto-Aerodynamics," *Journal of Aerospace Science,* Vol. 25, No. 4, Pp. 235-245, 258 (1958).

13. Edwin L. Resler, Jr. and William R. Sears, "Magneto-Gasdynamic Channel Flow," *Zeitschrift für Angewandte Mathematik und Physik (ZAMP),* Vol. 9, Nos. 5-6, Pp. 509-518 (1958).

14. Jack L. Kerrebrock, "Magnetohydrodynamic Generators with Nonequilibrium Ionization," *AIAA Journal,* Vol. 3, No. 4, Pp. 591-601 (1965).

15. Claudio Bruno and Paul A. Czysz, "An Electro-magnetic-chemical Hypersonic Propulsion System," *AIAA International Space Planes and Hypersonic Systems and Technologies Conference*, 8th, Norfolk, VA (1998).

16. Chul Park, David Bogdanoff, and Unmeel B. Mehta, "Theoretical Performance of Frictionless Magnetohydrodynamic-Bypass Scramjets," *Journal of Propulsion and Power,* Vol. 17, No. 3 (2001).

17. Chul Park, Unmeel B. Mehta, and David W. Bogdanoff, "Magnetohydrodynamics Energy Bypass Scramjet Performance with Real Gas Effects," *Journal of Propulsion and Power,* Vol. 17, No. 5 (2001).

18. Chul Park, David W. Bogdanoff, and Unmeel B. Mehta, "Theoretical Performance of a Magnetohydrodynamic-Bypass Scramjet Engine with Nonequilibrium Ionization," *Journal of Propulsion and Power*, Vol. 19, No. 4 (2003).

19. B.M. Burakhanov, A.P. Likhachev, S.A. Medin, V.A. Novikov, V.I. Okunev, V. Yu. Rickman, and V.A. Zeigarnik, "Advancement of Scramjet Magnetohydrodynamic Concept," *Journal of Propulsion and Power,* Vol. 17, No. 4 (2001).

20. David W. Riggins, "Analysis of the Magnetohydrodynamic Energy Bypass Engine for High-Speed Airbreathing Propulsion," *Journal of Propulsion and Power,* Vol. 20, No. 5 (2004).

21. E.G. Sheikin and A.L. Kuranov, "MHD Control in Hypersonic Aircraft," *AIAA Aerospace Sciences Meeting and Exhibit,* 43rd, Revo, NV (2005).

22. Mikhail N. Shneider and Sergey O. Macheret, "Modeling Plasma and MHD Effects in Hypersonic Propulsion Flowpath," *AIAA Plasmadynamics and Lasers Conference,* Toronto, Ontario, Canada (2005).

23. Chun-Hian Lee and Haoyu Lu, "Quasi-One-Dimensional Parametric Study for MHD Generator in MHD Bypass Scramjet System," *AIAA Aerospace Sciences Meeting and Exhibit*, 45th, Reno, NV (2007).

24. Zhenyu Xu and R.S. Amano, "Simulation of Supersonic MHD Channel Flow," *AIAA Aerospace Sciences Meeting and Exhibit,* 45th, Reno, NV (2007).

25. Daiki Gotoh, Toru Takahashi, Takayasu Fujino, Motoo Ishikawa, and John T, Lineberry, "Computational Analysis of the HVEPS Scramjet MHD Power Generation," *AIAA Plasmadynamics and Lasers Conference*, 38th, Miami, FL (2007).

26. J.T. Lineberry, L. Begg, J.H. Castro, and R.J. Litchford, "Scramjet Driven MHD Power Demonstration – HVEPS Program," *AIAA Plasmadynamics and Lasers Conference,* 37th, San Francisco (2006).

27. J.T. Lineberry, L. Begg, J.H. Castro, and R.J. Litchford, "Scramjet Driven MHD Power Demonstration – HVEPS Program Overview," *AIAA/AHI International Space Planes and Hypersonic Systems and Technologies Conference*, 14th, Canberra, Australia (2006).

28. J.T. Lineberry, L. Begg, J.H. Castro, R.J. Litchford, and J.M. Donohue, "HVEPS Scram-jet-Driven MHD Power Demonstration Test Results," *AIAA Plasmadynamics and Lasers Conference*, 38th, Maimi, FL (2007).

29. S. Gordon and B.J. McBride, "Computer Program for Calculation of Complex Chemical Equilibrium Composition and Applications I. Analysis," *NASA Reference Publication 1311* (October 1994).

30. *U.S. Standard Atmosphere, 1976,* U.S. Government Printing Office: Washington, D.C. (1976).

VITA

Nathan Lee Mundis was born on November 6, 1981 in Tulsa, Oklahoma. He attended Southside Elementary School, Charles N. Haskell Middle School, and North Intermediate High School in the Broken Arrow School District in Broken Arrow, Oklahoma. He graduated from Broken Arrow High School on May 11, 2000 with Distinction, Summa Cum Laude, as a National Merit Scholar and an Oklahoma Academic Scholar. He began attending the University of Missouri – Rolla in August, 2000, pursuing a Bachelor of Science in Aerospace Engineering. As a junior at UMR, Nathan won third place at the 2003 AIAA Region V Student Papers Conference with his paper entitled, "The Effect of Inlet Compression Angle on Scramjet Propulsion." Nathan completed his B.S. on May 15, 2004, graduating Summa Cum Laude and as an Honors Scholar. Shortly thereafter, Nathan began the pursuit of his Master of Science in Aerospace Engineering at the University of Missouri – Rolla. He was awarded the Extraordinary Student Leadership Award in April, 2006 for his efforts as UMR Student Council's Vice President of External Affairs from April, 2004 to May, 2006. Though still completing his M.S., Nathan began his career as a computational fluid dynamicist at Cessna Aircraft Company in June, 2007. Nathan received his Master of Science in Aerospace Engineering in December 2007.